STATISTICAL PERFORMANCE ANALYSIS OF TIME-VARYING VOLUMETRIC RANDOM ARRAYS BASED ON UAV SWARM

A Dissertation

by

ZHONG CHEN

Submitted to the Office of Graduate and Professional Studies of
Texas A&M University
in partial fulfillment of the requirements for the degree of

DOCTOR OF PHILOSOPHY

Chair of Committee,	Gregory H. Huff
Co-Chair of Committee,	Jean-Francois Chamberland
Committee Members,	Robert D. Nevels
	John Valasek
Head of Department,	Miroslav Begovic

December 2020

Major Subject: Electrical Engineering

ABSTRACT

This dissertation mainly focuses on the research of direction-of-arrival (DOA) estimation with micro-UAV swarm-based (MUSB) arrays, including signal model formulation, closed-form asymptotic mean square error (AMSE) derivation, Cramer-Rao bound (CRB) derivation in the presence of receiving antenna gain, phase, and position errors, system performance analysis with the derived equations, performing numerical simulation and practical experiments to verify the theoretical expectations.

This dissertation firstly reports on the DOA estimation with MUSB arrays. This work presents the mathematical model of MUSB array data collection system and introduces the iterative multiple signal classification (iterative-MUSIC) algorithm for MUSB arrays. System convergence of the MUSB array is examined by simulation and experiment to verify that the iterative-MUSIC algorithm works for the three-dimensional (3D) time-varying arrays based on UAV swarm.

Then statistical performance of iterative-MUSIC for the MUSB array is investigated by AMSE formulas and system limitation is examined by the derived CRB. This work also examines the applications of AMSE formula, such as studying the asymptotic efficiency and analyzing the asymptotic performance statistically. The CRB associated with DOAs in the presence of sensor gain and phase errors is also derived to reveal some direction-finding properties such as the global convergence, the impact of snapshots and the number of the arrays. Performance analysis with one-emitter case is also given to describe the CRB. A successive DOA refinement procedure with iterative-

MUSIC algorithm is provided based on the reconstructed arrays and spectrum from swarming UAVs to meet the requirement of high-precision DOA estimation.

Finally, the system performance analysis in the presence of small sensor gain, phase, and position errors is given. We firstly introduce the signal model with deterministic unknown location errors, and then extend the model to the cases when the location error is stochastic (Gaussian case). We also derived the joint CRB of DOAs, sensor gain, sensor phase, and sensor location errors for MUSB arrays, which can be applicable even if the number of sources exceeds the number of initial UAVs. Both numerical simulations and practical experiments will be given to verify the theoretical results.

ACKNOWLEDGEMENTS

I would like to thank my committee chair, Dr. Huff for his guidance, advice and full support throughout this dissertation work, which has been crucial to the success of the work. I am very grateful to have the opportunity working with him. I would also like to express my gratitude to my committee members, Dr. Chamberland, Dr. Novels, and Dr. Valasek for their unlimited time, advising and support throughout this research.

I also would like to express my thanks to my colleagues in the Electromagnetic and Microwave Laboratory (EML) for their many forms of help and friendship.

Finally, I would like to express my thanks to my dear father Yongji Chen, my mother Aizhen Tang, and my fiancée Zhenyue Tian for their understanding, supporting and encouragement in my research life.

CONTRIBUTORS AND FUNDING SOURCES

Contributors

This work was supervised by a dissertation committee consisting of Professors Huff, Chamberland, and Nevels of the Department of Electrical and Computer Engineering and Professor Valasek of the Department of Aerospace Engineering.

All work conducted for the dissertation was completed by the student, under the advisement of Dr. Huff and Dr. Chamberland of the Department of Electrical and Computer Engineering.

Funding Sources

Graduate study was supported by a one-year in-state tuition and 1000 dollars' scholarship from the Department of Electrical and Computer Engineering and three and half years' Graduate Teaching Assistant from the Department of Engineering Technology and Industrial Distribution at Texas A&M University.

There are no outside funding contributions to acknowledge related to the research and compilation of this document.

NOMENCLATURE

1D	1-dimension
2D	2-dimension
3D	3-dimension
AMSE	Asymptotic Mean Square Error
CRB	Cramer-Rao Bound
DOA	Direction of Arrival
GPS	Global Positioning System
LED	Light Emitting Diode
ML	Maximum Likelihood
MUSB	Micro-UAV Swarm-Based
MUSIC	Multiple Signal Classification
NLA	Nonuniform Linear Array
PCB	Printed Circuit Board
RF	Radio Frequency
RGB	Red, Green, Blue
RMSE	Root Mean Square Error
SNR	Signal to Noise Ratio
UAV	Unmanned Aerial Vehicle
UCA	Uniform Circular Array
ULA	Uniform Linear Array

URA	Uniform Rectangular Array
VNA	Vector Network Analyzer
VSWR	Voltage Standing Wave Ratio

TABLE OF CONTENTS

Page

LIST OF FIGURES

Page

LIST OF TABLES

Page

1. INTRODUCTION

1.1. Research Background

Array signal processing plays a very important role in the field of modern signal processing area and it has been used in a very wide range of applications, including radar, sonar, communications, navigation, oceanography, texture surveying, biomedical, radio astronomy, etc. Therefore, the research on array signal processing related technology has important theoretical signification and significant practical value.

One of the important research areas of array signal processing is the DOA estimation, which leverages the spatial information received from receiving sensor arrays to estimate the sources' directions. As we know, global positioning system (GPS) is widely used in modern digital system to help us locate the position due to the development of mobile technology, but it cannot be used reliably inside many buildings because the signal will be attenuated seriously. DOA estimation is one of the non-GPS positioning technologies.

Statistically analyzing the performance by deriving the AMSE and CRB formula is also a very important area of signal processing, which is a very good tool to evaluate the performance of array system and algorithm.

1.2. Two Important Research Topics in DOA Estimation

At present, the research on DOA estimation area mainly includes two aspects: one is to investigate the antenna structure; the other is to examine the DOA algorithms.

For the research on antenna array structure, there are a lot of different dimensional antenna arrays that have been proposed, such as one-dimensional (1D), two-dimensional (2D), and 3D antenna arrays. There are some known arrays among them, such as uniform linear array (ULA), nonuniform linear array (NLA), uniform circular array (UCA), uniform rectangular array (URA), cubic array, and spherical array, etc. 1D antenna array is usually applied in 1D DOA estimation (only azimuth angle estimation), 2D and 3D antenna arrays can be applied in 2D DOA estimations (azimuth and elevation estimations).

3D array system has some advantages in DOA estimation compared with 1D and 2D arrays. Due to the symmetry of array structure, planar arrays like ULA and UCA cause the aliasing problem in DOA estimation when the internal spacing of array is equal and greater than half wavelength [2]. However, 3D arrays can overcome the aliasing problems when internal spacing of arrays is half wavelength. But when the internal spacing is increased to ten wavelengths, some 3D arrays also have aliasing problems. Furthermore, when the planar array (2D array) is used for DOA estimation, the elevation estimation accuracy is relatively low because of the limited elevation directional aperture of the planar array. However, 3D antenna array has both high azimuth and elevation estimation accuracy because it has large apertures in both azimuth and elevation directions [3-4]. Moreover, random array structure can also overcome the symmetry of array structure and thus it can overcome the aliasing problem in DOA estimation.

DOA estimation algorithms have been researched for decades and it is still a popular topic in signal processing area. Most of the algorithms are only suitable for 1D DOA estimation with 1D uniform linear array (ULA). Even though many algorithms have

been proposed to perform DOA estimations, MUSIC algorithm remains quite prevalent since it offers a very robust eigen-based decomposition of the signal space [1-2]. MUSIC algorithm is a super-resolution algorithm and can be applied for 1D and 2D DOA estimation with any type of antenna array. However, MUSIC algorithm requires high snapshots and high signal-noise-ratio (SNR) to guarantee the estimation accuracy. Furthermore, MUSIC algorithm has a weakness of heavy computation because it needs to search 2D angle space step by step. Therefore, some search-free algorithms like root-MUSIC algorithm and Fourier-domain root-MUSIC algorithm are developed to reduce calculation [5-7]. Many of other algorithms based on MUSIC algorithm are also developed. But root-MUSIC and Fourier-domain and root-MUSIC algorithm are only used for 1-D DOA estimation.

1.3. Summarized Contributions Made by This Dissertation

The first contribution of this dissertation is to formulate the mathematic model of DOA estimation with MUSB array system. The MUSB arrays reconstructed from swarming UAVs are volumetric random time-varying arrays, so that they have all the advantages of 3D random antenna arrays presented in section 2 for DOA estimation.

The second contribution of this dissertation is that we present an iterative-MUSIC algorithm which can be used to estimate the DOAs with MUSB arrays under the environment with very low SNR and low number of snapshots. Traditional MUSIC algorithm needs high snapshots to reduce the noise floor and improve the DOA estimation accuracy, so the traditional MUSIC algorithm cannot work in the MUSB array system.

But the iterative-MUSIC algorithm can be used in low snapshot or even one snapshot system by multiplying or summing the MUSIC spectrum at each iteration to improve the DOA estimation accuracy. We compare the performance of iterative-MUSIC algorithm and CRB. Furthermore, we performed practical 3D random time-varying antenna array experiment in the anechoic chamber room using "Medusa", which is a platform with 16 moveable and rotatable antennas. I will explain this platform in Chapter 3.

The third contribution of this dissertation is to derive the AMSE formulas for iterative-MUSIC algorithm and apply the formula to evaluate the performance of iterative-MUSIC. We proof that the iterative-MUSIC algorithm is capable for time-varying arrays in low snapshot and low SNR conditions, and this algorithm has the advantage to eliminate the impact of sensor gain, phase, and position errors. The convergence efficiency of the iterative-MUSIC is better than the traditional MUSIC algorithm at the extreme condition, such as 3-element array for 2D DOA estimation, very low SNR, and very low number of snapshots.

The fourth contribution is to derive the CRB for MUSB system. Since we use swarming UAVs to construct the 3D random time-varying arrays and apply it into multiple source direction estimations, the snapshot in each sample position will be low and receiving array structure will be changed at each sample position. We prove that the total Fisher information matrix (FIM) can be summed based on each sample when the UAVs swarm.

The fifth contribution of this dissertation is that we investigate the DOA estimation performance with MUSB arrays in the presence of sensor gain, phase, and position errors.

In practice, the swarming UAVs always have sensor gain, phase, and position errors. We derived the joint CRB with DOAs, sensor gain, phase, and location errors, and then we compare the DOA estimation performance using iterative-MUSIC algorithm with CRB in the presence of sensor gain, phase, and position errors. We also investigated the impact of sensor location errors for different error levels under different types of arrays.

1.4. Dissertation Organization

This dissertation firstly introduces the research background and significance of DOA estimation in array signal processing and the advantages of 3D random arrays applied in robust DOA estimation under high noise and low snapshot environment. MUSIC and modified MUSIC algorithms are still very popular in the modern DOA estimation. Chapter 2 describes the MUSB array system by constructing the mathematic model of the system. Chapter 3 introduces the iterative-MUSIC algorithm and applies it for MUSB system to analyze the DOA estimation performance by investigating the synthetic DOA estimation convergence. Chapter 4 derives the AMSE of iterative-MUSIC and the CRB for MUSB system and use one source case to analyze the DOA estimation performance. Chapter 5 analyzes the performance of DOA estimation with MUSB arrays in the presence of sensor gain, phase, and position errors. Chapter 6 concludes this dissertation.

Glossary of notation is listed below:

$C^{k\times p}$ = the space of $k\times p$ complex-valued matrices;

E = expectation operator;

A_{ij} = the *i, j* element of a general matrix $A \in C^{k \times p}$;

A^T = the transpose of $A \in C^{k \times p}$;

A^H = the conjugate transpose of $A \in C^{k \times p}$;

Re (A) = the real part of $A \in C^{k \times p}$;

Im (A) = the image part of $A \in C^{k \times p}$;

tr (A) = the trace of $A \in C^{k \times k}$;

det (A) = the determinant of $A \in C^{k \times k}$;

$A \odot B$ = the Schur-Hadamard matrix product of $A, B \in C^{k \times p}$, defined by $[A \odot B]_{ij} = A_{ij} B_{ij}$

$A \otimes B$ = the Kronecker matrix product of $A, B \in C^{k \times p}$, defined by

$$A \otimes B = \begin{bmatrix} a_{11}B & \cdots & a_{1_j}B \\ \vdots & \ddots & \vdots \\ a_{i1}B & \cdots & a_{ij}B \end{bmatrix}$$

$z \sim cN(\mu(\alpha), \zeta(\alpha))$ = the complex Gaussian distribution of the complex random vector z with mean μ and variance ζ, and α is a real-valued parameter vector that completely and uniquely specifies the distribution of z (see [8]).

2. SIGNAL MODEL FORMULATION FOR APERIODIC MUSB ANTENNA ARRAYS*

2.1. Introduction

The presented antenna arrays reconstructed from swarming UAVs are time-varying 3D random arrays, which have the advantages of 3D arrays, random arrays, and time-varying arrays. There is one antenna in each UAV and one moving UAV is represented as a moving antenna in this dissertation. The gain and phase of the receiving antennas will also vary, and they are not uniform as the UAVs move. Therefore, the MUSB array signal model should include gain and phase errors of the receiving antennas.

The MUSB array is not a static array, so that it will sample at different locations and the snapshots cannot be high at the sample position due to the high moving speed of the UAV. Array structure always changes randomly and there are a lot of data information obtained from the array reconstructing process. Therefore, the total data will be summed from each iteration at each sample point to reduce the noise.

We assume the source is static in this dissertation, the source wavelength is comparable with the UAV speed, and we will use the moving distance at each time interval to represent the speed of the UAV.

---

*This chapter is partially based on Z. Chen, S. Yeh, JF Chamberland, and G. H. Huff, "A sensor-driven analysis of distributed direction-finding systems based on UAV swarms," *MDPI Sensors*, vol. 19 (12), pp. 2659-2677. Copyright [2019] by MDPI Sensors

2.2. MUSB Array

2.2.1. UAV Parameters

Assume there are M swarming UAVs and each UAV swarms in a cylinder region ($r = 10\lambda$, $h = 2$r, λ is wavelength and $\lambda = 1$m). Each UAV has an initial location (x, y, z) in the swarming region with a vector velocity in each iteration and the initial locations of the M UAVs are considered as the first iteration. The swarming short distance in each iteration is represented as a vector $\vec{d}_{i,m}$. The scalar quantity can be represented as d, which uses the following relation:

$$d = \beta_t \cdot \lambda / \rho \tag{1}$$

where $\beta_t \in R^{M\times 3}$ is a uniformly distributed random number matrix between zero and one, λ is wavelength and ρ is the coefficient determining the distribution mean of swarm distance. Figure 1 shows the distribution of the short distance with mean $\mu = 0.25$ wavelength. Here the range of d also depends on the speed of the UAV and data sampling interval and can be configured by the customer. We can obtain

$$\vec{d}_{i,m} = \vec{V}_{i,m} \cdot t \tag{2}$$

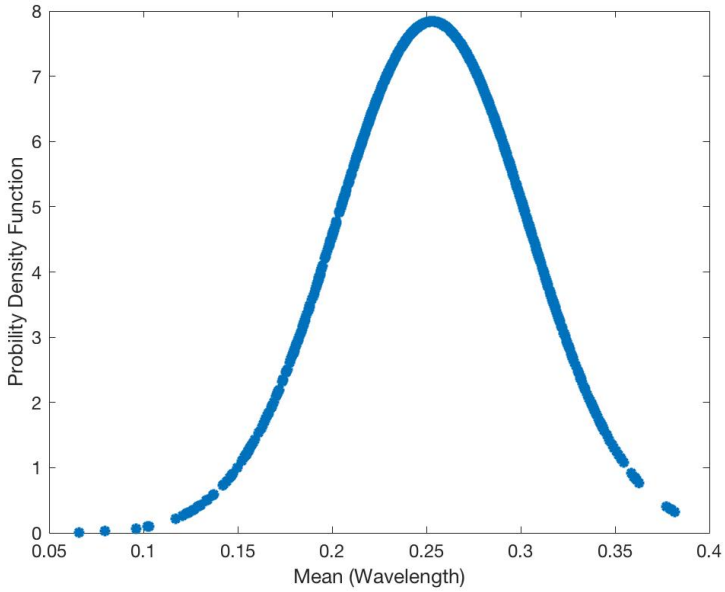

Figure 1. Distribution of distance that one UAV swarms

2.2.2. Swarming UAV Synthetic Aperture

A swarming UAV synthetic aperture was presented in our early published paper [9]. Figure 2 shows a graphical representation of a UAV swarm as it morphs in time (iteration I in this paper). Each of the M agents in the swarm has a location, orientation, and trajectory. Notionally, these have position $P_{m,i}\left(r,\theta,\phi\right)$, where m is the agent's index and i is the index of iteration. During swarming, the agents undergo rotations and translations, where a dual quaternion framework provides a convenient mechanism to handle this behavior. This motion rotates the agents' local (u,v,w) coordinate systems that describes the spatial orientation of their antenna radiation pattern with respect to the global coordinate system and incoming signal if interest $S\left(\theta_n,\phi_n\right)$, which is the nth source. The collection of these measurements over iteration creates a synthetic aperture that can be

used to calculate the parameters of interest (θ_n, ϕ_n). Notionally, K independent data is sampled for each agent in each iteration and K is usually called "snapshot". Since the UAV moves very fast, so K is relatively small compared to the static array in the most of practical applications.

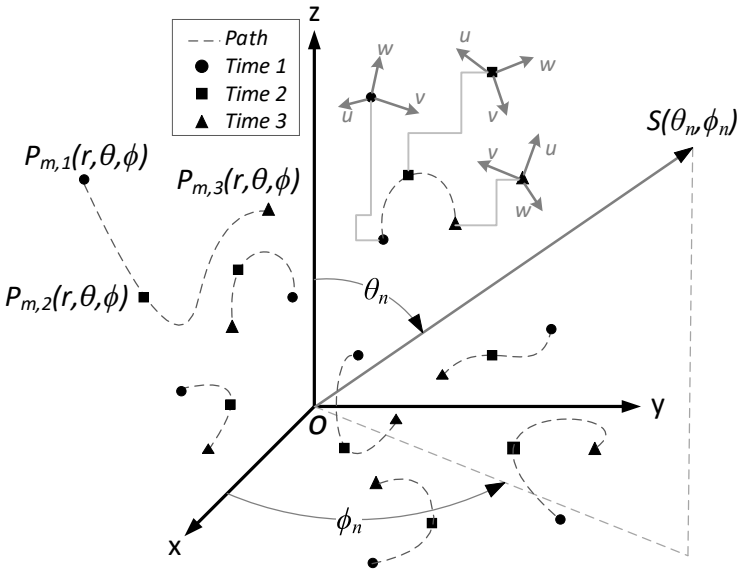

Figure 2. Morphing MUSB antenna array configuration

2.3. Signal Model

Friedlander et al. presented a mutual coupling model in the presence of sensor mutual coupling, gain, and phase uncertainties [10]. We ignore the mutual coupling effect in the signal model since the spacing of aperiodic array reconstructed from swarming UAVs is much larger than half wavelength. Furthermore, the MUSB array does not have mutual coupling and shading effects so long as the number of UAVs is small.

Consider an arbitrary array of M elements receive N uncorrelated incident signals in the far-field demonstrated in part 1. Thus, the received signal at the m-th sensor from the n-th source of the i-th iteration can be represented as

$$x_m^i(t) = \sum_{n=1}^{N} a_m^i s_n(t - \tau_{mn}^i - \psi_m^i) + w_m^i(t), \\ -T/2 \le t \le T/2;\ i = 1,2,\cdots,I;\ m = 1,2,\cdots,M \tag{3}$$

where $\{s_n^i(t)\}_{n=1}^N$ are the incident signals of the ith iteration, $\{w_m^i(t)\}_{m=1}^M$ are the additive noise along with the signals, and T is the observation period. $\{\tau_{mn}^i\}$ are delays from the nth source to the mth sensor of the ith iteration with respect to the signal propagation time. These parameters are the known functions of the incident angles and sensor array locations. In the end, a_m^i and ψ_m^i are the gain and the delay relative to the mth sensor of the ith iteration.

It is convenient for one to use Fourier coefficients to separate the parameters. It can be defined by

$$X_m^i(\omega_l) = \frac{1}{\sqrt{T}} \int_{-T/2}^{T/2} x_m^i(t) e^{-j\omega_l t} dt \tag{4}$$

where $\omega_l = 2\pi(l_1 + l)/T$, $l = 1, 2, \cdots, L$, and l_1 is a constant. The number of coefficients should be infinite to get all the signal information in theory. But the signals we are interested in here are narrow-band signals. Assume the spectrum is concentrated around ω_0, and the bandwidth is small relative to $2\pi/T$. Thus, L=1. Recall the Fourier coefficients of (4) on ω_0, we obtain

$$X_m^i = \sum_{n=1}^{N} a_m^i e^{-j\omega_0 \psi_m^i} \cdot e^{-j\omega_0 \tau_{mn}^i} S_n^i + W \qquad m = 1,2,\cdots,M,\ i = 1,2,\cdots,I \tag{5}$$

where S_n^i and W_m^i are the Fourier coefficients of $s_n^i(t)$ and $w_m^j(t)$, respectively. The gain a_m^i and phase ψ_m^i change with respect to element location based on orientation of UAV; τ_{mn}^i changes with respect to location; S_n^i is constant; W_m^i may change with respect to location, velocity of UAV, and environment. Equation (5) can be represented by

$$X_i(k) = \Gamma_i \cdot \tilde{\mathrm{A}}_i \cdot S_i(k) + W_i(k) \qquad k = 1,2,\cdots,K;\ i = 1,2,\cdots,I \tag{6}$$

where *k* is the snapshot (index of samples) of each iteration and

$$X_i(k) = [X_{1,1}(k),\cdots,X_{1,M}(k),\cdots,X_{i,1}(k),\cdots,X_{i,M}(k)]^T$$

$$S_i(k) = [S_{1,1}(k),\cdots,S_{1,N}(k),\cdots,S_{i,1}(k),\cdots,S_{i,N}(k)]^T$$

$$W_i(k) = [W_{1,1}(k),\cdots,W_{1,M}(k),\cdots,W_{i,1}(k),\cdots,W_{i,M}(k)]^T$$

$$\Gamma_i = diag\{g_{1,1}e^{-j\omega_0\psi_{1,1}},\cdots,g_{1,M}e^{-j\omega_0\psi_{1,M}},\cdots,g_{i,1}e^{-j\omega_0\psi_{i,1}},\cdots,g_{i,M}e^{-j\omega_0\psi_{i,M}}\}$$

$$\tilde{A}_{i,mn} = e^{-j\omega_0\tau_{i,mn}};\ m = 1,2,\cdots,M;n = 1,2,\cdots,N;i = 1,2,\cdots,I.$$

Then,

$$X(k) = \sum_{i=1}^{I} X_i(k) = \sum_{i=1}^{I}\left[\Gamma_i \cdot \tilde{\mathrm{A}}_i \cdot S_i(k) + W_i(k)\right] \tag{7}$$

where $S(k) = \sum_{i=1}^{I} S_i(k)$, $W(k) = \sum_{i=1}^{I} W_i(k)$, $\Gamma = \sum_{i=1}^{I} \Gamma_i$, and $\tilde{A} = \sum_{i=1}^{I} \tilde{A}_i$. Since the sources we consider here are in the far field from the observing array. It is easy to find that can be represented by

$$\tau_{i,mn} = -d_{i,mn} / c \tag{8}$$

$$d_{i,mn} = x_{i,m}\sin\theta_n\cos\phi_n + y_{i,m}\sin\theta_n\sin\phi_n + z_{i,m}\cos\theta_n \tag{9}$$

where $d_{i,mn}$ is the distance from origin (reference sensor) of the coordinate to the *m*th sensor in the direction of the *n*th source for the *i*th iteration, *c* is the propagating velocity in free space $(x_{i,m}, y_{i,m}, z_{i,m})$, are the coordinates of the *m*th sensor for the *i*th iteration, (θ_n, ϕ_n) are the DOAs of the *n*th source in the sphere coordinate. Figure 3 shows the geometry of one UAV swarming 8 times in the Cartesian coordinate system. From equations (8) and (9), the matrix $\tilde{A}$ can be obtained by

$$\tilde{A}_{i,mn} = e^{j(\omega_0/c)(x_{i,m}\sin\theta_n\cos\phi_n + y_{i,m}\sin\theta_n\sin\phi_n + z_{i,m}\cos\theta_n)} = e^{j(2\pi/\lambda)(x_{i,m}\sin\theta_n\cos\phi_n + y_{i,m}\sin\theta_n\sin\phi_n + z_{i,m}\cos\theta_n)} \tag{10}$$

where λ is the wavelength.

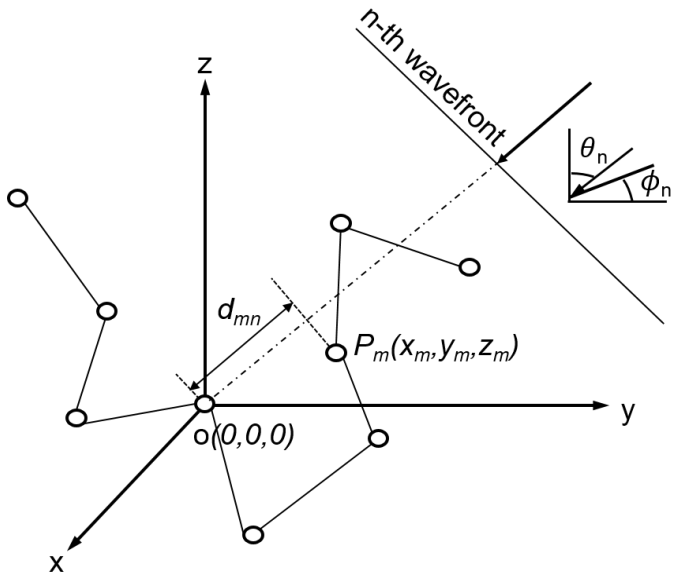

Figure 3. Geometry of MUSB antenna array

3. DOA ESTIMATION WITH APERIODIC MUSB ANTENNA ARRAYS*

3.1. Introduction

As proposed in Chapter 1, 1D array only can detect 1D DOA and 2D array can well estimate azimuth angles but cannot well estimate elevation angles due to its small antenna aperture in the elevation direction. In order to improve elevation angle estimation accuracy, one may put more elements, or to develop 3D array structure by putting more elements in the elevation direction to make large elevation aperture in elevation direction [3-4]. However, they require very big hardware and computational cost.

Furthermore, the linear and planar array will cause ambiguity problem (angle aliasing) due to the symmetry array structures [2,11,12]. Xia et al. proposed that the cubic arrays still have ambiguity problem and the spherical array can significantly reduce the angle ambiguity problem [2]. Recently, the 3D antenna array configurations have attracted much more research interest in array signal processing [13]-[18]. Most of those 3-D arrays above are constructed from regular structure (i.e. cubic, cylinder), extending the planar array (i.e. URA, UCA) or configuring virtual 3-D array based on the planar array. Even though those special 3-D arrays increase the elevation angle estimation accuracy, their array apertures are still small since the physical size of static arrays are restricted.

---

*This chapter is based on "A sensor-driven analysis of distributed direction-finding systems based on UAV swarms," by Zhong Chen, S. Yeh, Jean-Francois Chamberland, and Gregory H. Huff, 2019. *MDPI Sensors*, vol. 19 (12), pp. 2659-2677, Copyright [2019] by MDPI Sensors; Z. Chen, JF Chamberland, and G. H. Huff, "Impact of UAV swarm density and heterogeneity on synthetic aperture DOA convergence," *IEEE APS-URSI Conf.* Copyright [2017] by IEEE.

The conventional investigations in DOA require the number of the sensors be more than the number of the receiving signals, which increase the hardware cost and system complexity. In contrast, time-variant arrays whose element positions change over time have been examined to tradeoff between processing time and hardware cost by time-divided sampling rather than simultaneously sampling as a static array. Many researchers have reported that using moving arrays to improve the system performance of DOA estimation [19]-[25]. Instead of using a set of different elements to process the incident signals, time-variant array can only use one or small number of elements to reconstruct the virtual antenna arrays by sweeping 1-D or 2-D regular arrays. Wan et al. proposed a method of combining the characteristics of arbitrary virtual baseline to construct virtual 3-D array [19]. However, the number of sub-array elements is too less and do not have high resolution. Liu examined a rotating long baseline interferometer whose length is much larger than one wavelength to estimate 2-D DOA by constructing the virtual 2-D circular array [20]. However, the 2-D circular array has limited elevation aperture and still cannot well estimate the elevation angle.

We herein propose to utilize the swarming UAVs to create the unstructured morphing antenna arrays that reduce ambiguity and improve convergence in sub-space DOA techniques. The reconstructed volumetric aperiodic array has high aperture in both azimuth and elevation directions, which increase the accuracy of both the azimuth and elevation angle estimation. Corner et al. proposed a parallel simulation of UAV swarm scenarios [26], and Saad et al. reported a testbed of vehicle swarm rapid prototyping [27]. Recently, many researchers investigated the methods and impact factors of designing the

robust micro-UAV-based antenna arrays for signal collection platforms [28]-[31]. However, those works are limited in the micro-UAV-based array constructing investigations including UAV positional precision, turbulence of the environment, and swarm-based real-time data collection. In this dissertation, 2D DOA estimation using UAV-swarm-based aperiodic array is firstly provided, a mathematical model of micro-UAV swarm-based data collection system for signal processing is provided firstly and the impact of the associated parameters on DOA accuracy and convergence in this model are analyzed. The MUSB arrays have the advantages of large aperture, no shading effect, significantly reduced mutual coupling effect and big spatial sampling data from different location in the space.

In the real-world application, the swarming UAV system for DOA estimation requires low snapshots and might be applied in low SNR scenarios, however the subspace-based techniques require adequate SNR and snapshots to guarantee good performance. We utilize the iterative method to lower the noise floor by multiply the MUSIC spectrum for each iteration, the details of the algorithm will be presented in section 4.

3.2. The Algorithm

3.2.1. Data Processing and Algorithm

When the UAV swarms, there will be a lot of data information due to the number of swarming UAVs and the number of iterations. Herein each location of each UAV is considered as one data point. Thus, when M UAVs morph I times, we have $M * I$ data points. Then we use those data points to reconstruct the virtually 3D aperiodic array to

calculate the MUSIC spectrum and estimate the DOAs. The number of data points (represented by N_d) we use to estimate the DOAs is equivalent to the number of elements for a static array.

One problem is how many data points should be used to compute the MUSIC spectrum at each signal processing iteration (Represented by *p-iteration*). Ten, hundred, or even more data points can be used to calculate the MUSIC spectrum at each p-iteration. We would like to use larger data in each p-iteration since more data points for MUSIC spectrum calculation each time means more array elements are used for data processing in a static antenna array, and more accurate for DOA estimation. However, more data processing points cause higher calculation cost. Thus, it is necessary to compromise the number of data points at each MUSIC spectrum calculation and computational complexity.

Another problem is the data collecting and processing methods. When the UAVs swarm, the data collected in the current processing period is called current data, and the date sampled and stored in the past is called previous data. There are several ways to process the data:

1) Only use the current data to compute the MUSIC spectrum.
2) Use the current and all previous data to compute the MUSIC spectrum.
3) Use the current and some previous data to compute the MUSIC spectrum

Type 1 requires high number of initial UAVs, type 2 requires heavy computation, so we choose type 3 to analyze the problems we are interested in. We will talk about the impact of different number of data sets at each p-iteration in section 6. Herein we take 3

data points for each group to examine the impact of other parameters but show the procedure of data processing using 6 data points in Figure 4.

Figure 4 shows the data processing schematic for 6 data points each set in the MUSB system. When UAV swarms to a certain location, we will sample 5 times (5 snapshots) and each snapshot takes the time d_t. After taking 5 snapshots, the program sets up a data point. After the number of data points $N_d = 6$ (i.e. number of elements of the new reconstructed aperiodic array is 6), the program computes the traditional MUSIC spectrum using the 6 data points and stores the result. Then UAV swarms again, we accumulate current data and 5 previous data points to calculate the MUSIC spectrum. Then we multiply the current MUSIC spectrum and previous MUSIC spectrum at each p-iteration where we obtain the iterative-MUSIC spectrum to reduce the noise level and improve the DOA performance. Note that if the p-iteration is too big, the value of the spectral points will be very small and might be taken as zero. If so, the correct DOA cannot be obtained. We may use dB instead of a number at that situation.

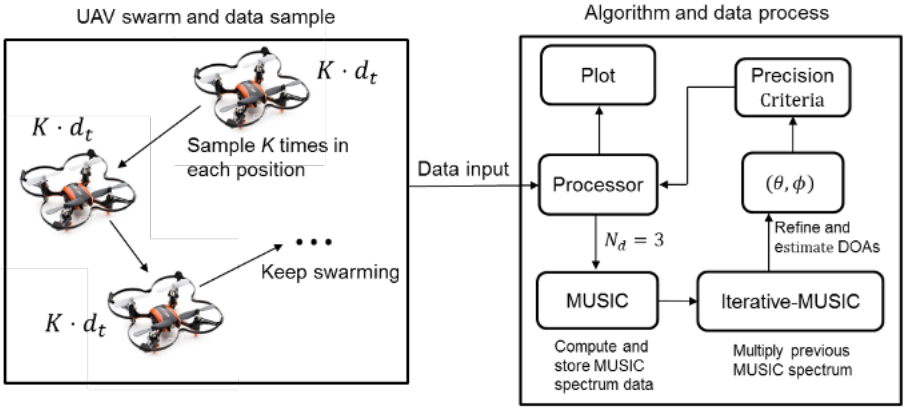

Figure 4. Data processing schematic for MUSB system

Consider the two problems above, the steps of the algorithm are:

Step 1: UAV swarms until the number of data points $N_d = 3$, then compute the MUSIC spectrum;

Step 2: UAV swarms again, and use current and some previous data points to calculate the MUSIC spectrum at each p-iteration;

Step 3: Multiply the current MUSIC spectrum and previous spectrum;

Step 4: Repeat step 2-3 until the MUSB system converges.

The algorithm flow chart is shown in Figure 5.

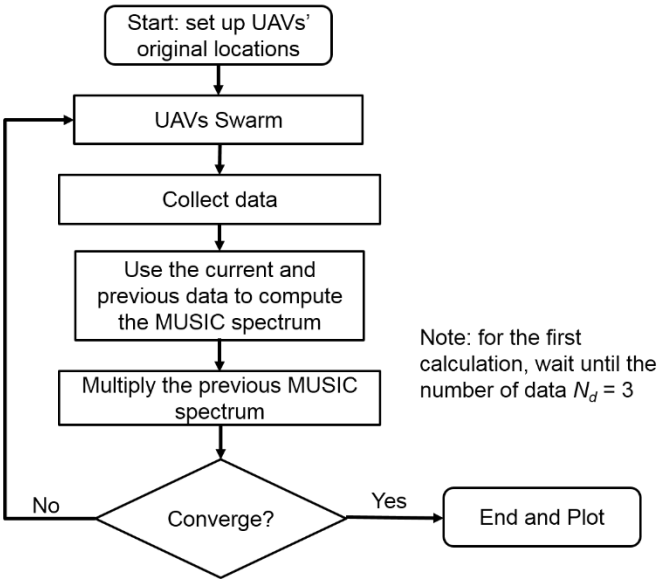

Figure 5. Flow chart of the algorithm

3.2.2. Iterative-MUSIC Algorithm

As already stated in part 2 of this section, the number of the reconstructed MUSB arrays is N_d. Here we rewrite the covariance of the signals listed in part 2 of Section 3 and give the first p-iteration (slightly different from the UAV swarming iteration) of the iterative-MUSIC algorithm.

Rewrite the data model (6), we obtain

$$X(k) = \Gamma \cdot \tilde{\mathrm{A}} \cdot S(k) + W(k) = A \cdot S(k) + W(k) \qquad k = 1, 2, \cdots, K \tag{11}$$

where $\left\{ X(k) \in C^{N_d \times 1} \right\}$ are the vectors of sampled data, $\left\{ S(k) \in C^{N \times 1} \right\}$ are the source signals, $\left\{ \Gamma \in C^{N_d \times N_d} \right\}$ are the gain and phase of the sensors and $\left\{ \tilde{A} \in C^{N_d \times N} \right\}$ are the regular steering vectors. Thus, the covariance of $X(k)$ is

$$R = E\left[X(k) X^H(k) \right] = \Gamma \tilde{A} P \tilde{A}^H \Gamma^H + \sigma^2 I_0 = A P A^H + \sigma^2 I_0 \tag{12}$$

Define

$$R_s = A P A^H \tag{13}$$

R_s is the $N_d \times N_d$ matrix with rank N. Therefore, it has the $N_d - N$ repeated eigenvectors corresponding to the minimum eigenvalues σ^2. Let e_i be such an eigenvector so that $R_s e_i = 0$ or $A^H e_i = 0$, thus, the $N_d - N$ eigenvectors e_i corresponding to the minimal eigenvalues are orthogonal to each of the N signal columns of $A = \Gamma \tilde{A}$, proved in [1]. $N_d - N$ dimensional subspace spanned by the noise eigenvectors is defined as noise subspace and N dimensional subspace spanned by the incident signal mode vectors is defined as signal subspace.

Let Q_n be the $N_d \times (N_d - N)$ matrix of the noise eigenvectors, then the MUSIC spatial spectrum function is given by

$$P_{MU}(\theta,\phi) = \frac{1}{\tilde{a}(\theta,\phi)^H \Gamma^H Q_n Q_n{}^H \Gamma \tilde{a}(\theta,\phi)} = \frac{1}{\left\| Q_n{}^H \Gamma \tilde{a}(\theta,\phi) \right\|^2} = \frac{1}{\left\| Q_n{}^H a(\theta,\phi) \right\|^2} \tag{14}$$

Then, search the spectrum peaks in the range of θ and ϕ, and the peak spectrum points we obtain are the estimation of the arrival angles of the incident waves.

3.3. Convergence Check

The algorithm performs the calculation until the system converges. The convergence can be guaranteed since the estimated DOA is a convergent series.

When the signal is covered by a high noise level, the estimated DOA might be far from the ground truth and cannot be judged for the convergence. But as the iteration increases, the noise level is reduced and the estimated DOA is converged gradually. Avoiding the misjudgment, the equation for judging the convergence is given by

$$DOA_{i+1} - DOA_i \le \varepsilon, \qquad i = 1, 2, \cdots I_m \tag{15}$$

where I_m is the number of *p-iteration* and ε is the preset threshold.

3.4. Simulation and Results

In this section, several groups of simulations will be carried out to demonstrate the performance of the presented distributed directional finding system in this paper. As the framework of the system established in this paper is mentioned for the first time, we focus

mainly on analyzing the impact of various factors on the feasibility of the MUSB distributed directional finding system.

The wavelength of the signal is fixed at 1 meter (m) and the simulation in each scenario is repeated for 500 times. The elevation angle of the source emitter is 85° and the azimuth angle is 270°. As one UAV swarms till the number of data points is N_d, the iterative-MUSIC algorithm begins to sample the [0° 179°] space for elevation angle and [0° 359°] space for azimuth angle with 1° interval to form the overcomplete MUSIC spectrum for each p-iteration. The UAV keeps swarming and the iterative-MUSIC algorithm keeps computing the MUSIC spectrum before the precision of DOA estimation is satisfied. When the preset threshold is satisfied, the UAV stops flying, and the reconstructed process of the phased arrays based on swarming UAVs is terminated. The refined DOA estimations are obtained by scanning the reconstructed signal peaks from the iterative-MUSIC algorithm with 0.1° step during the refinement procedure for 10 times.

Moreover, the speed of the UAV will influence the snapshot at each location where the system samples the source emitter. The snapshot at each location should be very low if the UAV swarms very fast and the snapshot can be high when the swarming rate of the UAV is pretty low. The speed of UAV in this paper will be represented by the distance between two iterations of the swarming UAVs. Assume we take three data points (one UAV swarms two times) to compute the MUSIC spectrum, the distribution of the sum of two short distances between two iterations will be given in part 2.

Firstly, the system convergence is studied in a typical scenario. Secondly, the DOA estimation performance using iterative-MUSIC algorithm will be compared with CRB in various scenarios.

The average root-mean-square error (RMSE) of the incident signals is used for statistical DOA estimation precision evaluation, which is defined as

$$RMSE_{\theta,\phi} = \sqrt{\sum_{w=1}^{W}\sum_{n=1}^{N}\left[\left(\hat{\theta}_n^w - \theta_n^w\right)^2 + \left(\hat{\phi}_n^w - \phi_n^w\right)^2\right] \Big/ 2WN} \tag{16}$$

where W is the number of Monte Carlo simulations, $\left(\theta_n^w, \phi_n^w\right)$ represent the true DOAs of the nth signal, $\left(\hat{\theta}_n^w, \hat{\phi}_n^w\right)$ and represent the estimated DOAs of the nth signal in the wth simulation.

3.4.1. System Convergence

In order to prove the system convergence presented in part 4 of section 5, assume one UAV swarms and the number of data points is 3, snapshot is 1, and SNR is 0 dB for 500 trails. Figure 6 shows the MUSB distributed directional finding system gradually converges to the ground truth.

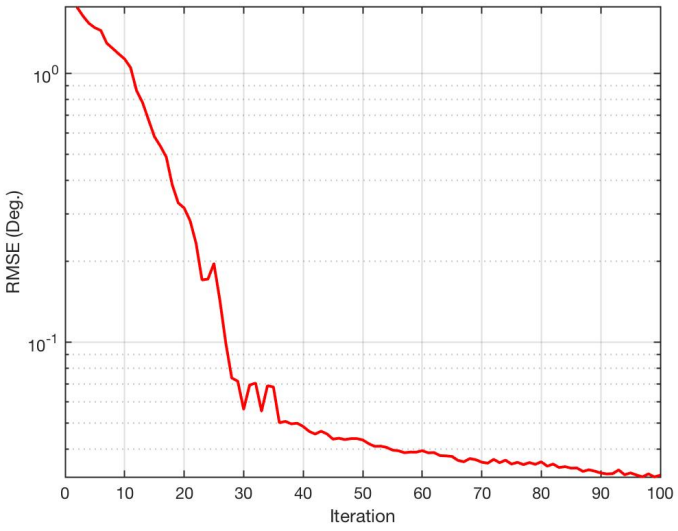

Figure 6. DOA estimation convergence for the MUSB system

3.4.2. DOA Estimation with Iterative-MUSIC via MUSB Arrays

In simulations, we set a DOA with an azimuth of 300° and elevation of 60°, SNR to be -15 dB. Then we compare the spectrum with spectrum for one and twenty iterations to check iterative-MUSIC spectrum intuitively. Figure 7 shows the simulated spectrum intuitively and the iterative-MUSIC can well estimate the DOAs under a low SNR and low snapshot condition.

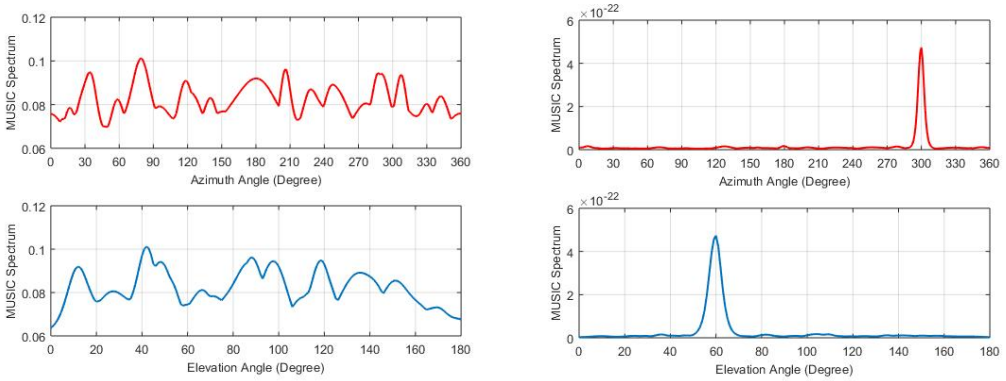

(a) (b)

Figure 7. Simulated MUSIC spectrum: an incident signal with a SNR = -15 dB, and a direction of arrival with an azimuth of 300° and elevation of 60°. (a) number of iteration t = 1, (b) number of iteration t = 20.

3.5. Experiment

3.5.1. Experiment Platform

Figure 8 shows a 16-channel movable and rotatable antenna system named after Medusa. We use this system to simulate the MUSB array system. The position of each element can be automatically obtained from spatial recognition system. A block diagram of MUSB system is shown in Figure 9.

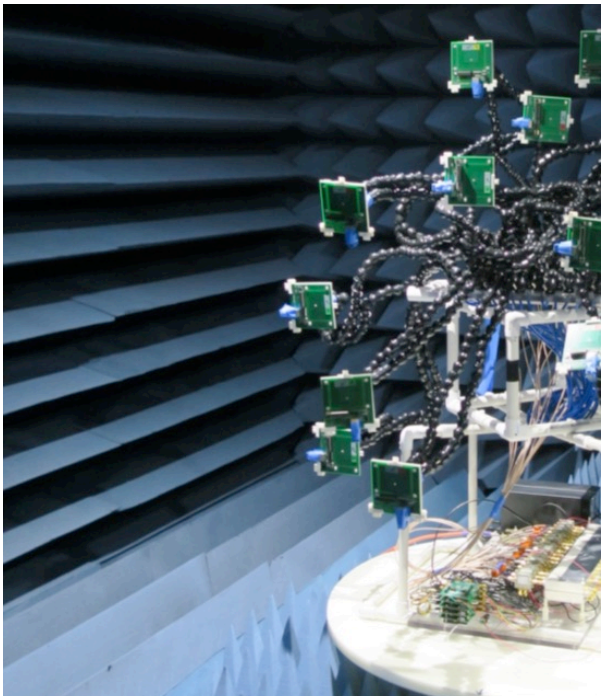

Figure 8. MUSB array experiment system - Medusa

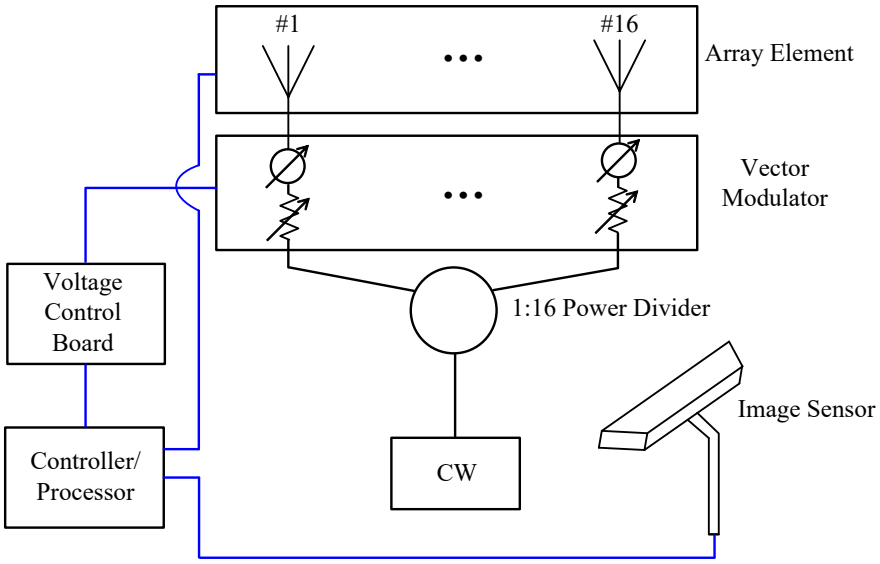

Figure 9. Diagram of the Medusa system (Reprinted from [57])

3.5.1.1. Antenna

Figure 10 shows the microstrip patch antenna with LED, microcontroller, voltage regulation, etc. Figure 11 shows the measured VSWR of the patch antenna and Figure 12 shows the measured radiation pattern. The 9DOF IMU on the patch antenna board is programmable to monitor and log motion, transmit Euler angles over a serial port or even act as a step-counting pedometer. Four RGB (red, green, and blue) LEDs are placed around the patch antenna and they are used to locate the antenna position.

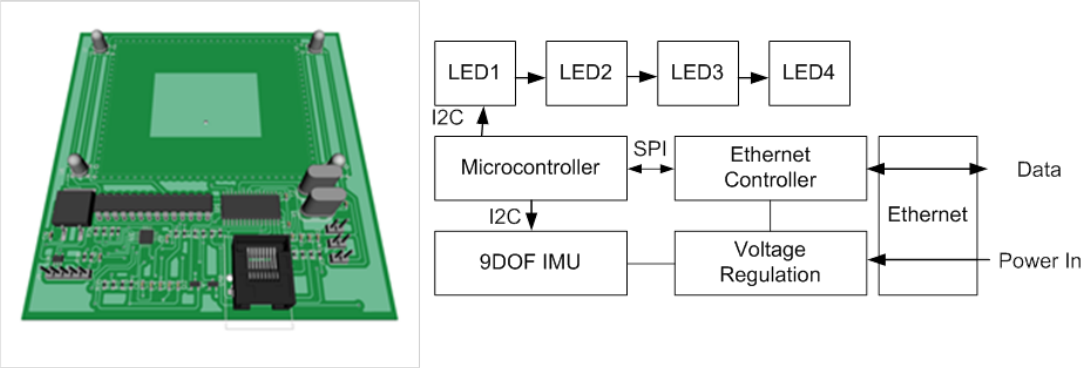

(a) (b)

Figure 10. Microstrip patch antenna. (a) PCB of patch antenna; (b) Components on the PCB board of patch antenna. (Reprinted from [57])

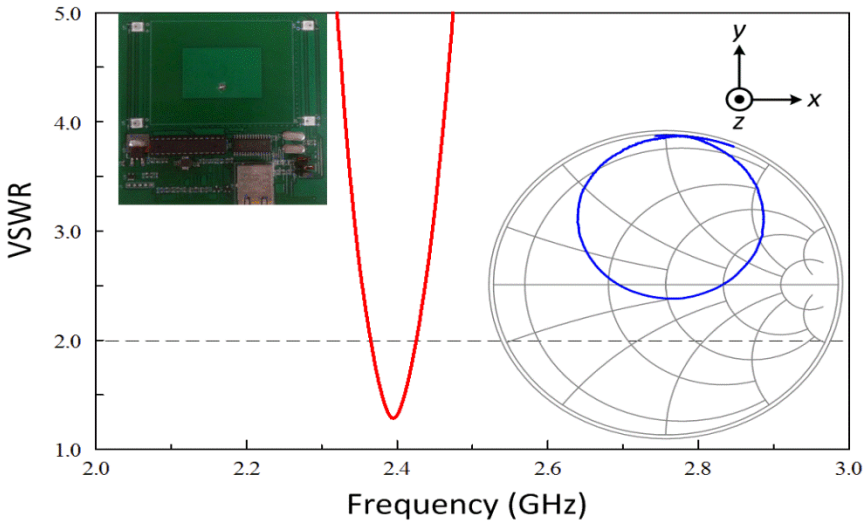

Figure 11. Measured VSWR and Smith chart of the patch antenna. (Reprinted from [57])

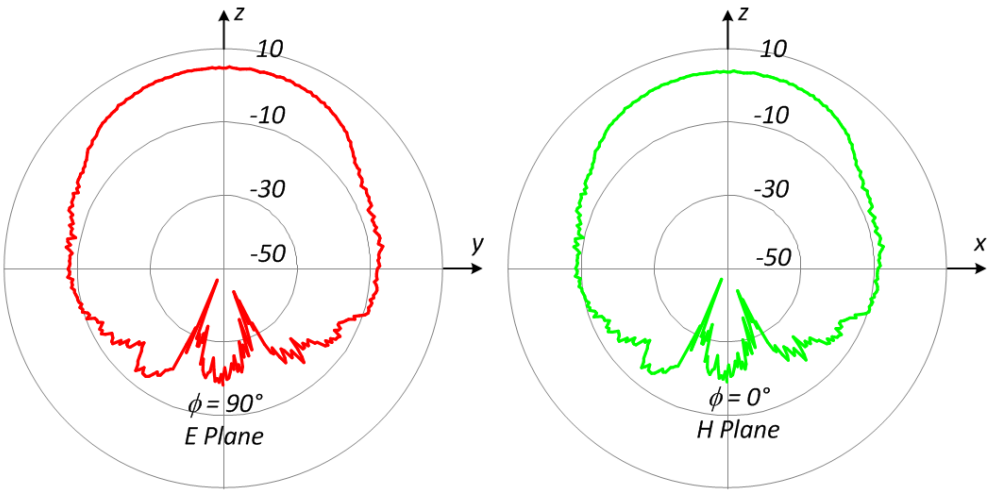

Figure 12. Measured radiation pattern of the patch antenna (dB) (Reprinted from [57])

3.5.1.2. Vector Modulator

This analog vector modulator shown in Figure 13 has both continuous 360˚ phases and 40 dB gain controls.

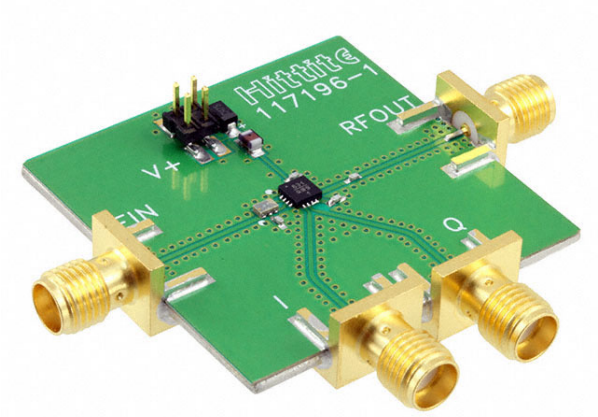

Figure 13. PCB layout of vector modulator for Medusa (Reprinted from [57])

3.5.1.3. Voltage Controller Board

The voltage control board for Medusa is shown in Figure 14.

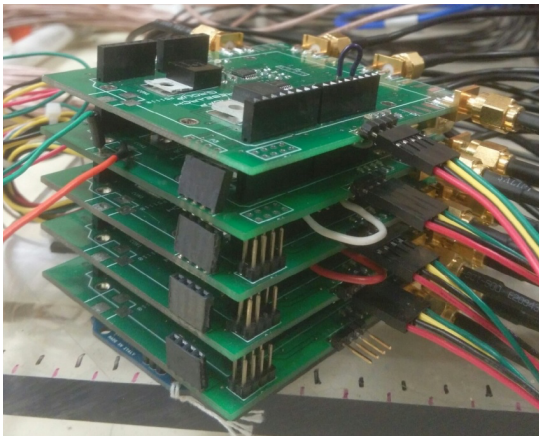

Figure 14. PCB layout of voltage control board for Medusa ([57])

3.5.1.4. Visual Spatial Recognition System

Figure 15 shows that a camera is set up in the front of Medusa to capture the positions of LEDs on the patch antenna board to locate the antenna position (x, y, z). Figure 16 shows the image processing of LEDs and the theory of positioning the antenna.

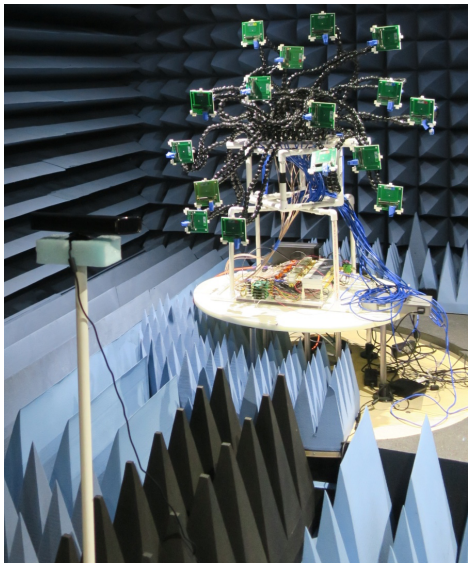

Figure 15. Medusa with camera

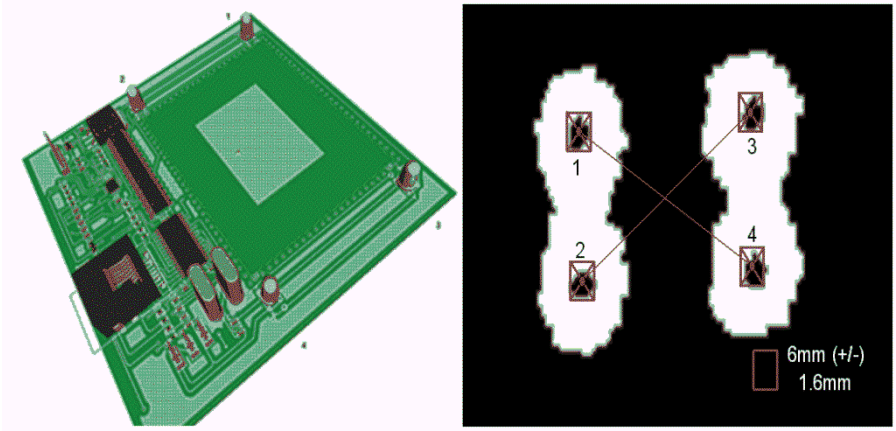

(a) (b)

Figure 16. Visual spatial recognition system. (a) PCB layout of patch antenna; (b) Image processing of antenna position. (Reprinted from [57])

3.5.2. Experiment Results

Figure 17 shows the test diagram where we use two ports of vector network analyzer (VNA) to test the phase difference between the receiving antenna and source.

Figure 18 shows the relative position of the source and receiving antennas in practical measurements, (a) and (b) have the source 1 and source 2 separately. Source 2 is relatively farther from the receiving antenna array center than source 1 to make sure the source is in the far-field.

We firstly test the DOA of the source 1 and source 2 when the receiving antennas are identical (all the receiving antennas are in the same direction without any rotation). We move one antenna 60 times to simulate a UAV flying and measure the phase difference between the receiving antenna and the source at each moving point. Then we rotate the antenna to make it be not identical (rotate 0 ~ 45 degrees around x, y, z axis randomly) to simulate the MUSB array in practice.

Figure 19 shows the measured spectrum for a 16-element MUSB array with element rotating randomly. Since it is not easy to measure 6 elements in our lab, the result has slight position error, so the spectrum has a noise floor from the system measurement error. Figure 20 and 21 show the results for one element moving multiple times to simulate the UAV swarm. Compared with Figure 18, these two figures have much lower noise floor. From Figure 20, we can find that the UAV rotation does not cause high noise, even though the measured DOA errors are a little higher shown from Table 1 and Table 2. From Figure 21, we can find that the iterative method can reduce the noise and gradually close to the ground truth.

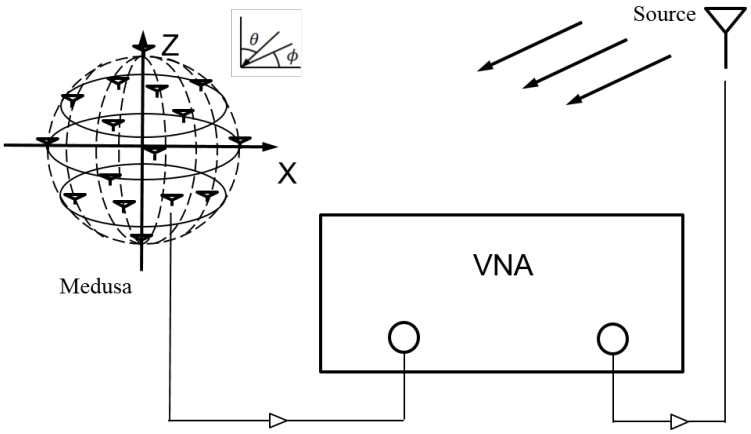

Figure 17. Test diagram

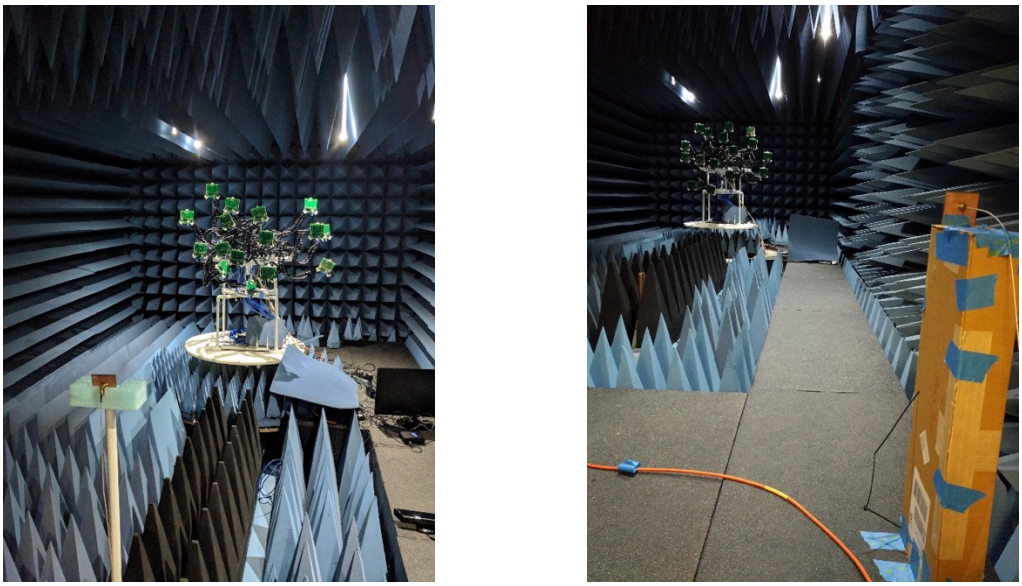

(a) (b)

Figure 18. Practical measurement schematic diagram. (a) Source 1; (b) Source 2.

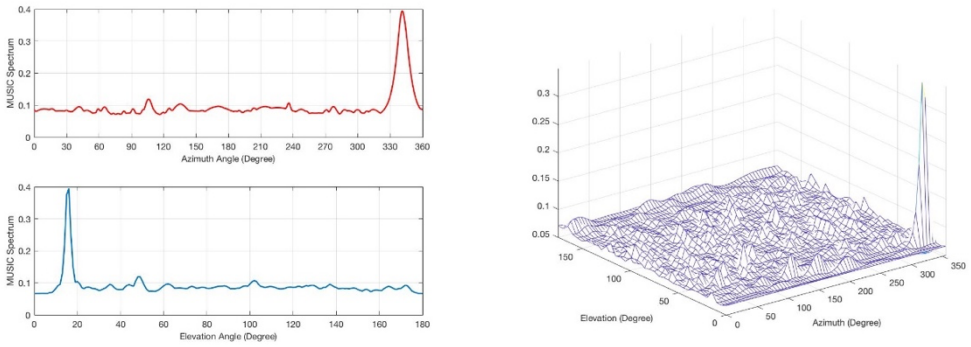

(a) (b)

Figure 19. Measured spectrum for the 16-element MUSB array. (a) 2D spectrum; (b) 3D spectrum.

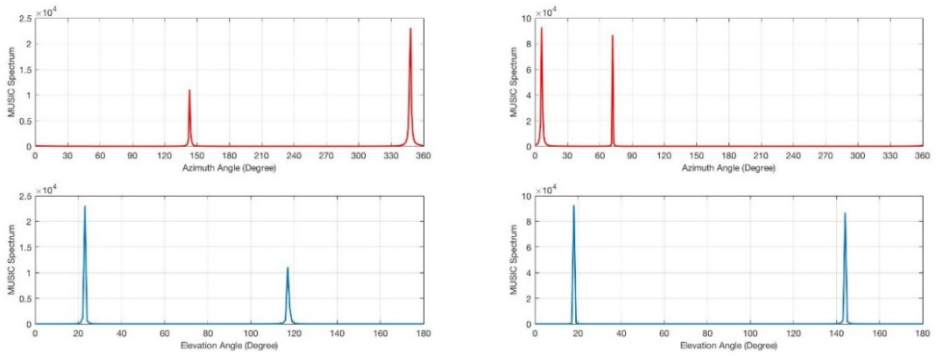

(a)

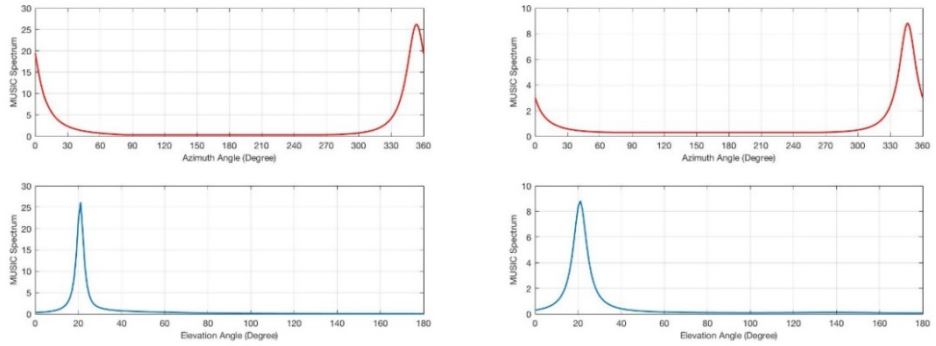

(b)

Figure 20. 2D spectrum. (a) 3-element array; (b) 16-element array; (c) 60-element array. (left figure is for identical array, right figure is for non-identical array)

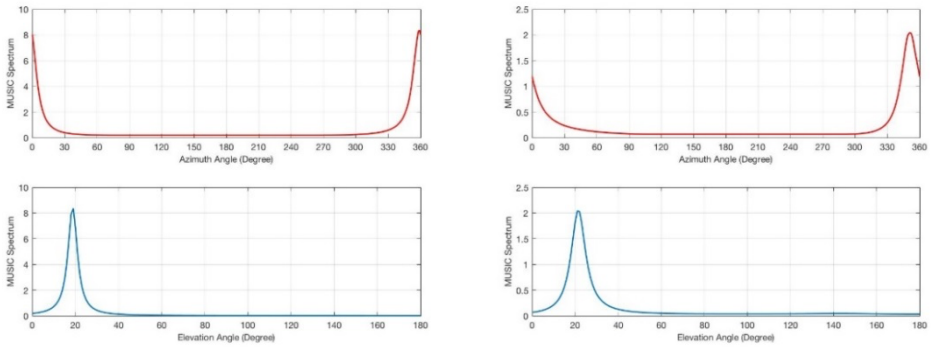

(c)

Figure 20 Continued.

Table 1. Measured DOAs of 3, 16, 60-element array reconstructed from one UAV swarm without element rotation

	3 elements	16 elements	60 elements
Measured Azimuth	348	353	359
Measured Elevation	23	21	19
Theoretical Azimuth	356.3		
Theoretical Elevation	18		

Table 2. Measured DOAs of 3, 16, 60-element array reconstructed from one UAV swarm with element rotation

	3 elements	16 elements	60 elements
Measured Azimuth	6	346	351
Measured Elevation	18	21	21
Theoretical Azimuth	357		
Theoretical Elevation	18		

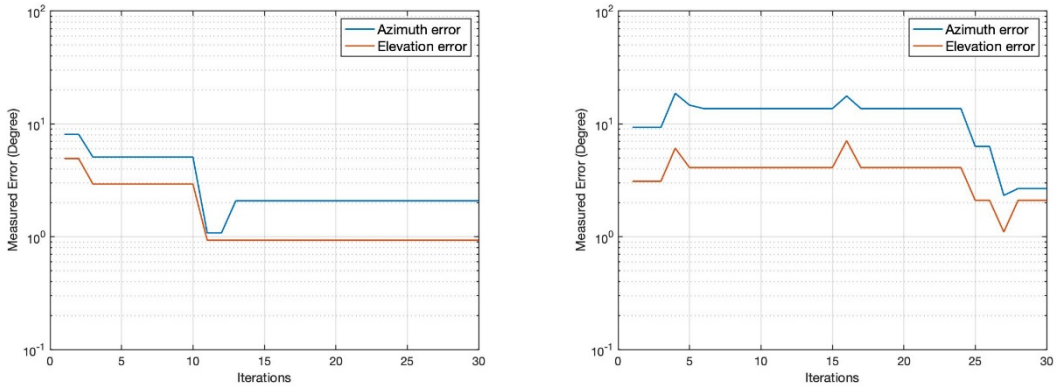

(a) (b)

Figure 21. Measured DOA errors as iterations. (a) Identical MUSB array; (b) MUSB array with elements rotation randomly.

3.6. Chapter Summary

This chapter introduces the iterative-MUSIC algorithm for MUSB array and use numerical simulation and lab experiment to verify the DOA estimation convergence performance. Theoretical results are given to reveal the performance of the MUSB phased array system used for 2D DOA estimation, which supports the feasibility of the system. Iterative-MUSIC algorithm is applied for the framework and it can estimate the DOAs efficiently only with 1 snapshot in each iteration when the UAV swarms very fast. The UAV speed controls the structure of the reconstructed phased arrays from the MUSB system. Our results will benefit to future research on performance analysis and optimal design of time-varying antenna arrays based on UAV swarm.

4. STATISTICAL PERFORMANCE ANALYSIS OF MUSB ARRAYS*

4.1. Introduction

Statistical performance analysis is still one of the most important area among array signal processing. Stoica et al. analyzed the performance of traditional MUSIC and MUSIC-related algorithms statistically by deriving the closed-form AMSE formulas, analyzing their statistical efficiency, and giving general joint CRB of DOA, noise variance, and signal power in [33-36]. However, it cannot be applied for time-varying antenna arrays. Rieken et al. presented general MUSIC for multiple noncoherent arrays in [53], and Wen et al. addressed the improved MUSIC algorithm for noncoherent subarrays by deriving the CRB formulas [54]. They utilized the summation of the MUSIC spectrums calculated from multiple subarrays to estimate DOAs, but the number of subarrays is limited. Furthermore, it requires large snapshots in each subarray so that it cannot be applied in low snapshot scenario.

In this chapter, we consider the statistical performance of MUSB arrays by deriving the CRB of the MUSB system and the AMSE formula of the iterative-MUSIC algorithm. We first derive the closed-form asymptotic MSE expression for the iterative-MUSIC algorithm and investigate their properties. We then derive the joint CRB of DOA,

---

*This chapter is partially based on Z. Chen, S. Yeh, JF Chamberland, and G. H. Huff, "A sensor-driven analysis of distributed direction-finding systems based on UAV swarms," *MDPI Sensors*, vol. 19 (12), pp. 2659-2677. Copyright [2019] by MDPI Sensors.

sensor gain, and sensor phase for MUSB arrays. We analyze the performance of one-emitter case for MUSB array and simplify the CRB formula.

4.2. Asymptotic MSE of Iterative-MUSIC

4.2.1. Asymptotic DOA Estimation Errors

In practice, we use limited number of sampling to estimate R_i with $\hat{R}_i = \frac{1}{K_i}\sum_{k=1}^{K_i} x_i(k)x_i^H(k)$, such that we have DOA estimation errors from limited sampling data. Therefore, we derive the DOA estimation error expression as iteration goes to infinity to analyze the performance of iterative-MUSIC for MUSB arrays.

Theorem 1: Let $\hat{\alpha}_n = (\hat{\theta}_n, \hat{\phi}_n)$ denote the estimated values of the n-th DOAs by iterative-MUSIC algorithm and $\Delta r_i = vec(\hat{R}_i - R_i)$. Then the estimation error of iterative-MUSIC can be represented by

$$\Delta\alpha_n = (\hat{\alpha}_n - \alpha_n) \doteq -(s_n\rho_n)^{-1}\sum_{i=1}^{I}\mathrm{Re}(\xi_{i,n}^T\Delta r_i) \tag{17}$$

where $\doteq$ denotes asymptotic equality, and

$$\xi_{i,n} = \nu_{i,n} \otimes \mu_{i,n} \tag{18}$$

$$\mu_{i,n}^T = -e_n^T A_i^\dagger \tag{19}$$

$$\nu_{i,n} = A_i^\perp d_i(\alpha_n) \tag{20}$$

$$\rho_n = \sum_{i=1}^{I}\left[d_i^H(\alpha_n)A_i^\perp d_i(\alpha_n)\right] \tag{21}$$

$$A_i^{\perp} = Q_{n,i} Q_{n,i}^H \tag{22}$$

Proof: Appendix A.

It is easy to proof that $\nu_{i,n}, \xi_{i,n} \neq 0$ for $n = 1, 2, \cdots, N$. $\nu_{i,n} \neq 0$ ensures that ρ_n^{-1} exist and equation 17 is well-defined, while $\xi_{i,n} \neq 0$ ensures that equation depends on Δr and cannot be trivially zero [51].

Theorem 1 gives a unified analysis of DOA estimation errors for the iterative-MUSIC algorithm applied in the MUSB arrays, so we can then obtain the AMSE formula in Theorem 2 in subsection 4.2.2.

4.2.2. Asymptotic MSE

Theorem 2: Based on the same assumptions of Theorem 1, we can have the AMSE formula:

$$E\left[\left(\hat{\alpha}_{n1} - \alpha_{n1}\right)\left(\hat{\alpha}_{n2} - \alpha_{n2}\right)\right] = \left(s_{n1}\rho_{n1}\right)^{-1}\left(s_{n2}\rho_{n2}\right)^{-1} \sum_{i=1}^{I} \frac{1}{K_i} \mathrm{Re}\left(\xi_{i,n1}^H \left(R_i \otimes R_i^T\right) \xi_{i,n2}\right) \tag{23}$$

Proof: Appendix B.

Thus, we can obtain the unified AMSE expression of iterative-MUSIC for MUSB arrays

$$\varepsilon\left(\alpha_n\right) = \left(s_n \rho_n\right)^{-2} \sum_{i=1}^{I} \frac{1}{K_i} \mathrm{Re}\left(\xi_{i,n}^H \left(R_i \otimes R_i^T\right) \xi_{i,n}\right) \tag{24}$$

Therefore, we can observe that the AMSE expression only depends on the physical array geometry at each iteration.

4.3. The CRB

4.3.1. Previous Results of CRB for the Static Array

In theory, for the static array, the steering vector $\tilde{A}$ is considered invariant over different snapshot since the array geometry is invariant. Assume

$$z \sim cN(\mu(\alpha),\zeta(\alpha)) \tag{25}$$

where α is a real-valued parameter vector that completely and uniquely specifies the distribution of z. Then, the m,n-th general formula of FIM on the covariance matrix of any unbiased estimate of α is:

$$F_{mn} = tr\left[\zeta^{-1}(\alpha)\frac{\partial\zeta(\alpha)}{\partial\alpha_m}\zeta^{-1}(\alpha)\frac{\partial\zeta(\alpha)}{\partial\alpha_n}\right] + 2\,\mathrm{Re}\left\{\frac{\partial\mu(\alpha)}{\partial\alpha_m}\zeta^{-1}(\alpha)\frac{\partial\mu(\alpha)}{\partial\alpha_n}\right\} \tag{26}$$

where α_m denotes the m-th component of α. The general formula has been presented in [34] and proved in [35]. Petre et al. presented the deterministic and stochastic CRB in [35].

For deterministic CRB, the parameters, mean, and variance of the complex distribution are given by $\alpha = \left\{\theta, \left\{\mathrm{Re}\left[s(t)\right], \mathrm{Im}\left[s(t)\right]\right\}_{k=1}^{K}, \sigma^2\right\}$, $\mu(\alpha) = \left[As(k)\right]_{k=1}^{K}$, $\zeta(\alpha) = block - diag\left(\sigma^2 I\right)$. Then, the m,n-th FIM is

$$F_{mn} = K\frac{\mu}{\sigma^4}\frac{\partial\sigma^2}{\partial\alpha_m}\frac{\partial\sigma^2}{\partial\alpha_n} + \frac{2}{\sigma^2}\cdot\sum_{k=1}^{K}\left[\frac{\partial}{\partial\alpha_m}As(k)\right]^H\left[\frac{\partial}{\partial\alpha_n}As(k)\right] \tag{27}$$

For stochastic CRB, the parameters, mean and variance of the complex distribution is given by $\alpha = \left\{\theta, \left\{\mathrm{Re}\left(P_{mn}\right), \mathrm{Im}\left(P_{mn}\right)\right\}_{m,n=1}^{K}, \sigma^2\right\}$, $\mu(\alpha) = 0$, $\zeta(\alpha) = block - diag(R)$, Then, the m,nth FIM is

$$F_{mn} = K\,tr\left[R^{-1}(\alpha)\frac{\partial R(\alpha)}{\partial \alpha_m} R^{-1}(\alpha)\frac{\partial R(\alpha)}{\partial \alpha_n} \right] \tag{28}$$

Since the signals estimated cannot be known completely and the signals in practice are stochastic, this paper considers the stochastic CRB.

4.3.2. The CRB for MUSB Arrays

Before we derive the CRB, we assume that the signals are stationary and ergodic complex Gaussian random process with zero mean and nonsingular covariance matrix, uncorrelated with noise. It is also assumed that the noise is stationary and ergodic complex Gaussian random process with zero mean and covariance, uncorrelated with each other. The columns of are linearly independent. An additional assumption is that the number of array elements reconstructed from swarming UAVs is greater than the number of sources. Therefore, the matrix of steering vector has full column rank.

The covariance matrices of the signal, noise and observation vectors for ith iteration are given by

$$P_i = E\left[S_i S_i^H \right] \;\; \sigma_i^2 I_0 = E\left[W_i W_i^H \right] \tag{29}$$

$$R_i = E\left[X_i(k) X_i^H(k) \right] = \Gamma_i \tilde{A}_i P_i \tilde{A}_i^H \Gamma_i^H + \sigma_i^2 I_0 = A_i P_i A_i^H + \sigma_i^2 I_0 \tag{30}$$

where $\tilde{A}_i$ is the steering vector for *i*th iteration and $A_i = \Gamma_i \tilde{A}_i$. It is useful to observe that if we let the sample data covariance matrix $\hat{R}_i = \frac{1}{K}\sum_{k=1}^{K} X_i(k) X_i^H(k)$, and $\hat{R} = \frac{1}{I}\sum_{i=1}^{I} \hat{R}_i$, then $\lim_{K\to\infty} \hat{R}_i = R_i$, and $\lim_{I\to\infty} \hat{R} = R$.

The log-likelihood function of K independent samples in the ith iteration of a zero-mean complex Gaussian random process $X_i(k)$ whose statistics depend on a parameter vector α is given by

$$\begin{aligned} L_i(\alpha) &= -K \ln\left[\det\left(R_i \pi\right)\right] - \sum_{k=1}^{K} x_i^H(k) R_i^{-1} x_i(k) \\ &= const - K \ln\left[\det\left(R_i\right)\right] - \sum_{k=1}^{K} x_i^H(k) R_i^{-1} x_i(k) \end{aligned} \tag{31}$$

where *const* denotes the constant term of the log-likelihood function, det(R) represents the determinant of the matrix R, and R_i is the time-varying covariance matrix with respect to the iteration. Thus, the log-likelihood function of $X(k)$ is:

$$\begin{aligned} L(\alpha) &= -K \sum_{i=1}^{I} \ln[\det(R_i \pi)] - \sum_{i=1}^{I} \sum_{k=1}^{K} x_i^H(k) R_i^{-1} x_i(k) \\ &= \sum_{i=1}^{I} \{const - K \ln[\det(R_i)] - \sum_{k=1}^{K} x_i^H(k) R_i^{-1} x_i(k)\} = \sum_{i=1}^{I} L_i(\alpha) \end{aligned} \tag{32}$$

Therefore, the m,n-th elements of the FIM for the i-th iteration are given by

$$\begin{aligned} F_{mn} &= -E\left[\frac{\partial^2 L(\alpha)}{\partial \alpha_m \partial \alpha_n}\right] = -\sum_{i=1}^{I} E\left[\frac{\partial^2 L_i(\alpha)}{\partial \alpha_m \partial \alpha_n}\right] \\ &= \sum_{i=1}^{I} \left\{ K\, tr\left[R_i^{-1}(\alpha) \frac{\partial R_i(\alpha)}{\partial \alpha_m} R_i^{-1}(\alpha) \frac{\partial R_i(\alpha)}{\partial \alpha_n} \right] \right\} = \sum_{i=1}^{I} F_{i,mn} \end{aligned} \tag{33}$$

It follows that the FIM's submatrix F_{mn} for the UAV swarming data collecting system can be obtained by summing the single-iteration $F_{i,mn}$ of FIM over the iterations. Furthermore, the FIM's submatrix $F_{i,mn}$ can be obtained by multiplying the single-snapshot $F_{i,mn}$ and the number of snapshots. Thus, we only need to know the single-snapshot FIM $F_{i,mn}$ for the *i*-th iteration. The problem of the major interest is the estimation of the incident angles of the sources. Expression of CRB for 1D DOA of each iteration for the present problem is listed in [35]. CRB of 2D DOA with arbitrary array for the *i*th iteration, which can be considered as an arbitrary static array, presented in this paper is given in Appendix C. The detailed derivation of the CRB with joint gain *g*, phase ψ, DOAs θ and ϕ is given in Appendix D.

4.4. Analysis of Single-Emitter Case

In this section, we investigate in more details of the MUSB data collecting system using single-emitter cases. The unknown parameters we consider here are the 2D DOAs (θ,ϕ). Assume the source variance is *P*, the noise variance is σ^2, the snapshot for each iteration is K_i, and the iteration is *I*. From the Appendix A, we have the formula of CRB with respect to the 2D DOAs in the *i*th iteration of the MUSB system.

$$F_{i,s,2}=\begin{bmatrix} F_{i,\theta\theta} & F_{i,\theta\phi} \\ F_{i,\phi\theta} & F_{i,\phi\phi} \end{bmatrix}=\frac{2K_i}{\sigma^2}\left\{\mathrm{Re}\left[D_i^H A_i^{\perp} D_i \odot 1_2 1_2^T \otimes U_i\right]\right\} \tag{34}$$

The *m*th element of the steering vector for the *i*th iteration is given by

$$a_{i,m}(\theta,\phi)=\gamma_{i,m}\cdot\exp[j\frac{2\pi}{\lambda}(x_{i,m}\sin\theta\cos\phi+y_{i,m}\sin\theta\sin\phi+z_{i,m}\cos\theta)] \tag{35}$$

where $\gamma_{i,m}$ is the gain and phase parameters, which can be represented as

$$\gamma_{i,m}=g_{i,m}e^{-j\omega_0\psi_{i,m}} \tag{36}$$

Taking the derivative of $a_i(\theta,\phi)$ for the *i*-th iteration, we obtain

$$d_{i,\theta}=\frac{d}{d\theta}a_i(\theta,\phi)=j\frac{2\pi}{\lambda}b_{i,m}\odot a_i(\theta,\phi) \tag{37}$$

$$d_{i,\phi}=\frac{d}{d\phi}a_i(\theta,\phi)=j\frac{2\pi}{\lambda}q_{i,m}\odot a_i(\theta,\phi) \tag{38}$$

where $b_{i,m}=x_{i,m}\cos\theta\cos\phi+y_{i,m}\cos\theta\sin\phi-z_{i,m}\sin\theta$, $q_{i,m}=-x_{i,m}\sin\theta\sin\phi+y_{i,m}\sin\theta\cos\phi$.

Note

$$A_i^H A_i=\sum_{m=1}^{M}g_{i,m}^2=G_{i,M} \tag{39}$$

Therefore, it is straightforward to verify that

$$D_i^H(\theta)D_i(\theta)=\left(-j\frac{2\pi}{\lambda}b_iA_i^H\right)\left(j\frac{2\pi}{\lambda}b_iA_i\right)=\frac{4\pi^2}{\lambda^2}\sum_{m=1}^{M}b_{i,m}^2g_{i,m}^2 \tag{40}$$

$$D_i^H(\phi)D_i(\phi)=\left(-j\frac{2\pi}{\lambda}q_iA_i^H\right)\left(j\frac{2\pi}{\lambda}q_iA_i\right)=\frac{4\pi^2}{\lambda^2}\sum_{m=1}^{M}q_{i,m}^2g_{i,m}^2 \tag{41}$$

$$D_i^H(\theta)D_i(\phi)=\left(-j\frac{2\pi}{\lambda}b_iA_i^H\right)\left(j\frac{2\pi}{\lambda}q_iA_i\right)=\frac{4\pi^2}{\lambda^2}\sum_{m=1}^{M}b_{i,m}q_{i,m}g_{i,m}^2=D_i^H(\phi)D_i(\theta) \tag{42}$$

Substituting the equations (38), (39), and (40), we can obtain

$$
\begin{aligned}
D_i^H(\theta) A_i^{\perp} D_i(\theta) &= D_i^H(\theta)\left(I_0 - A_i\left(A_i^H A_i\right)^{-1} A_i^H\right) D_i(\theta) \\
&= D_i^H(\theta) D_i(\theta) - \frac{D_i^H(\theta) A_i A_i^H D_i(\theta)}{G_{i,M}} \\
&= \frac{4\pi^2}{\lambda^2}\sum_{m=1}^{M} b_{i,m}^2 g_{i,m}^2 - \frac{4\pi^2}{\lambda^2}\frac{1}{G_{i,M}}\left(\sum_{m=1}^{M} b_{i,m} g_{i,m}^2\right)^2 \\
&= \frac{4\pi^2}{\lambda^2}\left\{\sum_{m=1}^{M} b_{i,m}^2 g_{i,m}^2 - \frac{1}{G_{i,M}}\left(\sum_{m=1}^{M} b_{i,m} g_{i,m}^2\right)^2\right\}
\end{aligned}
\tag{43}
$$

Using the same derivative procedure,

$$
D_i^H(\phi) A_i^{\perp} D_i(\phi) = \frac{4\pi^2}{\lambda^2}\left\{\sum_{m=1}^{M} q_{i,m}^2 g_{i,m}^2 - \frac{1}{G_{i,M}} \cdot \left(\sum_{m=1}^{M} q_{i,m} g_{i,m}^2\right)^2\right\} \tag{44}
$$

$$
\begin{aligned}
D_i^H(\theta) A_i^{\perp} D_i(\phi) &= \frac{4\pi^2}{\lambda}\left\{\sum_{m=1}^{M} b_{i,m} q_{i,m} g_{i,m}^2 - \frac{1}{G_{i,M}} \cdot \left(\sum_{m=1}^{M} b_{i,m} g_{i,m}^2 \sum_{m=1}^{M} q_{i,m} g_{i,m}^2\right)\right\} \\
&= D_i^H(\theta) A_i^{\perp} D_i(\phi)
\end{aligned}
\tag{45}
$$

Furthermore,

$$
\begin{aligned}
U_i &= P A_i^H R_i^{-1} A_i P = P^2 A_i^H \left(A_i^H P A_i + \sigma^2 I_0\right)^{-1} A_i \\
&= P^2 G_{i,M}\left(P G_{i,M} + \sigma^2\right)^{-1} = \frac{P^2 G_{i,M}}{P G_{i,M} + \sigma^2}
\end{aligned}
\tag{46}
$$

Therefore,

$$
F_{i,\theta\theta} = \frac{8K\pi^2}{\lambda^2\sigma^2}\frac{P^2 G_{i,M}^2}{P G_{i,M} + \sigma^2}\left\{\frac{1}{G_{i,M}}\sum_{m=1}^{M} b_{i,m}^2 g_{i,m}^2 - \left(\frac{1}{G_{i,M}}\sum_{m=1}^{M} b_{i,m} g_{i,m}^2\right)^2\right\} \tag{47}
$$

$$
F_{i,\phi\phi} = \frac{8K\pi^2}{\lambda^2\sigma^2}\frac{P^2 G_{i,M}^2}{P G_{i,M} + \sigma^2}\left\{\frac{1}{G_{i,M}}\sum_{m=1}^{M} q_{i,m}^2 g_{i,m}^2 - \left(\frac{1}{G_{i,M}}\sum_{m=1}^{M} q_{i,m} g_{i,m}^2\right)^2\right\} \tag{48}
$$

$$F_{i,\theta\phi} = \frac{8K\pi^2}{\lambda^2\sigma^2}\frac{P^2G_{i,M}^2}{PG_{i,M}+\sigma^2}\left\{\frac{1}{G_{i,M}}\sum_{m=1}^{M}b_{i,m}q_{i,m}g_{i,m}^2 - \left(\frac{1}{G_{i,M}^2}\sum_{m=1}^{M}b_{i,m}g_{i,m}^2\sum_{m=1}^{M}q_{i,m}g_{i,m}^2\right)\right\} \quad (49)$$
$$= F_{i,\phi\theta}$$

Assume

$$B_i = \frac{1}{G_{i,M}}\sum_{m=1}^{M}b_{i,m}^2g_{i,m}^2 - \left(\frac{1}{G_{i,M}}\sum_{m=1}^{M}b_{i,m}g_{i,m}^2\right)^2 \quad (50)$$

$$Q_i = \frac{1}{G_{i,M}}\sum_{m=1}^{M}q_{i,m}^2g_{i,m}^2 - \left(\frac{1}{G_{i,M}}\sum_{m=1}^{M}q_{i,m}g_{i,m}^2\right)^2 \quad (51)$$

$$V_i = \frac{1}{G_{i,M}}\sum_{m=1}^{M}b_{i,m}q_{i,m}g_{i,m}^2 - \left(\frac{1}{G_{i,M}^2}\sum_{m=1}^{M}b_{i,m}g_{i,m}^2\sum_{m=1}^{M}q_{i,m}g_{i,m}^2\right) \quad (52)$$

$$C_i = \frac{G_{i,M}^2SNR^2}{G_{i,M}SNR+1} \quad (53)$$

where $SNR = P/\sigma^2$. Thus, summing over iteration, we obtain

$$F_{\theta\theta} = \frac{8K\pi^2}{\lambda^2}\sum_{i=1}^{I}C_iB_i \quad (54)$$

$$F_{\phi\phi} = \frac{8K\pi^2}{\lambda^2}\sum_{i=1}^{I}C_iQ_i \quad (55)$$

Therefore, the CRB is given by

$$CRB = \begin{bmatrix} F_{\theta\theta} & F_{\theta\phi} \\ F_{\phi\theta} & F_{\phi\phi} \end{bmatrix}^{-1} \quad (56)$$

If we ignore the sensor orientation (i.e. $\Gamma = 1$) and let snapshot *K*=1, then $A_i^HA_i = M$ and the FIM with respect to 1D DOA is given by

$$F_\theta = \frac{8\pi^2}{\lambda^2}\frac{M^2 \cdot SNR^2}{M \cdot SNR + 1} B \tag{57}$$

where $B = \sum_{i=1}^{I} B_i$ and $B_i = \frac{1}{M}\sum_{m=1}^{M} b_{i,m}^2 - \left(\frac{1}{M}\sum_{m=1}^{M} b_{i,m}\right)^2$, which coincides with the result in [45].

4.5. Numerical Simulation

In this section, we numerically analyze the performance of MUSB arrays based on the iterative-MUSIC algorithm. We first investigate the DOA estimation performance, then we use the derived closed-form AMSE formula to check the application of this formula.

4.5.1. DOA Estimation Performance

The performance of the DOA estimation depends on the factors such as SNR, snapshot number *K*, the number of data processing points N_d and the velocity of UAV. Furthermore, the performance also depends on the diversity of the observation models associated with different iterations. Such diversity can be reflected by the distinctness of the array geometries at different time instants.

In this section, we only consider the single-emitter case. When a single emitter is present, a typical scenario is set in which the UAV swarm short distance mean $\mu = 2\lambda$, the Monte-Carlo simulation number and angles of the source are the same as before. The fixed and changed settings are listed below. Scenario 1: vary the SNR of one signal from -20 to 20 dB; snapshot $K = 1$, $N_d = 3$; Scenario 2: vary the snapshot number, i.e., *K* is from 1 to

99; SNR = 0 dB, N_d = 3; Scenario 3: vary the speed of UAV; K = 1, N_d = 3, SNR = 0 dB; Scenario 4: Set N_d = 10 to compare with scenario 1. The RMSE of the elevation and azimuth angles estimated from the iterative-MUSIC algorithm are shown in Figure 22, compared with CRB calculated from the derived CRB formula in subsection 4.3.

These groups of simulations demonstrate the performance of the MUSB system. From Figure 22(a), the RMSE of iterative-MUSIC is smaller than 1° when the SNR exceeds -7 dB; (b) shows that the system can estimate the DOAs even when snapshot K = 1; (c) shows that when the distance between two locations increases, the precision of DOA estimation increases; (d) compares with (a), and shows that the data processing number N_d significantly increases the DOA estimation precision (RMSE of iterative-MUSIC is smaller than 1° when the SNR exceeds -13 dB).

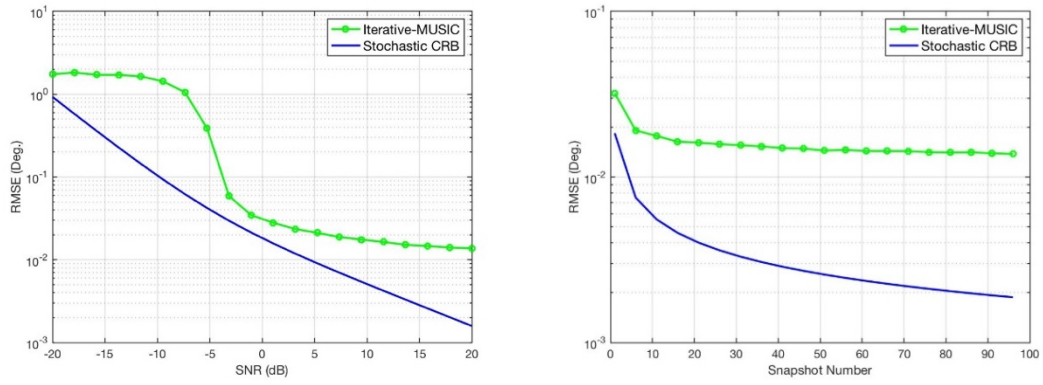

(a) (b)

Figure 22. DOA estimation RMSE of iterative-MUSIC and CRB in different scenarios. (a) Varying SNR (N_d = 3). (b) Varying snapshot number. (c) Vary the speed of UAV. (d) Varying SNR (N_d = 10).

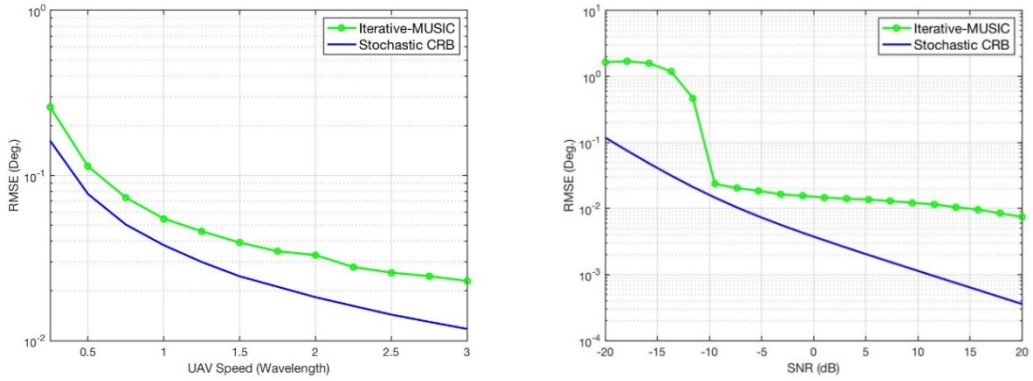

(c) (d)

Figure 22 Continued.

4.5.2. Asymptotic Efficiency Study

In this section, we will use formula (24) to investigate the asymptotic statistical efficiency of the iterative-MUSIC algorithm for MUSB arrays with different apertures and parameters. We define the average efficiency as

$$\kappa = \frac{tr\left(CRB_{\alpha}\right)}{\sum_{n=1}^{N} \varepsilon\left(\alpha_n\right)} \tag{58}$$

We expect $\kappa = 1$ for efficient estimators and $0 \le \kappa < 1$ for inefficient estimators.

We first compare the average efficiency varying SNR for different number of data processing points. We consider three cases: n = 1, n = 3, and n = 5. All sources have the same power. As shown in Figure 23, we can see that when n = 1 and n = 5, κ is complicated as SNR increases, while the curve is smoother when n = 3. However, the results here are not converged to zero like the results in traditional MUSIC [1], [35].

Next, we analyze the impact of angular separation to κ. Two sources are located at $30^\circ - \Delta\alpha/2$ and $30^\circ + \Delta\alpha/2$, then vary $\Delta\alpha$. In this section, the number of snapshots

at each iteration is 10, the number of iterations is 30, and the number of Monte Carlo simulation is 1000. The overall average efficiency of iterative-MUSIC decreases as SNR increases from -10 to 20. We also can find that the relation between κ and $\Delta\alpha / \pi$ is very complex, opposed to traditional MUSIC algorithm [1], [35]. Figures 23 and 24 show that the statistical efficiency of the iterative-MUSIC depends on the array geometry and angular separation.

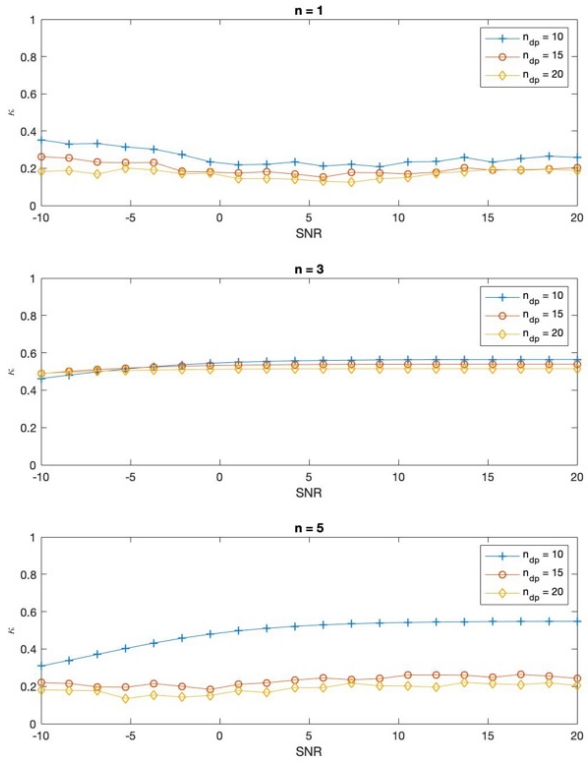

Figure 23. κ vs. SNR for MUSB array with different number of elements under different number of incident angles cases. K_i = 10, I = 30.

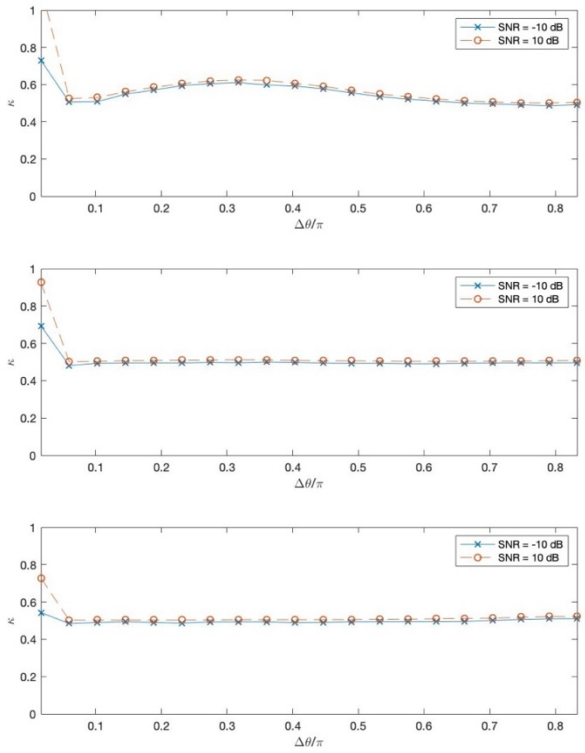

Figure 24. κ vs. angular separation for MUSB array with different SNR under different number of incident angles cases. K_i = 10, I =30.

4.5.3. AMSE vs. Number of Data Points (Elements)

We examine how the number of data processing affects the MSE in this section. We consider two cases: vary number of data point, K = 1000, I = 1; vary number of data points at each iteration, K = 10, I = 30. We set SNR to be 0 dB, number of trails to be 1000. For both cases, we compare three different arrays with different interelement spacing (2 wavelength, 3 wavelength and 4 wavelength).

In Figure 25 and 26, we observe that MSE decreases as number of elements increases, but the curves are not as smooth as traditional MUSIC in [1], [35]. When the

number of data points is very small, especially for the extreme case (N_{dp}= 3), iterative-MUSIC for MUSB arrays has better performance than traditional MUSIC for static array.

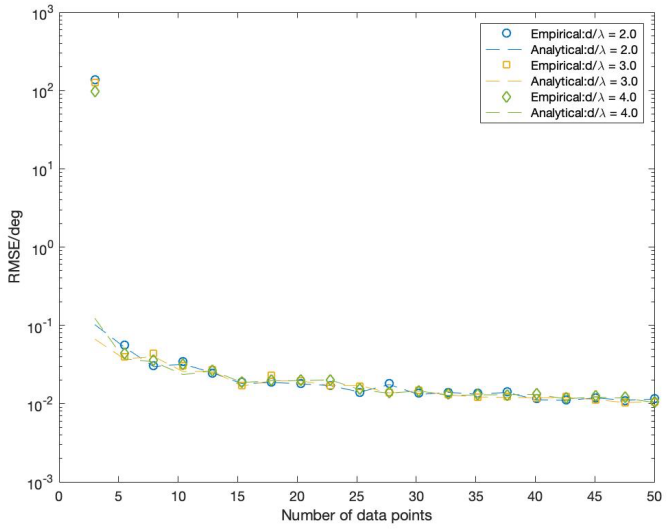

Figure 25. RMSE vs. Number of data points for MUSB array with different interelement spacing. K_i = 1000, *I* = 1.

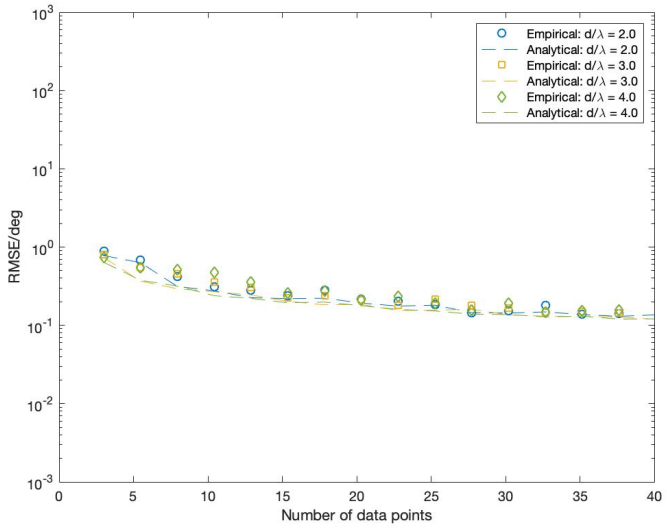

Figure 26. RMSE vs. Number of data points for MUSB array with different interelement spacing. K_i = 10, *I* =30.

4.6. Experiment

In this section, we will analyze the performance by experiment in the Chamber room of our research lab. One 2.45 GHz monopole antenna is randomly located in the platform with 32 random positions. Then we move one monopole antenna to simulate one UAV swarming in a cylinder region. We repeatedly measure the phase differences to estimate the DOAs to simulate the Monte Carlo simulations by rotating the holder of the anechoic chamber room under the antenna platform. Figures 28 and 29 show that the system can converge well and estimate correct DOAs. Figure 30 shows that the DOA estimation errors gradually decrease to around 4 degrees as the number of iterations increases. However, as the number of iterations increases, it cannot converge to less than 4 degrees because we have a system errors from measurement of sensor positions by hand.

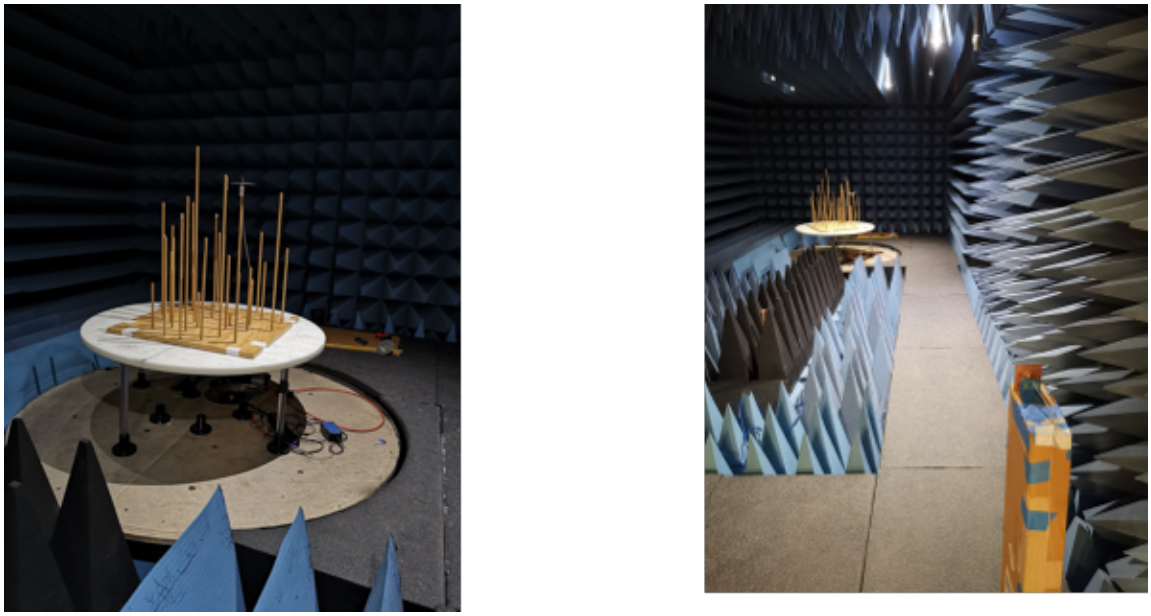

Figure 27. Test platform

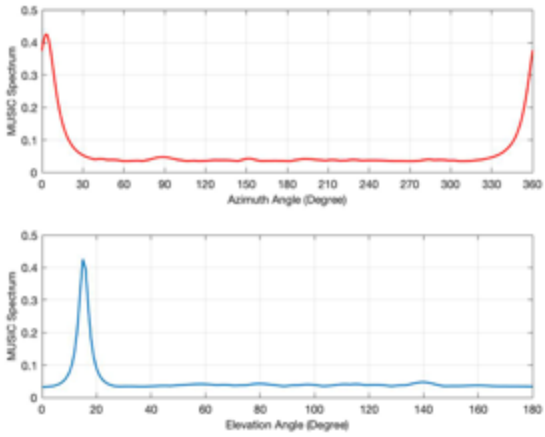

Figure 28. 2D spectrum for MUSB array with an incident angle of azimuth 3.6 and elevation 14.86 degrees.

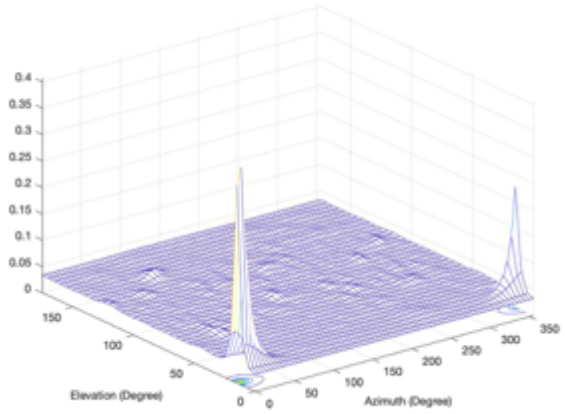

Figure 29. 3D spectrum for MUSB array with an incident angle of azimuth 3.6 and elevation 14.86 degrees.

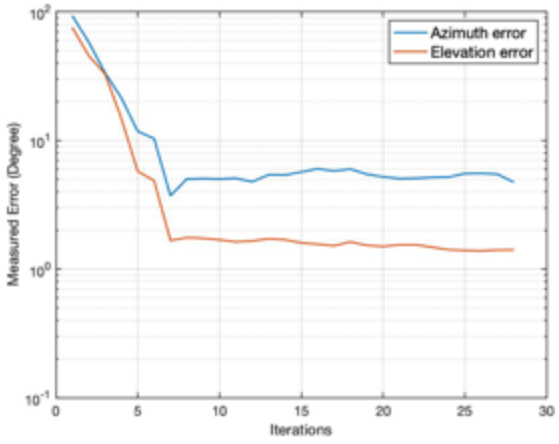

Figure 30. RMSE vs. number of iterations. Average errors of 30 good measured data for one UAV swarming 32 times.

4.7. Summary

This chapter derives the closed-form AMSE formula of iterative-MUSIC and the CRB formula of MUSB array. We apply the AMSE formula to study the asymptotic efficiency. We analyze the CRB with one-emitter case in detail and it coincides with the results of other paper. We also do the experiment with one monopole antenna moving around 32 locations randomly located in a platform in the Anechoic Chamber room. Simulation and experiment results verify our analytical results.

5. STATISTICAL PERFORMANCE ANALYSIS OF MUSB ARRAYS IN THE PRESENCE OF SENSOR GAIN, PHASE, AND POSITION ERRORS*

5.1. Introduction

The purpose of this section is to analyze the performance of DOA estimation based on MUSB arrays in the presence of sensor gain, phase, and location errors. In paper [55], the MUSB array does not have any errors, however, there are a variety of array imperfections, such as sensor gain and phase errors [43], and position errors [44] in practice, which degrades the estimation performance [42], [37-38], [45-50]. Various work has been done in analyzing the sensitivity of DOA estimation algorithms, asymptotic MSE of MUSIC-based algorithms and CRB in the presence of array imperfections [39-41]. In [39], the authors derived the asymptotic MSE of MUSIC using second order Taylor series to capture the performance in the presence of large sensor location errors, but they only derive the expression for 1D DOA with static 1D uniform linear array (ULA). Furthermore, they only consider the impact of sensor location errors. In [45], the authors derived the AMSE of MUSIC and CRB formulas in the presence of general model errors including sensor gain, phase, mutual coupling, sensor location errors, etc. However, they only consider 1D DOA with ULA.

---

* This chapter is partially based on Z. Chen, S. Yeh, JF Chamberland, and G. H. Huff, "A sensor-driven analysis of distributed direction-finding systems based on UAV swarms," *MDPI Sensors*, vol. 19 (12), pp. 2659-2677. Copyright [2019] by MDPI Sensors; Z. Chen, S. Yeh, JF Chamberland, and G. H. Huff, "Impact of position errors on synthetic aperture DOA convergence based on swarming UAVs," *IEEE APS-URSI Conf.* Copyright [2020] by IEEE.

We will mainly analyze the performance of MUSB array system with the iterative-MUSIC algorithm in the presence of small sensor gain, phase, and location errors in this chapter. It is more difficult for us to analyze the performance due to the non-linearity of location errors compared with sensor gain and phase errors.

5.2. Problem Formulation

5.2.1. Swarming UAV Synthetic Aperture in the Presence of Position Errors

A swarming UAV synthetic aperture with position errors was presented in our early published paper [56]. Compared with Figure 2, we add the stochastic position errors in Figure 31. The actual agent positions shown by filled symbols are ideal without any error and the measured agent locations embrace with stochastic location errors around the local coordination (u,v,w) which are represented by unfilled symbols.

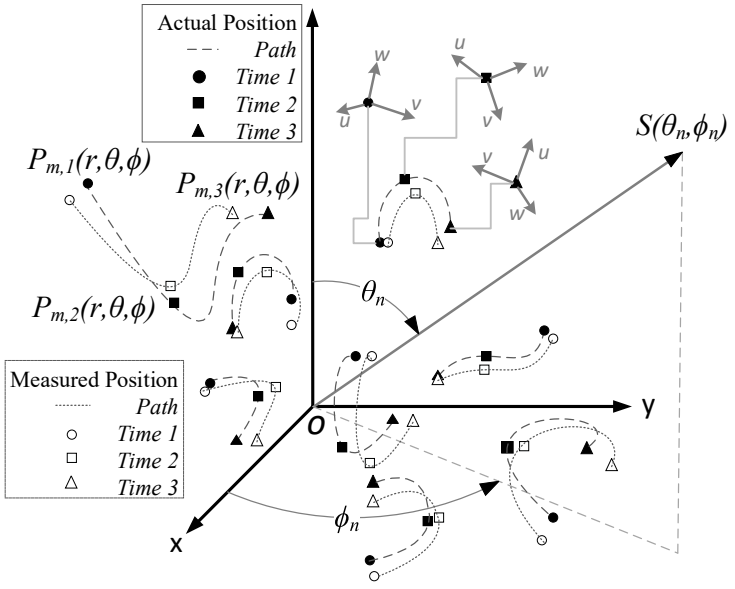

Figure 31. Morphing MUSB array configuration with location errors.

5.2.2. Signal Model

We consider that an arbitrary array of *M* elements receives *N* uncorrelated incident signals in the far-field demonstrated in subsection 5.2.1. Thus, the *K-th* snapshot received by the array at the *i*-th iteration can be represented as

$$x_i(t) = A_i(\alpha,\beta)s_i(t) + w_i(t), \quad t = 1,2,\cdots,K_i;\ i = 1,2,\cdots,I \tag{59}$$

$$A_i(\alpha,\beta) = \Gamma_i(\alpha)\,\overline{A}_i(\beta) \tag{60}$$

where *K* is the snapshot (index of samples) of each iteration, $s_i(t)$ denotes source signals at *i*-th iteration, $A_i(\alpha,\beta)$ denotes the array steering vectors at the *i*-th iteration, $\Gamma_i(\alpha)$ denotes the sensor gain and phase, $w_i(t)$ denotes additional noise at the *i*-th iteration and $\alpha = \left[\theta^T\ \phi^T\right]^T$, $\beta = \left[g^T\ \psi^T\right]^T$, $g_i = \left[g_{i,1},\cdots,g_{i,M}\right]^T$, $\psi_i = \left[\psi_{i,1},\cdots,\psi_{i,M}\right]^T$.

Herein, we denote the nominal sensor location for the *i*-th iteration as $\varsigma_i = \{(x_{i,1},y_{i,1},z_{i,1}),\cdots,(x_{i,M},y_{i,M},z_{i,M})\}$. Without sensor location errors, $a_i(\theta_N,\phi_N)$ at sensor *M* at the *i*-th iteration can be expressed as

$$\begin{aligned} a_{i,M}(\theta_N,\phi_N) = \gamma_{i,M}\cdot\exp(j\frac{2\pi}{\lambda}(x_{i,M}\sin\theta_N\cos\phi_N \\ + y_{i,M}\sin\theta_N\sin\phi_N + z_{i,M}\cos\theta_N)) \end{aligned} \tag{61}$$

Where $\gamma_{i,M}$ includes the gain and phase errors of the sensor *M* at the *i*-th iteration.

In this dissertation, we make the following assumptions that both incident signals and noise are stationary, the ergodic complex Gaussian random process with zero mean and nonsingular covariance matrix is uncorrelated with each other. An additional assumption is that the number of array elements reconstructed from swarming UAVs is

greater than the number of sources n. Therefore, the matrix of the steering vector has a full column rank.

In the signal model of chapter 2, we assume that no sensor error at each sensor exists, while there are sensor gain, phase, and location errors in our MUSB array system in practice.

We will introduce the position errors firstly in this chapter and the sensor gain and phase errors can be analyzed using the same way. In order to obtain a more general perturbation model, we assume array position errors are along *x*-axis, *y*-axis, and *z*-axis. We use $u=[u_1,u_2,\cdots,u_M]^T$, $v=[v_1,v_2,\cdots,v_M]^T$, $w=[w_1,w_2,\cdots,w_M]^T$ to denote the position errors along the x-axis, y-axis, and z-axis separately. The perturbed sensor locations are then given by

$$\varsigma=\{(x_1+u_1,y_1+v_1,z_1+w_1)\cdots(x_M+u_M,y_M+v_M,z_M+w_M)\},$$

when the array position errors are large, the MUSB array will be destroyed, which leads to large DOA estimation errors that are tough to characterize. Therefore, we will mainly focus on the performance analysis of relatively small sensor position errors of MUSB array in this dissertation.

Let $\delta=[u^T\,v^T\,w^T]^T$ denote the parameters of array position errors, so we can obtain the expression of the *K* snapshots of the perturbed array in the *i*-th iteration:

$$\tilde{x}_i(t)=\tilde{A}_i\left(\alpha,\beta,\delta\right)s_i(t)+w_i(t),\quad t=1,2,\cdots,K;\ i=1,2,\cdots,I \tag{62}$$

where $\tilde{A}_i(\alpha,\beta,\delta)$ is the perturbed steering matrix. Refer to paper [51], we also name this as deterministic error model where sensor position errors do not change for different *K* snapshots in different iterations.

Then, we name the case that sensor array errors are time-dependent as the stochastic error model, which is shown below

$$\tilde{x}(t) = \tilde{A}_i\left(\alpha,\beta(t),\delta(t)\right)s_i(t) + w_i(t),\ \ t = 1,2,\cdots,K;\ i = 1,2,\cdots,I \tag{63}$$

5.3. The Deterministic Error Model

Based on the definition in section 5.2, we can obtain the perturbed covariance matrix for the deterministic error model as

$$\tilde{R}_i = \tilde{A}_i(\alpha,\beta_i,\delta_i)P\tilde{A}_i^H(\alpha,\beta_i,\delta_i) + \sigma^2 I_0 \tag{64}$$

In this subsection, we will omit subscript *i* of iteration to derive the formulas. In paper [56], the authors give the fundamental derivation of AMSE formula for coarrays, we will follow their procedure for the AMSE derivation of iterative-MUSIC of our MUSB array system. Firstly, we link the DOA estimation errors to the MUSB array perturbations by the perturbed steering matrix $\tilde{A}$ introduced above. Then, because $\tilde{A}$ is analytical around $\delta = 0$, we can linearize it using the first-order Taylor expansion under the assumption that location errors are small compared with the exact positions:

$$\tilde{A} = A + U\tilde{A}_u + V\tilde{A}_v + W\tilde{A}_w + G\tilde{A}_u + \Psi\tilde{A}_u + o(\delta) \tag{65}$$

where we omit the subscript *i* and

$$U = diag(u_1,u_2,\cdots,u_M) \tag{66}$$

$$V = diag(v_1, v_2, \cdots, v_M) \tag{67}$$

$$W = diag(w_1, w_2, \cdots, w_M) \tag{68}$$

$$G = diag(g_1, g_2, \cdots, g_M) \tag{69}$$

$$\Psi = diag(\psi_1, \psi_2, \cdots, \psi_M) \tag{70}$$

$$\tilde{A}_u = j\frac{2\pi}{\lambda} AQ_x \tag{71}$$

$$\tilde{A}_v = j\frac{2\pi}{\lambda} AQ_y \tag{72}$$

$$\tilde{A}_w = j\frac{2\pi}{\lambda} AQ_z \tag{73}$$

$$\tilde{A}_g = A / g \tag{74}$$

$$\tilde{A}_\psi = jA \tag{75}$$

$$Q_x = diag\left(\sin\theta_1 \cos\phi_1, \sin\theta_2 \cos\phi_2, \cdots, \sin\theta_n \cos\phi_n\right) \tag{76}$$

$$Q_y = diag\left(\sin\theta_1 \sin\phi_1, \sin\theta_2 \sin\phi_2, \cdots, \sin\theta_n \sin\phi_n\right) \tag{77}$$

$$Q_z = diag\left(\cos\theta_1, \cos\theta_2, \cdots, \cos\theta_n\right) \tag{78}$$

and $o(\delta)$ is the higher order terms w.r.t. δ. We can write the perturbed covariance matrix $\tilde{R}$ as

$$\begin{aligned}\tilde{R} = R + U\tilde{A}_u PA^H + AP\tilde{A}_u^H U + V\tilde{A}_v PA^H + AP\tilde{A}_v^H V + W\tilde{A}_w PA^H + AP\tilde{A}_w^H W \\ G\tilde{A}_g PA^H + AP\tilde{A}_g^H G + \Psi\tilde{A}_\psi PA^H + AP\tilde{A}_\psi^H \Psi + o(\delta)\end{aligned} \tag{79}$$

In practice, we can only obtain the estimate of $\hat{R}_i$ by samping the data in each snapshot at each iteration, and so $\hat{R}_i = 1/K_i \sum_{t=1}^{K_i} X_i(t) X_i^H(t)$. Therefore, the covariance matrix errors could be decomposed into two parts and given by

$$\Delta R = \hat{R} - R = \underbrace{\hat{R} - \tilde{R}}_{E} + \underbrace{\tilde{R} - R}_{G} \tag{80}$$

where E is the estimation errors resulting from finite number of snapshot and iterations, and G is the estimation errors resulting from sensor gain, phase, and position errors. In order to derive the AMSE expression of iterative-MUSIC in the presence of sensor errors, we derive the AMSE expression of iterative-MUSIC without sensor errors first.

In order to derive the AMSE of iterative-MUSIC, we need to recall the equation (17). Then, we will add sensor location errors into the AMSE formulas. From (17) and (80), it is straight to obtain the DOA estimation errors

$$\Delta\alpha_n \doteq -\left(s_n \rho_n\right)^{-1} \sum_{i=1}^{I} \mathrm{Re}\left[\xi_{i,n}^T \left(e_i + g_i\right)\right] \tag{81}$$

where $e_i = vec\left(E_i\right)$, and $g_i = vec\left(G_i\right)$. Thus, when there is a large snapshot or iteration, the AMSE can be represented by

$$\varepsilon\left(\alpha_n\right) = E\left[\Delta\alpha_n^2\right] \doteq \left(s_n \rho_n\right)^{-2} E\left\{\sum_{i=1}^{I} \mathrm{Re}\left[\xi_{i,n}^T \left(e_i + g_i\right)\right]\right\}^2 \tag{82}$$

Because $\mathrm{Re}\left(AB\right) = \mathrm{Re}\left(A\right)\mathrm{Re}\left(B\right) - \mathrm{Im}\left(A\right)\mathrm{Im}\left(B\right)$, we can obtain the numerator in (82) as follows:

$$
\begin{aligned}
E\left\{\sum_{i=1}^{I}\mathrm{Re}\left[\xi_{i,n}^{T}\left(e_i+g_i\right)\right]\right\}^2 &= \sum_{i=1}^{I}E\left\{\left[\mathrm{Re}\left(\xi_{i,n}^{T}\left(e_i+g_i\right)\right)\right]^2\right\} \\
&= \sum_{i=1}^{I}\mathrm{Re}\left(\xi_{i,n}\right)^{T}E\left[\mathrm{Re}\left(e_i+g_i\right)\mathrm{Re}\left(e_i+g_i\right)^{T}\right]\mathrm{Re}\left(\xi_{i,n}\right) \\
&\quad+\sum_{i=1}^{I}\mathrm{Im}\left(\xi_{i,n}\right)^{T}E\left[\mathrm{Im}\left(e_i+g_i\right)\mathrm{Im}\left(e_i+g_i\right)^{T}\right]\mathrm{Im}\left(\xi_{i,n}\right) \\
&\quad-2\sum_{i=1}^{I}\mathrm{Re}\left(\xi_{i,n}\right)^{T}E\left[\mathrm{Re}\left(e_i+g_i\right)\mathrm{Im}\left(e_i+g_i\right)^{T}\right]\mathrm{Im}\left(\xi_{i,n}\right)
\end{aligned}
\tag{83}
$$

Because E[e] = 0, we have

$$
E\left[\mathrm{Re}\left(e_i+g_i\right)\mathrm{Re}\left(e_i+g_i\right)^{T}\right]=E\left[\mathrm{Re}\left(e_i\right)\mathrm{Re}\left(e_i\right)^{T}\right]+\mathrm{Re}\left(g_i\right)\mathrm{Re}\left(g_i\right)^{T} \tag{84}
$$

$$
E\left[\mathrm{Im}\left(e_i+g_i\right)\mathrm{Im}\left(e_i+g_i\right)^{T}\right]=E\left[\mathrm{Im}\left(e_i\right)\mathrm{Im}\left(e_i\right)^{T}\right]+\mathrm{Im}\left(g_i\right)\mathrm{Im}\left(g_i\right)^{T} \tag{85}
$$

$$
E\left[\mathrm{Re}\left(e_i+g_i\right)\mathrm{Im}\left(e_i+g_i\right)^{T}\right]=E\left[\mathrm{Re}\left(e_i\right)\mathrm{Im}\left(e_i\right)^{T}\right]+\mathrm{Re}\left(g_i\right)\mathrm{Im}\left(g_i\right)^{T} \tag{86}
$$

Based on the derivation of asymptotic MSE in chapter 4, we can obtain

$$
\begin{aligned}
&E\left\{\sum_{i=1}^{I}\mathrm{Re}\left[\xi_{i,n}^{T}\left(e_i+g_i\right)\right]\right\}^2 \\
&=\sum_{i=1}^{I}\left\{\mathrm{Re}\left(\xi_{i,n}\right)^{T}E\left[\mathrm{Re}\left(e_i\right)\mathrm{Re}\left(e_i\right)^{T}\right]\mathrm{Re}\left(\xi_{i,n}\right)+\mathrm{Im}\left(\xi_{i,n}\right)^{T}E\left[\mathrm{Im}\left(e_i\right)\mathrm{Im}\left(e_i\right)^{T}\right]\mathrm{Im}\left(\xi_{i,n}\right)\right. \\
&\quad-2\mathrm{Re}\left(\xi_{i,n}\right)^{T}E\left[\mathrm{Re}\left(e_i\right)\mathrm{Im}\left(e_i\right)^{T}\right]\mathrm{Im}\left(\xi_{i,n}\right)+\sum_{i=1}^{I}\left\{\mathrm{Re}\left(\xi_{i,n}\right)^{T}\mathrm{Re}\left(g_i\right)\mathrm{Re}\left(g_i\right)^{T}\mathrm{Re}\left(\xi_{i,n}\right)\right. \\
&\quad\left.\left.+\mathrm{Im}\left(\xi_{i,n}\right)^{T}\mathrm{Im}\left(g_i\right)\mathrm{Im}\left(g_i\right)^{T}\mathrm{Im}\left(\xi_{i,n}\right)-2\mathrm{Re}\left(\xi_{i,n}\right)^{T}\mathrm{Re}\left(g_i\right)\mathrm{Im}\left(g_i\right)^{T}\mathrm{Im}\left(\xi_{i,n}\right)\right\}\right. \\
&=I\sum_{i=1}^{I}\mathrm{Re}\left[\xi_{i,n}^{H}\left(\tilde{R}_i\otimes\tilde{R}_i^{T}\right)\xi_{i,n}\right]\Big/K_i+I\sum_{i=1}^{I}\mathrm{Re}\left(g_i^{T}\xi_{i,n}\right)^{T}\mathrm{Re}\left(g_i^{T}\xi_{i,n}\right)
\end{aligned}
\tag{87}
$$

The first three terms are expressed as $\sum_{i=1}^{I}\mathrm{Re}\left[\xi_{i,n}^{H}\left(\tilde{R}_i\otimes\tilde{R}_i^{T}\right)\xi_{i,n}\right]\Big/K_i$, which is same as the formula in Chapter 4. The latter three terms can be expressed as $\sum_{i=1}^{I}\mathrm{Re}\left(g_i^{T}\xi_{i,n}\right)^{T}\mathrm{Re}\left(g_i^{T}\xi_{i,n}\right)$

.

Then, we need to expand g_i in terms of δ_i. Let $D = diag(d)$ be a diagonal matrix. Then $vec(DX) = (X^T \circ I)d$ and $vec(XD) = (I \circ X)d$ for any matrix X with a proper shape [52].

Therefore, we can rewrite g as $B\delta + o(\delta)$, where $B = \begin{bmatrix} B_u & B_v & B_w & B_g & B_\psi \end{bmatrix}$ and

$$B_u = I \circ \left(AP\tilde{A}_u^H \right) + \left(AP\tilde{A}_u^H \right)^* \circ I \tag{88}$$

$$B_v = I \circ \left(AP\tilde{A}_v^H \right) + \left(AP\tilde{A}_v^H \right)^* \circ I \tag{89}$$

$$B_w = I \circ \left(AP\tilde{A}_w^H \right) + \left(AP\tilde{A}_w^H \right)^* \circ I \tag{90}$$

$$B_g = I \circ \left(AP\tilde{A}_g^H \right) + \left(AP\tilde{A}_g^H \right)^* \circ I \tag{91}$$

$$B_\psi = I \circ \left(AP\tilde{A}_\psi^H \right) + \left(AP\tilde{A}_\psi^H \right)^* \circ I \tag{92}$$

Substituting the expression of g back into (78), we can get the AMSE formula as follow:

$$\begin{aligned} \varepsilon(\alpha_n) &= E\left[\Delta\alpha_n^2 \right] \\ &\doteq \frac{1}{s_n^2 \rho_n^2} \sum_{i=1}^{I} \left\{ \frac{1}{K_i} \xi_{i,n}^H \left(\tilde{R}_i \otimes \tilde{R}_i^T \right) \xi_{i,n} + \mathrm{Re}\left(B_i^T \xi_{i,n} \right)^T \delta_i \delta_i^T \mathrm{Re}\left(B_i^T \xi_{i,n} \right) \right\} \end{aligned} \tag{93}$$

From this formula, we can find that the first term is from sampling error, the second term is for sensor gain, phase, and position errors. However, the first term is also affected by sensor perturbations since $\tilde{R}_i$ depends on sensor gain and phase errors β_i, and sensor position errors δ_i. When iteration I is very small, and a sufficient small number of snapshots K_i at each iteration will make the effect negligible. The second term cannot be

vanished when K_i goes to infinity if I is small, but it will be vanished as I goes to infinity since $\rho_n = \sum_{i=1}^{I}\left[d_i^H(\alpha_n)A_i^{\perp}d_i(\alpha_n)\right]$ in denominator.

5.4. The Stochastic Error Model

We assume the sensor gain, phase, and position errors vary with each snapshot at each iteration for the stochastic error model, therefore the k-th snapshot at each iteration is represented by

$$\tilde{x}_i(t) = \tilde{A}_i\left(\alpha, \beta_i(t), \delta_i(t)\right)s_i(t) + w_i(t),\ t = 1,2,\cdots,K;\ i = 1,2,\cdots,I \tag{94}$$

where $\beta_i(t)$ and $\delta_i(t)$ follow a certain stochastic model. We make an additional assumption for the stochastic error model as: the array gain, phase, and location errors are i.i.d. and uncorrelated with source signals and additive noise.

Different from the deterministic error model, $\tilde{x}_i(t)$ does not follow the complex circularly-symmetric Gaussian distribution because $\tilde{A}_i\left(\alpha, \beta_i(t), \delta_i(t)\right)$ is nonlinear. It is pretty tough to derive the distribution of $\tilde{R}_i$ in a finite number of snapshots or iterations for the stochastic error model. Furthermore, the impact of sensor gain, phase, and location errors for DOA estimation performance dominates mainly at a sufficiently large snapshot or iteration. Hence, we mainly analyze the impact of sensor gain, phase, and position errors when the snapshot or iteration goes to infinity.

Under the conditions listed in Chapter 3, the perturbed covariance matrix can be represented as

$$\tilde{R}_i = E\left[\tilde{x}_i^H(t)x_i(t)\right] = \underbrace{E\left[\tilde{A}_i\left(\beta_i(t),\delta_i(t)\right)s_i(t)s_i^H(t)\tilde{A}_i^H\left(\beta_i(t),\delta_i(t)\right)\right]}_{J} + \sigma^2 I_0 \tag{95}$$

where the cross terms are vanished because signal and noise have zero mean and uncorrelated. J can be expressed as

$$J_i = \sum_{j=1}^{N}\sum_{l=1}^{N} E\left[\tilde{a}_i\left(\alpha_j,\beta_i(t),\delta_i(t)\right)s_{i,j}(t)s_{i,l}^H(t)\tilde{a}_i^H\left(\alpha_l,\beta_i(t),\delta_i(t)\right)\right] \tag{96}$$

whose (x,y)-th element is given by

$$J_{i,xy} = \sum_{j=1}^{N}\sum_{l=1}^{N} E\left[\tilde{a}_{i,x}\left(\alpha_j,\beta_i(t),\delta_i(t)\right)\tilde{a}_{i,y}^H\left(\alpha_l,\beta_i(t),\delta_i(t)\right)s_{i,j}(t)s_{i,l}^H(t)\right] \tag{97}$$

Herein, $E\left[s_{i,j}(t)s_{i,l}^H(t)\right] = p_l$ only if $j = l$, and otherwise 0, if $j \neq l$. Thus, we only consider the terms where $j = l$. We can obtain

$$\begin{aligned} J_{i,xy} &= \sum_{n=1}^{N} p_{i,n} E\left[\tilde{a}_{i,x}\left(\alpha_n,\beta_i(t),\delta_i(t)\right)\tilde{a}_{i,y}^H\left(\alpha_n,\beta_i(t),\delta_i(t)\right)\right] \\ &= \sum_{n=1}^{N} p_{i,n} a_{i,x}\left(\alpha_n\right)a_{i,y}^H\left(\alpha_n\right)E\left\{\exp\left[j\left(t_{i,n,x} - t_{i,n,y}\right)^T\delta_i\right]\right\} \\ &= \sum_{n=1}^{N} p_{i,n} a_{i,x}\left(\alpha_n\right)a_{i,y}^H\left(\alpha_n\right)\varphi_{i,\delta}\left(t_{i,n,x} - t_{i,n,y}\right) \end{aligned} \tag{98}$$

where $\varphi_{i,\delta}\left(t_{i,n,x} - t_{i,n,y}\right)$is the characteristic function of $\delta_i(t)$, $t_{i,n,x} = \dfrac{2\pi}{\lambda}\begin{bmatrix} e_X^y \sin\theta\cos\phi \\ e_X^y \sin\theta\sin\phi \\ e_X^y \cos\theta \end{bmatrix}$,

and e_X^y is an X-dimensional vector with only the y-th element being one and other elements being zero. Therefore, we can express the covariance matrix as

$$\tilde{R}_i = \sum_{n=1}^{N} p_{i,n} a_i\left(\alpha_n\right)a_i^H\left(\alpha_n\right) \odot \varphi_{i,n} + \sigma^2 I \tag{99}$$

where $p_{i,n} = E\left[s(t)s^H(t)\right]$, $\varphi_{n,\delta}(k) = \exp\left(-1/2k_n^T C k_n\right)$, and we consider $\delta_i(t)$ follows zero-mean Gaussian distribution with the covariance matrix C, which can be

$$C = \begin{bmatrix} C_{gg} & C_{g\psi} & C_{gu} & C_{gv} & C_{gw} \\ C_{\psi g} & C_{\psi\psi} & C_{\psi u} & C_{\psi v} & C_{\psi w} \\ C_{ug} & C_{u\psi} & C_{uu} & C_{uv} & C_{uw} \\ C_{vg} & C_{v\psi} & C_{vu} & C_{vv} & C_{vw} \\ C_{wg} & C_{w\psi} & C_{wu} & C_{wv} & C_{ww} \end{bmatrix}$$

Based on the conclusion in paper [52], we know that the effect of random sensor position errors is DOA dependent, but the effect will be independent of DOAs if all error variables have the same distribution zero-mean Gaussian with the same variance.

Let $\delta_i(t) \sim N\left(0, \sigma_p^2 I\right)$, then

$$\tilde{R}_i = C_1\left\{A_i P A_i^H + \frac{1}{C_1}\left[\sigma^2 + (1-C_1)\sum_{n=1}^{N} p_n\right] I\right\} \tag{100}$$

where $C_1 = \exp\left(-4\pi^2\sigma_p^2/\lambda^2\right)$.

We observe that the effect of sensor position errors could be modeled as additive white noise as the number of snapshots or iterations goes to infinity. The signal subspace is unchanged, and we can approximate AMSE of iterative-MUSIC for the n-th DOA:

$$\varepsilon(\alpha_n) = E\left[\Delta\alpha_n^2\right] \doteq \frac{1}{s_n^2\rho_n^2}\sum_{i=1}^{I}\frac{1}{K_i}\xi_{i,n}^H\left(R_i \otimes R_i^T\right)\xi_{i,n} \tag{101}$$

with the original noise variance σ^2 replaced with $\frac{1}{C_1}\left[\sigma^2 + (1-C_1)\sum_{n=1}^{N} p_n\right]$ which is the same as the result in paper [52] for static array.

5.5. The Joint CRBs of DOAs, Sensor Gain, Phase, and Position Errors

In this subsection, we will derive the joint CRBs for the general MUSB array under the stochastic error model. Apart from the source powers, noise powers, and the DOAs, we also treat the gain, phase, and position errors of sensors as unknown parameters. Hereby we assume that the precise sensor gains, phases, and positions are known. Therefore, the FIM with unknown sensor gain, phase, and position errors is given by

$$FIM = CRB^{-1}\left(g,\psi,\theta,\phi,u,v,w\right) = \begin{bmatrix} F_{gg} & F_{g\psi} & F_{g\theta} & F_{g\phi} & F_{gu} & F_{gv} & F_{gw} \\ F_{\psi g} & F_{\psi\psi} & F_{\psi\theta} & F_{\psi\phi} & F_{\psi u} & F_{\psi v} & F_{\psi w} \\ F_{\theta g} & F_{\theta\psi} & F_{\theta\theta} & F_{\theta\phi} & F_{\theta u} & F_{\theta v} & F_{\theta w} \\ F_{\phi g} & F_{\phi\psi} & F_{\phi\theta} & F_{\phi\phi} & F_{\phi u} & F_{\phi v} & F_{\phi w} \\ F_{ug} & F_{u\psi} & F_{u\theta} & F_{u\phi} & F_{uu} & F_{uv} & F_{uw} \\ F_{vg} & F_{v\psi} & F_{v\theta} & F_{v\phi} & F_{vu} & F_{vv} & F_{vw} \\ F_{wg} & F_{w\psi} & F_{w\theta} & F_{w\phi} & F_{wu} & F_{wv} & F_{ww} \end{bmatrix} = \frac{2K}{\sigma^2}\left\{\mathrm{Re}\left[\tilde{D}_i^H A_i^{\perp}\tilde{D}_i \odot 1_7 1_7^T \otimes U_i\right]\right\} \tag{102}$$

herein $\tilde{D}_i = \left[\tilde{d}_{i,g} \quad \tilde{d}_{i,\psi} \quad \tilde{d}_{i,\theta} \quad \tilde{d}_{i,\phi} \quad \tilde{d}_{i,u} \quad \tilde{d}_{i,v} \quad \tilde{d}_{i,w}\right]$, and where

$$F_{\theta\theta} = \sum_{i=1}^{I} F_{i,\theta\theta} \tag{103}$$

$$F_{i,\theta\theta} = \frac{2K}{\sigma^2}\mathrm{Re}\left\{\tilde{D}_{i,\theta}^H \tilde{A}_i^{\perp}\tilde{D}_{i,\theta} \odot U_i\right\} \tag{104}$$

$$F_{i,\phi\phi} = \frac{2K}{\sigma^2}\mathrm{Re}\left\{\tilde{D}_{i,\phi}^H \tilde{A}^{\perp}\tilde{D}_{i,\phi} \odot U_i\right\} \tag{105}$$

$$\tilde{D}_{i,\theta} = \frac{\partial \tilde{A}_i}{\partial \theta} \tag{106}$$

$$\tilde{D}_{i,\phi} = \frac{\partial \tilde{A}_i}{\partial \phi} \tag{107}$$

$$\tilde{A}_i^{\perp} = I_0 - \tilde{A}_i \left(\tilde{A}_i^H \tilde{A}_i \right)^{-1} \tilde{A}_i^H \tag{108}$$

$$U_i = P_i \tilde{A}_i^H \tilde{R}_i^{-1} \tilde{A}_i P_i \tag{109}$$

Here we only give part of the FIMs, all the other components of FIMs and partial derivative of steering vectors A w.r.t. g, ψ, u, v, w can be obtained by following the same idea.

Proof: See Appendix E.

5.6. Simulation Results

5.6.1. Numerical Analysis of the Deterministic Error Model

In this section, we verify the closed-form AMSE for deterministic error model first. We consider 1 source located in $(60°, 60°)$ and set the SNR to 20 dB. We use a zero-mean Gaussian distribution with covariance matrix $\sigma_p^2 I$ to generate the sensor location errors and the magnitude of position errors can be tuned by σ_p.

We investigate how the position errors affect the DOA estimation errors by varying σ_p / λ with two cases: the first case is with the same number of elements array; the second case is with the same average interelement spacing (refer as same aperture). They are plotted in Figure 32 and 33 separately. We observe that the RMSE errors increase as the position errors increase for the first case and the interelement spacing should be not too big or too small. In our results, when the interelement spacing is 2.5 wavelength, the

RMSE is relatively smaller. For the second case, we can also find that RMSE increases as the position errors increase and more element has lower RMSE, which coincides with our analysis.

Then, we investigate that how the position errors affect the DOA estimation errors as SNR increases. We consider one source is located at $(60°, 60°)$. We also consider two cases: in the first case we set snapshots at each position to be 1000 and number of iteration to be 1 (static array); in the second case, we set snapshots at each position to be 10 and number of iteration to be 30 (swarming array). In Figure 34 and Figure 35, we find that as SNR increases to infinity, the gap between different position errors is not changed because the position errors cannot be omitted by increasing SNR, which agrees with our analysis in section 4. Furthermore, we find that the iterative-MUSIC algorithm has more capacity of position errors than the traditional MUSIC when the variance of position errors over wavelength is above 0.08. In Figure 34, the traditional MUSIC cannot converge when δ_p = 0.08, while iterative-MUSIC can estimate DOAs well in Figure 35. In Figures 36 and 37, we examine the impact of sensor gain error and find that it won't affect the DOA estimation performance a lot.

Finally, we investigate that how the sensor phase errors affect the DOA estimation errors as SNR increases. We consider one source is located at $(60°, 60°)$. We also consider two cases: in the first case we set snapshots at each position to be 1000 and number of iteration to be 1 (static array); in the second case, we set snapshots at each position to be 10 and number of iteration to be 30 (swarming array). In Figure 38 and Figure 39, we find

that as SNR increases to infinity, the gap between different phase errors is not changed because the phase errors cannot be omitted by increasing SNR, which agrees with our analysis in section 4. Furthermore, we find that the iterative-MUSIC algorithm has more capacity of phase errors than the traditional MUSIC when the variance of phase errors is above 30 degrees. We observe that the trend of the impact of sensor phase errors and position errors has the similar effect.

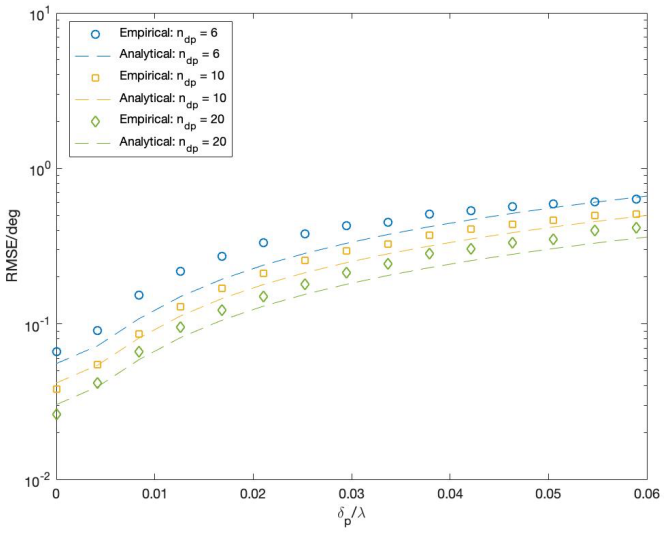

Figure 32. RMSE vs. sensor position error level for MUSB array with different number of elements: K_i = 10, *I* = 30, and the empirical MSE is averaged from 1000 trails.

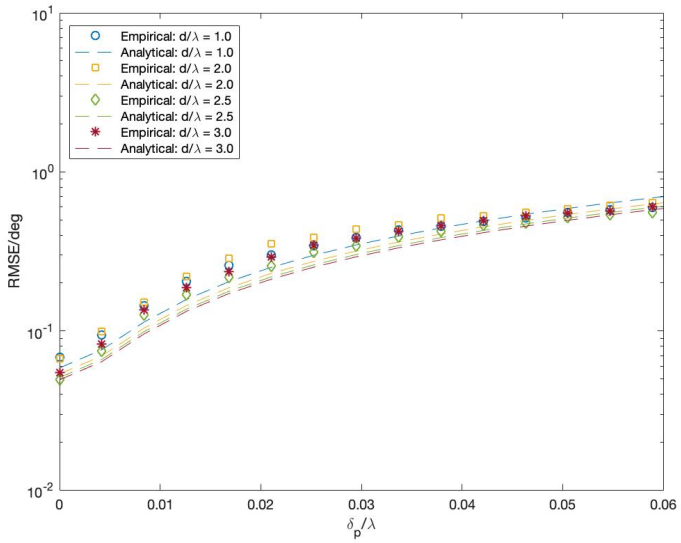

Figure 33. RMSE vs. sensor position error level for MUSB array with different average inter-element spacing: K_i = 10, I = 30, and the empirical MSE is averaged from 1000 trails.

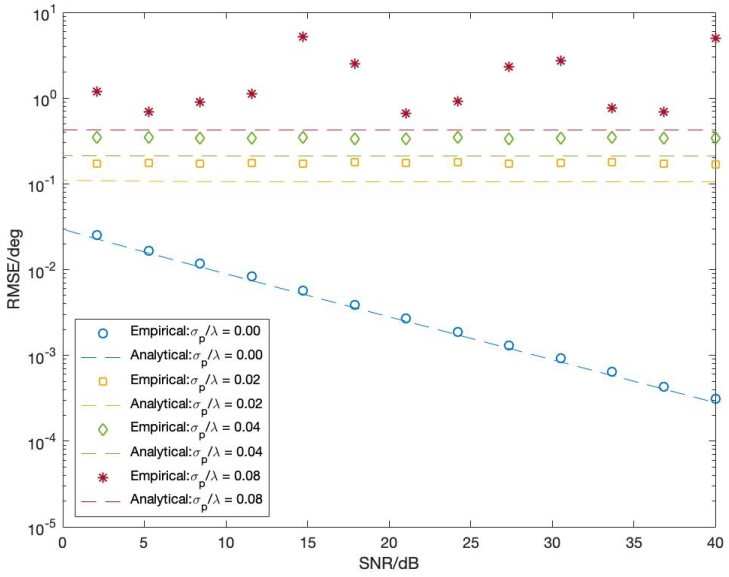

Figure 34. RMSE vs. SNR for MUSB array with sensor position error level: K_i = 1000, I = 1, and the empirical MSE is averaged from 1000 trails.

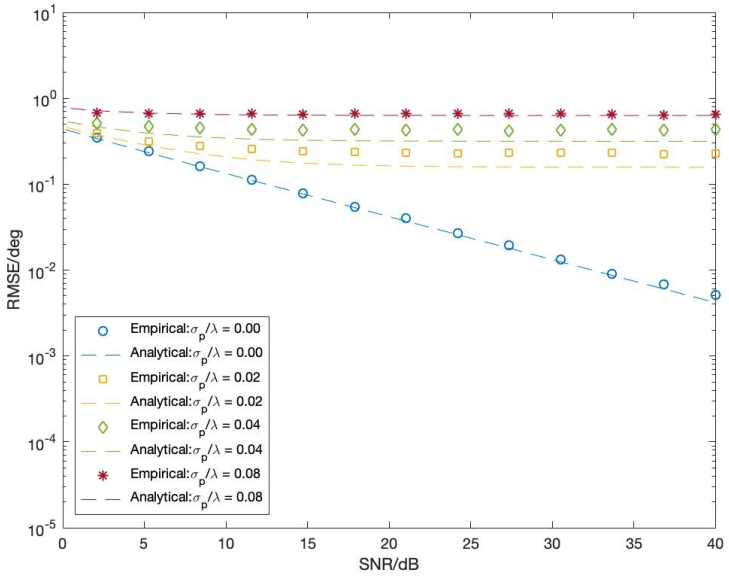

Figure 35. RMSE vs. SNR for MUSB array with sensor position error level: K_i = 10, *I* = 30, and the empirical MSE is averaged from 1000 trails.

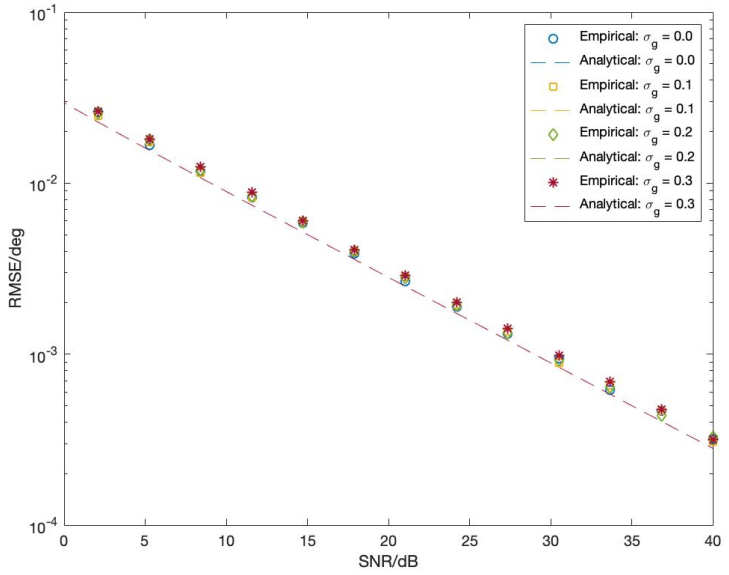

Figure 36. RMSE vs. SNR for MUSB array with different gain error level: K_i = 1000, *I* = 1, and the empirical MSE is averaged from 1000 trails.

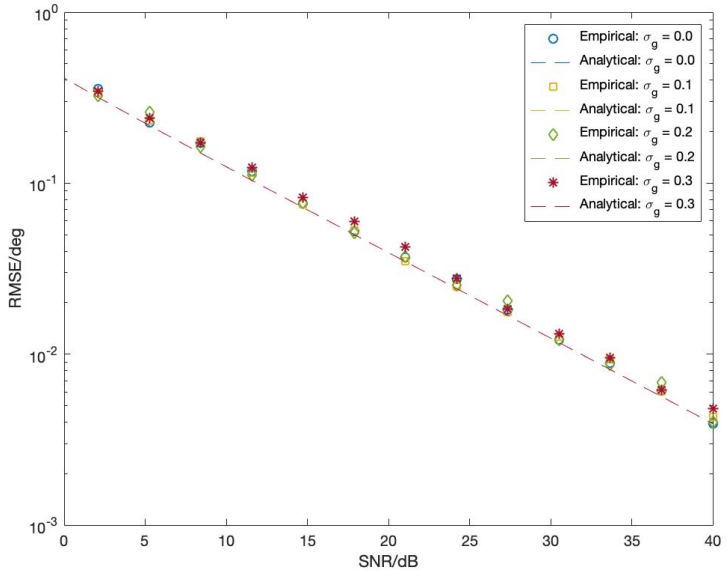

Figure 37. RMSE vs. SNR for MUSB array with different gain error level: K_i = 10, *I* = 30, and the empirical MSE is averaged from 1000 trails.

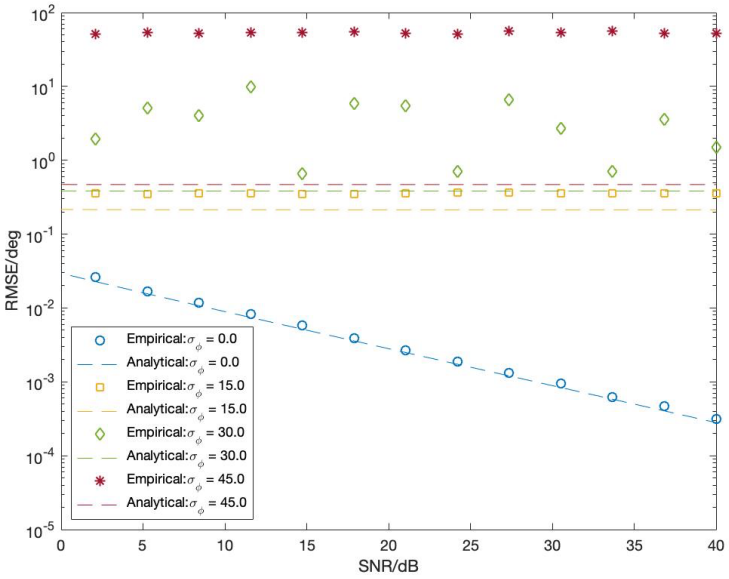

Figure 38. RMSE vs. SNR for MUSB array with different gain error level: K_i = 1000, *I* = 1, and the empirical MSE is averaged from 1000 trails.

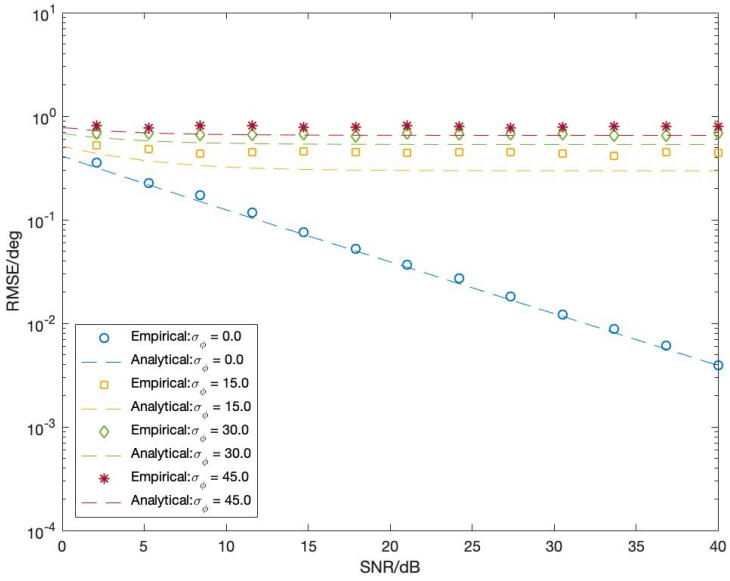

Figure 39. RMSE vs. SNR for MUSB array with different gain error level: K_i = 10, *I* = 30, and the empirical MSE is averaged from 1000 trails.

5.6.2. Numerical Analysis of the Stochastic Error Model

In this subsection, we examine the impact of snapshots and iteration by varying number of snapshots and number of iterations for different number of element arrays under the stochastic error models. Therefore, we also consider two cases: in the first case we set the iteration to be 30 and vary the snapshots at each iteration; in the second case, we set the snapshots to be 10 and vary iteration. We set the position error standard deviation σ_p to be 0.1 and fix the SNR to be 20 dB for both of cases

The results are plotted in Figure 40, it shows that the trend of empirical MSE agrees with our analytical formula and becomes closer to our theoretical results as the snapshot increases, because we assume the snapshots or iteration goes to infinity when we derive our AMSE formulas. We also can find that as the number of iteration increases, the RMSE

does not decrease a lot because the iterative-MUSIC algorithm converges to the saturation earlier as the number of iteration increases.

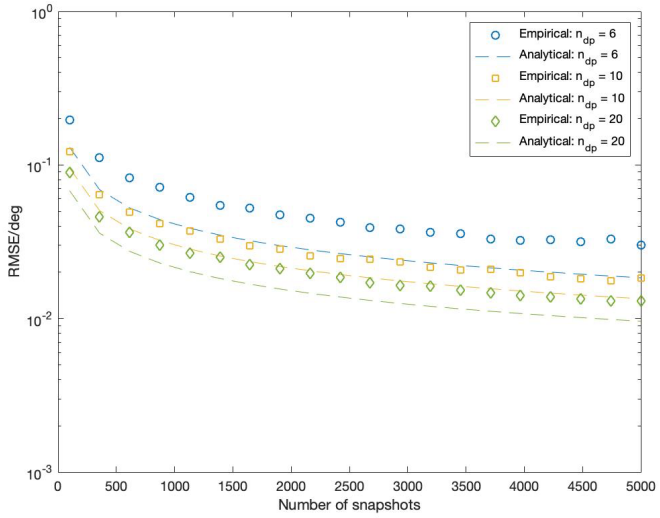

Figure 40. RMSE vs. number of snapshots for MUSB array with different number of elements: I = 30, and the empirical MSE is averaged from 1000 trails.

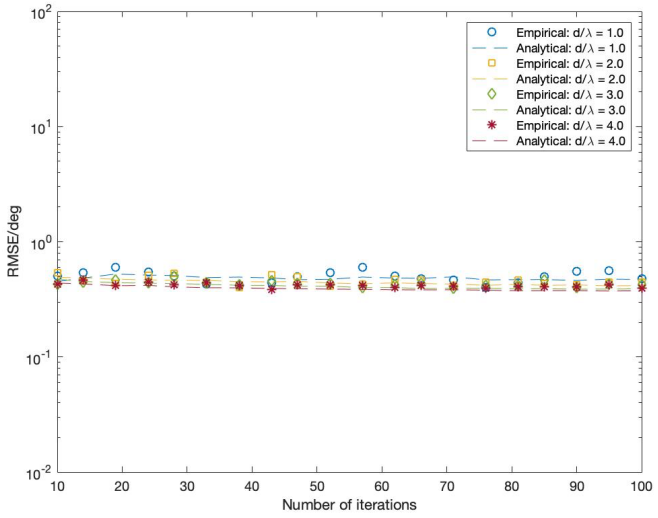

Figure 41. RMSE vs. number of iterations for MUSB array with different number of interelement spacing corresponding to wavelength: K_i = 10, and the empirical MSE is averaged from 1000 trails.

5.6.3. Numerical Analysis of the CRB

We close this subsection with the CRB results for one source case. We located the source at 60°, and compare two cases: the first one is with 1000 snapshots and one iteration (No swarm case); the second one is with large snapshots and small iterations.

The results are plotted in Figures 42 and 43, we observe that the gap between free-error CRB and fixed error CRB does not change as the SNR increases because the position error cannot be omitted by increasing SNR for the traditional MUSIC algorithm without UAV swarming, which coincides with our analysis before. However, when we add iteration to the CRB, the CRB with position error approaches gradually to the error-free CRB. That means that the position error is decreased by increasing the number of iterations. Furthermore, the CRB cannot be decreased more by increasing the number of iterations when the iteration is greater than a certain value. From (a), (c) in Figure 42, we also observe that the gap is not increased a lot as δ_p increases from $\delta_p = 0.01$ to 0.05.

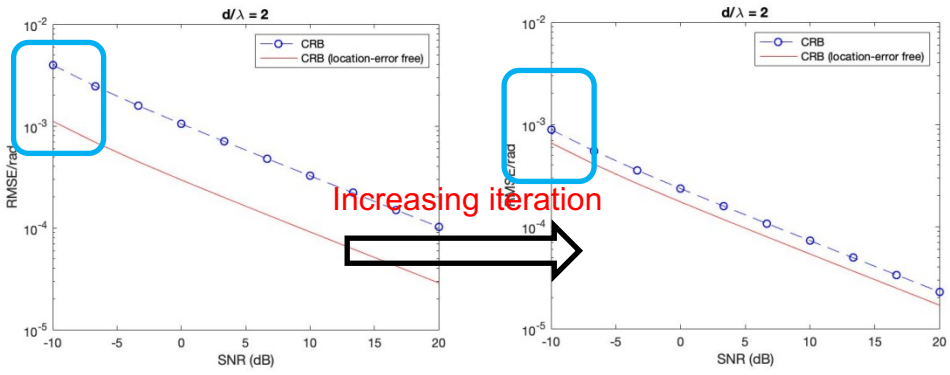

(a) (b)

Figure 42. CRB vs. SNR for MUSB array: K_i = 1000: (a) K_i = 1000, I = 1, δ_p = 0.01; (b) K_i = 1000, I = 10, δ_p = 0.01; (c) K_i = 1000, I = 1, δ_p = 0.1; (d) K_i = 1000, I = 10, δ_p = 0.1; (e) K_i = 10, I = 1, δ_p = 0.1; (f) K_i = 10, I = 10, δ_p = 0.1.

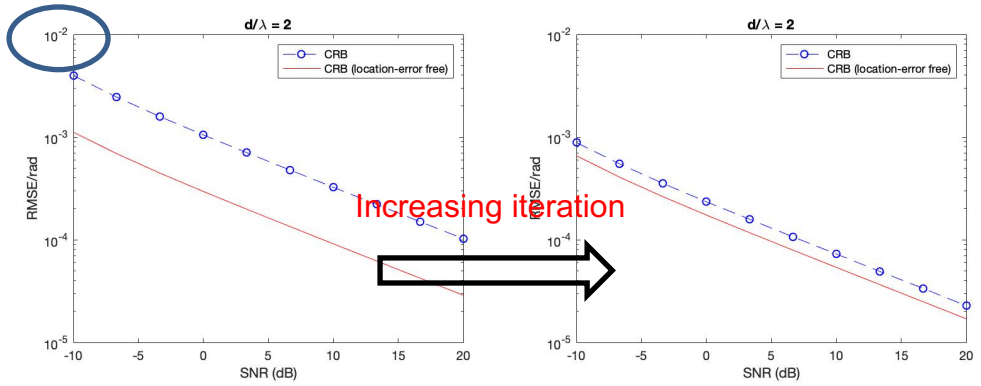

(c) (d)

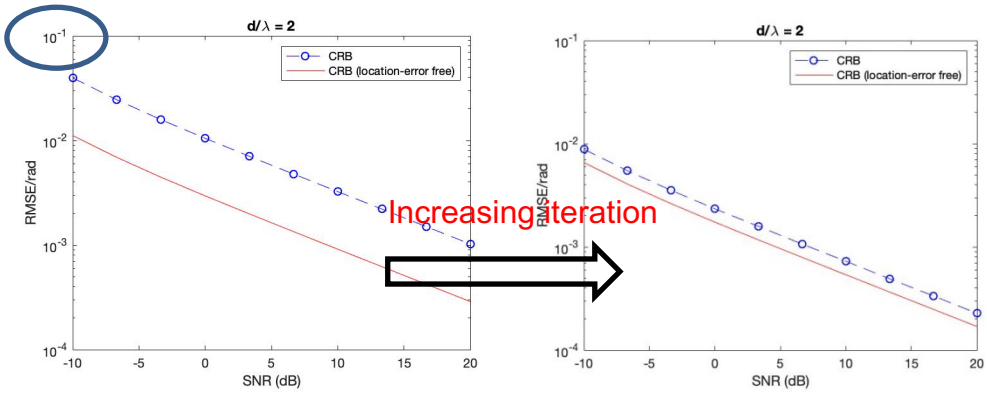

(e) (f)

Figure 42 Continued.

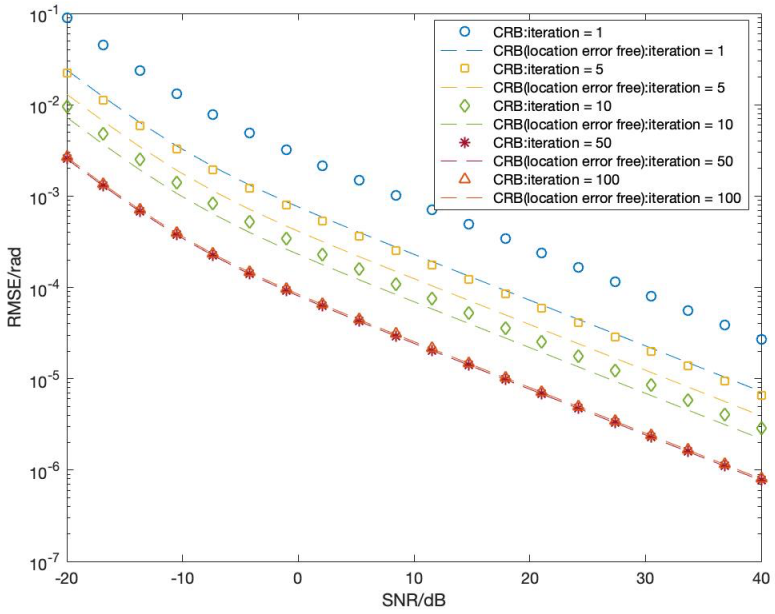

Figure 43. CRB vs. SNR for MUSB array with different number of iterations.

5.7. Experiment

The data collection process assumes the target is stationary and narrowband in the far field, and that one or more of the swarming UAVs can process the information from the source. The conjecture assumes that the position error will degrade the DOA estimation performance and the system can still converge in certain number of iterations via iterative-MUSIC algorithm. To study this, a test-bed is constructed with thirty possible locations that an agent can occupy (One agent swarms). The iterative data collection process begins at time $t = 1$, when $N_d = 3$. We choose the extreme case, 3-element array for 2-D DOA estimation, to demonstrate the performance in this paper. The process iterates for t times until the convergence criteria is met or some other instruction is received.

The position errors for each iteration can be selected using the following relation:

$$\alpha_i = \beta_i \cdot std \tag{110}$$

where β_i is the standard normally distributed random numbers for each swarming iteration i and std is the standard deviation of the position errors.

5.7.1. Experiment Results

In experiments, the test fixture provides a convenient platform to study this morphing in time and we use two different platforms to verify our expectation and analysis. In Figure 44, Randomly positioned monopole antennas designed for 2.45 GHz are used with a fixed morphing volume provided by a sphere with a 380 mm radius to estimate the DOAs. Thus, the wavelength is 122.45 mm for the designed frequency and 1 mm location error with respect to wavelength will cause about 3° phase difference shift from source to sensor. If each agent has 1 mm location error, the maximum measured phase difference errors will be 6°.

Figure 45 shows the RMSE vs. number of iterations with UAV swarms in the presence of stochastic location errors (std = 0, 5, 10, and 15 mm). The DOA estimation errors increase as the location error increases and DOA estimation errors decrease as the iteration increases. This system can converge with certain iterations when location errors exist. In Figure 46, we use Medusa platform to investigate the performance of our system in the presence of sensor gain and phase errors by rotating the antenna in a range of 0 to 45 degrees. However, we cannot control the exact value for sensor gain and phase errors

in practice. Figure 47 shows that when UAVs rotate, the system will be more difficult to converge compared with no rotation case.

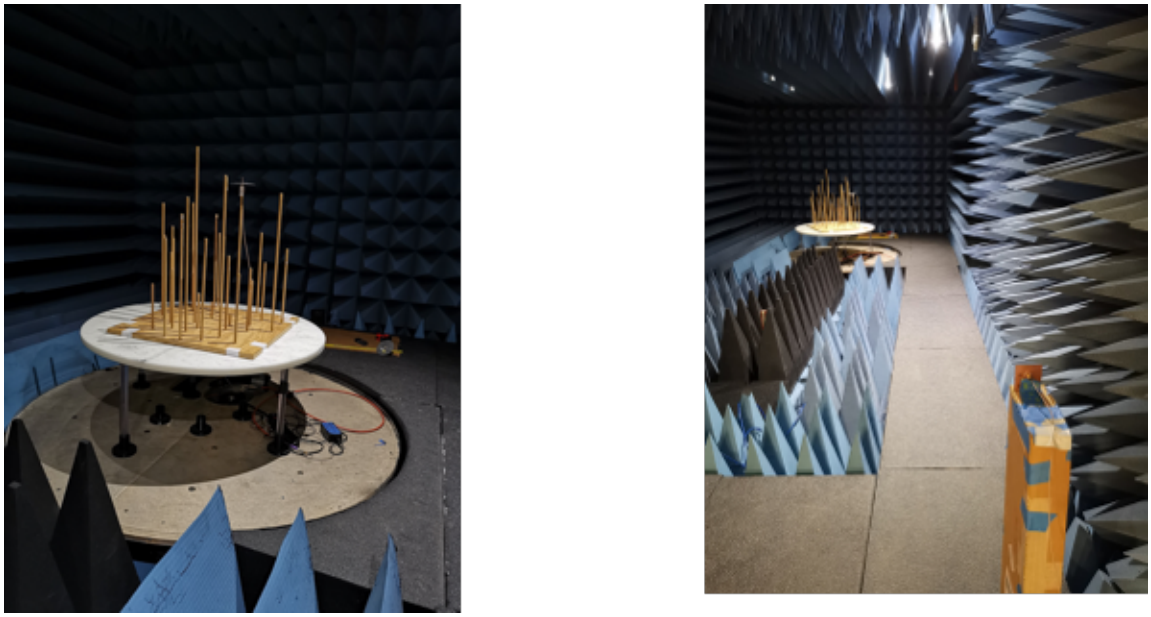

(a) (b)

Figure 44. Practical measurement schematic diagram: (a) One monopole antenna located at the test platform with 32 random positions; (b) Test diagram with one source in the far field.

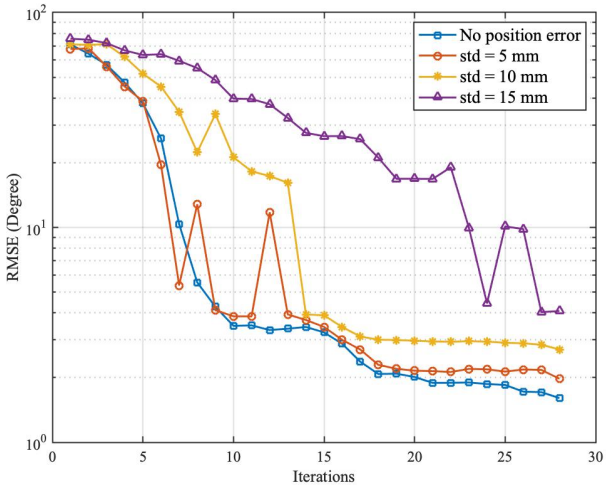

Figure 45. DOA estimation RMSE of experiment vs. iterations for different sensor position error level

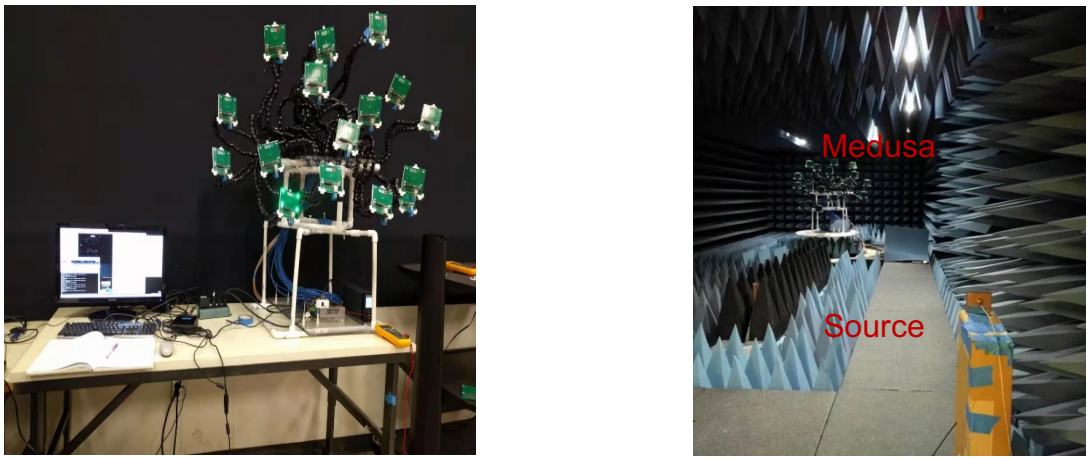

(a) (b)

Figure 46. Practical measurement schematic diagram: (a) Medusa test platform with patch antenna attached to 16 rotatable arms; (b) Test diagram with one source in the far field.

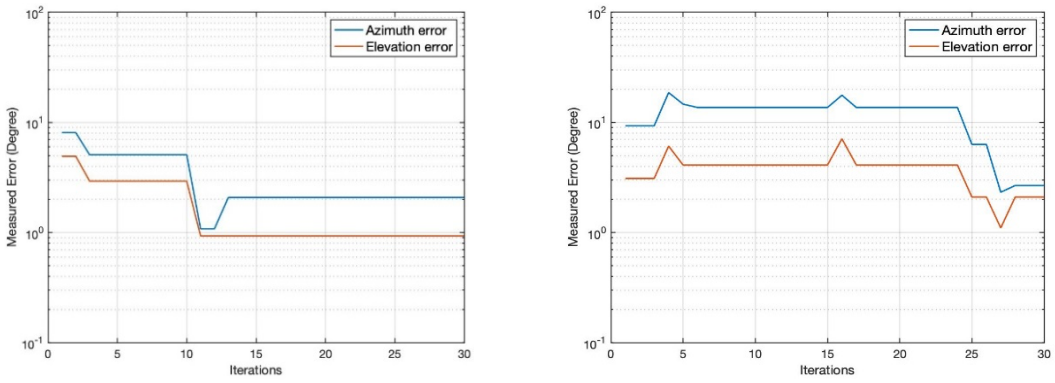

(a) (b)

Figure 47. DOA estimation RMSE of experiment vs. iterations: (a) without UAV rotation; (b) with random UAV rotation in a range of 0 to 45 degrees

5.8. Chapter Summary

This chapter statistically analyzes the performance of iterative-MUSIC algorithm for the MUSB array. We derive the closed-form AMSE formula of iterative-MUSIC in the presence of small and deterministic sensor gain, phase, and position errors, as well as the joint CRB formulas of sensor gain, phase, position errors, and DOAs for the MUSB array. We also extended the deterministic error model to stochastic error model with the Gaussian distribution case. Our results proof that the iterative-MUSIC algorithm has the advantages than the traditional MUSIC algorithm in the condition with low SNR and low snapshot case, as well as the iterative-MUSIC algorithm can eliminate the sensor gain, phase, and position errors.

6. CONCLUSION

This work has shown that it is possible to develop a signal model for the swarming array that includes sensor errors to account for both directional antenna radiation behavior (rotational errors) and position uncertainties (translational errors), and use this model to derive an iterative formulation of the MUSIC algorithm to study the convergence and fundamental statistical limitations of the swarming DOA estimation system and inform an experimental campaign that been able to successfully demonstrate and validate the key aspects of the system's behavior. We formulated the signal model to account for dynamic behavior of UAV swarm, developed framework for iterative MUSIC-based algorithm suitable for UAV swarm, derived closed-form asymptotic MSE and CRB expressions for statistical performance analysis of swarming array, and derived closed-form asymptotic MSE and CRB expressions with sensor gain, phase, and position errors to analyze the performance of swarming array theoretically (with experimental validation). Our results will benefit to future research on performance analysis and optimal design of time-varying antenna arrays based on UAV swarm.

REFERENCES

[1] R. O. Schmidt, “Multiple emitter location and signal parameter estimation,” IEEE Trans. Antennas Propag., vol. 34, pp. 276-280, 1986.

[2] Z. Xia, G. H. Huff, JF Chamberland, H. Pfister, and R. Bhattacharya, “Direction of arrival estimation using canonical and crystallographic volumetric element configurations,” The 6th European Conference Antenna and Propagation (EUCAP), Prague, 26-30 March 2012, pp. 1436-1439.

[3] D. Vu, A. Renaux, R. Boyer, and S. Marcos, "Performance analysis of 2D and 3D antenna arrays for source localization," Proc. European Signal Processing Conference, pp. 661-665, Aug. 2010.

[4] H. Hotta, M. Teshima, T. Amano, "Estimation of radio propagation parameters using antennas arrayed 3-Dimensional space," TEICE Technical Report, no. AP2005-87, Oct. 2005.

[5] A. J. Barabell. “Improving the resolution performance of eigenstructure-based direction-finding algorithms,” Proc. ICASSP. pp. 336-339, 1983.

[6] B. D. Rao and K. V. Hari, “Performance of analysis of root-MUSIC,” IEEE Trans. on ASSP. vol. 37(12), pp. 1939-1949, 1989.

[7] M. Rubsamen and A. B. Gershman. “Direction-of-arrival estimation for nonuniform sensor arrays: from manifold separation to Fourier domain MUSIC methods,” IEEE Trans. on SP. vol.57(2), pp. 588-599, 2009.

[8] N. R. Goodman, “Statistical analysis based on a certain multivariate complex distribution (an itroduction),” Ann. Math. Stat., vol. 34, pp. 152-177, Mar. 1963.

[9] Z. Chen, JF Chamberland, and G. H. Huff, “Impact of UAV swarm density and heterogeneity on synthetic aperture DoA convergence,” IEEE USNC-URSI Radio Science Meeting (Joint with AP-S Symposium), July 2017.

[10] B. Friedlander, and A. J. Weiss, “Direction finding in the presence of mutual coupling,” IEEE Trans. on APS, vol. 39(3), Mar. 1991.

[11] L. C. Godara and A. Cantoni, “Uniqueness and linear independence of steering vectors in array space,” J. Acoust. Soc. Amer., vol. 70(2), pp. 467–475, Aug. 1981.

[12] H. Gazzah, and K. Abed-Meraim, “Optimum ambiguity-free directional and omnidirectional planar antenna arrays for DOA estimation,” IEEE Trans. on SP. vol. 57(10), Oct. 2009.

[13] S. Kiani and A. M. Pezeshk, “A comparative study of several array geometries for 2D DOA estimation,” Procedia Computer Science. vol. 58, pp. 18-25, 2015.

[14] H. Moriya, Y. Doi, K. Ichige, and H. Arai, “Cuboid array: a novel 3-D array configuration for high resolution 2-D DOA estimation,” IEEE Workshop on Signal Processing Systems, 2013.

[15] H. Moriya, K. Ichige, H. Arai, T. Hayashi, H. Matsuno, and M. Nakano, “High resolution 2-D DOA estimation by 3-D array configuration based on CRLB formulation,” IEEE 11th ICSP Proceedings, 2012.

[16] S. Poormohammad and F. Farzaneh, “Precision of direction of arrival (DOA) estimation using novel 3-dimensional array geometries,” Int. J. Electron Comm. vol. 75, pp. 35-45, 2017.

[17] S. Asgari, A. M. Ali, T. C. Collier, Y. Yao, R. E. Hudson, K. Yao, and C. E. Taylor, “Theoretical and experimental study of DOA estimation using AML algorithm for an isotropic and non-isotropic 3D array,” SPIE the Int. Society for Optical Engineering, 2007.

[18] R. Zhang, S. Wang, X. Lu, W. Duan, and L. Cai, “Two-dimensional DoA estimation for multipath propagation characterization using the array response of PN sequences,” IEEE Trans. on Wireless Comm. vol. 15(1), pp. 341-356, Jan. 2016.

[19] L. Wan, L. Liu, G. Han, and J. Rodrigues, “A low energy consumption DOA estimation approach for conformal array in ultra-wideband,” Future Internet, vol. 5, pp. 611-630, 2013.

[20] Z. M. Liu and F. C. Guo, “Azimuth and elevation estimation with rotating long-baseline interferometers,” IEEE Trans. on SP. vol. 63(9), pp. 2405-2419, May 2015.

[21] Z. M. Liu, “Direction-of-arrival estimation with time-varying arrays via Bayesian multitask learning,” IEEE Trans. on Vehicular Tech, vol. 63(8), pp. 3762-3773, Oct. 2014.

[22] T. G. Dvorkind and E. Greenberg, “DOA estimation and signal separation sing antenna with time varying response,” IEEE 22th European EUSIPCO, 2014.

[23] A. Naaz and R. Rao, “DOA estimation-a comparative analysis,” Int. J. of Comp. and Comm. Eng. vol. 3(2), Mar. 2014.

[24] B. Demissie, M. Oispuu, and E. Ruthotto, “Localization of multiple sources with a moving array using subspace data fusion,” 11th Int. Conf. on Info. Fusion, 2008.

[25] J. R. Kendra, “Motion-extended array synthesis-part I: theory and method,” IEEE Trans. Geoscience Remote Sens., vol. 55, pp. 2028–2044, 2017.

[26] J. J. Corner and G. B. Lamont, “Parallel simulation of UAV swarm scenarios,” Proceedings of the 2004 Winter Simulation Conf.

[27] E. Saad, J. Vian, G. J. Clark, and S. Bieniawski, “Vehicle swarm rapid prototyping testbed,” Aerospace Research Conf., Apr. 2009.

[28] J. S. Petko, and D. H. Werner, “Positional tolerance analysis and error correction of micro-UAV swarm-based antenna arrays,” IEEE Antenna and propag. Society Int. Sympo., 2009.

[29] M. Almeida, H. Hildmann, and G. Solmaz, “Distributed UAV-swarm-based real-time geomatic data collection under dynamically changing resolution requirements,” The Int. Archives of Photogrammetry, Remote Sensing and Spatial Information Science, Vol. XLII-2/W6, pp. 5-12, 2017.

[30] F. Namin, J. S. Petko, and D. H. Werner, “Design of robust aperiodic antenna array formations for micro-UAV swarms,” IEEE APSURSI, 2010.

[31] F. Namin, J. S. Petko, and D. H. Werner, “Analysis and design optimization of robust aperiodic micro-UAV swarm-based antenna arrays,” IEEE Trans. on APS, vol. 60(5), pp. 2295-2308, May 2012.

[32] H. Hung and M. Kaveh, "On the statistical sufficiency of the coherently averaged covariance matrix for the estimation of the parameters of wide-band sources," IEEE Int. Conf. Acoust., Speech, Signal Processing, Mar. 1987, pp. 33-36.

[33] P. Stoica and A. Nehorai, "MODE, maximum likelihood, and Cramer-Rao bound: conditional and unconditional results," Center Syst. Sci., Yale University, New Haven, CT, Rep. 8901, Jan. 1989.

[34] P. Stoica and A. Nehorai, "Performance study of conditional and unconditional direction-of-arrival estimation," IEEE Trans. on Acoust. Speech. And Signal Processing, vol. 38(10), pp. 1783-1795, Oct. 1990.

[35] P. Stoica and A. Nehorai, "MUSIC, maximum likelihood, and Cramer-Rao bound," IEEE Trans. on Acoust. Speech. and Signal Processing, vol. 37(5), pp. 1783-1795, May 1989.

[36] P. Stoica and A. Nehorai, "MUSIC, maximum likelihood, and Cramer-Rao bound: further results and comparisons," IEEE Trans. on Acoust. Speech. and Signal Processing, vol. 38(12), pp. 2140-2150, Dec 1990.

[37] M. Zhang and Z. Zhu, "DOA estimation with sensor gain, phase, and position perturbations," Proc. of the IEEE NAECON, May 1993, pp. 24-28.

[38] Y. Yardimci and J. A. Cadzow, "Direction-of-arrival estimation under sensor location uncertainty," IEEE Intel. Conf. on Acoust. Speech. and Signal Proceeding, Apr. 1993, pp. 27-30.

[39] A. Ferreol, P. Lcarzabal and M. Viberg, “On the asymptotic performance analysis of subspace DOA estimation in the presence of modeling errors: case of MUSIC,” IEEE Trans. on Signal Processing, vol. 54(3), pp. 907-920, March 2006.

[40] K. C. Ho, X. Lu and L. Kovavisaruch, “Localization using TDOA and FDOA measurements in the presence of receiver location errors: analysis and solution,” IEEE Trans. on Signal Processing, vol. 55(2), pp. 684-696, Feb. 2007.

[41] F. Li and R. J. Vaccaro, “Sensitivity analysis of DOA estimation algorithms to sensor errors,” IEEE Trans. on Aerospace and Electronic System, vol. 28(3), pp. 708-717, Jul. 1992.

[42] X. Lu and K. C. Ho, “Analysis of the degradation in source location accuracy in the presence of sensor location error,” IEEE Intel. Conf. on Acoust. Speech. and Signal Proceeding, May 2006, pp. 925-928.

[43] A. Zeira and B. Friedlander, “Direction finding with time-varying arrays,” IEEE Trans. on Signal Processing, vol. 43(4), Apr. 1995.

[44] K. C. Ho, X. Lu and L. Kovavisaruch, “Source localization using TDOA and FDOA measurement in the presence of receiver location errors: analysis and solution,” IEEE Trans. on Signal Processing, vol. 55(2), pp. 684-696, Feb. 2007.

[45] A. Lee Swindlehurst and T. Kailath, “A performance analysis of subspace-based methods in the presence of model errors, part I: the MUSIC algorithm” IEEE Trans. on Signal Processing, vol. 40(7), pp. 1758-1774, July 1992.

[46] X. Lu and K. C. Ho. “Analysis of the degradation in source location accuracy in the presence of sensor location error,” IEEE ICASSP., pp. 925-928, 2006.

[47] B. D. Rao and K. V. Hari, “Direction of arrival estimation by eigenstructure methods with unknown sensor gain and phase,” IEEE ICASSP. pp. 640-643, 2003.

[48] A. P. Ng. “Direction-of-arrival estimates in the presence of wavelength, gain, and phase errors,” IEEE Trans. on SP. vol.43(1). pp. 225-232, 1995.

[49] Y. Yardimci, “Direction-of-arrival estimation under sensor location uncertainty,” IEEE ICASSP, pp. 312-315, 1993.

[50] A. Ferreol, P. Larzabal, and M. Viberg, “Statistical analysis of the MUSIC algorithm in the presence of modeling errors, taking into account the resolution probability,” IEEE Trans. on SP. vol.58(8). pp. 4156-4166, 2010.

[51] M. Wang and A. Nehorai, “Coarrays, MUSIC, and the Cramer-Rao bound,” IEEE Trans. on SP, vol. 65(4), pp. 933-946, Nov. 2016.

[52] M. Wang, Z. Zhang, and A. Nehorai, “Performance analysis of coarray-based MUSIC in the presence of sensor location errors,” IEEE Trans. on SP, vol. 66(12), pp. 3074-3085, Apr. 2018.

[53] D. Rieken and D. Fuhrmann, “Generalizing MUSIC and MVDR for multiple noncoherent arrays,” IEEE Signal Processing Letters, vol. 52(9), Sep. 2004.

[54] F. Wen, Q. Wan, R. Fan, and H. Wei, “Improved MUSIC algorithm for multiple noncoherent subarrays,” IEEE Signal Processing Letters, vol. 21(5), May 2014.

[55] Z. Chen, Y. Yeh, JF Chamberland, and G. H. Huff, “A sensor-driven analysis of distributed direction-finding systems based on UAV swarms,” MDPI Sensors, vol.19(12), pp. 2659-2677, 2019.

[56] Z. Chen, S. Yeh, JF Chamberland, and G. H. Huff, “Impact of position errors on synthetic aperture DOA convergence based on swarming UAVs,” IEEE USNC-URSI Radio Science Meeting (Joint with AP-S Symposium), July 2020.

[57] S. Yeh, “Volumetric random phased arrays and their applications,” Ph.D. dissertation, Department of Electrical and Computer Engineering, Texas A&M University, College Station, Texas, 2018.

APPENDIX A

THE DOA ESTIMATION ERROR OF ITERATIVE-MUSIC

The eigendecomposition of R_i at *i*-th iteration is given by

$$R_i = Q_{s,i}\Lambda_{s,i}Q_{s,i}^H + Q_{n,i}\Lambda_{n,i}Q_{n,i}^H \tag{111}$$

where $Q_{s,i}$ and $Q_{n,i}$ are the eigenvectors of the signal subspace and noise subspace, and $\Lambda_{s,i}$, $\Lambda_{n,i}$ are the corresponding eigen values in the *i*-th iteration. Here we have $\Lambda_{n,i} = \sigma_i^2 I_0$.

Let $\tilde{R}_i = R_i + \Delta R_i$, $\tilde{Q}_{s,i} = Q_{s,i} + \Delta Q_{s,i}$, and $\tilde{\Lambda}_{n,i} = \Lambda_{n,i} + \Delta\Lambda_{n,i}$ be the perturbed versions of $R_i, Q_{s,i}$, and $\Lambda_{n,i}$. If the perturbation is small, we can omit the high-order terms and obtain [48], [49], [50]

$$A_i^H \Delta Q_{n,i} \doteq -S_i^{-1} A_i^{\dagger} \Delta R_i Q_{n,i} \tag{112}$$

Since *S* is diagonal, we have

$$a_i^H(\alpha_n)\Delta Q_{n,i} \doteq -s_n^{-1} e_n^T A_i^{\dagger} \Delta R_i Q_{n,i} \tag{113}$$

where e_n is the *n*-th column of the identity matrix $I_{n\times n}$.

The MUSIC spectrum in the *i*-th iteration is defined as

$$f_i(\alpha) = a_i^H(\alpha)\hat{Q}_{n,i}\hat{Q}_{n,i}^H a_i(\alpha) \tag{114}$$

Since the MUSIC spectrum in different iteration is independent, the total MUSIC spectrum is

$$f(\alpha)=\sum_{i=1}^{I} f_i(\alpha) \tag{115}$$

As $\hat{\alpha}_n$ is a minimum point of $f(\alpha)$, we must have

$$f'(\hat{\alpha}_n)=0 \tag{116}$$

where

$$f'(\hat{\alpha}_n)\triangleq \left.\frac{df(\alpha)}{d\alpha}\right|_{\alpha=\hat{\alpha}_n} = \sum_{i=1}^{I} f_i'(\alpha_n) \tag{117}$$

In order to analyze the distribution of the estimation errors $\{\hat{\alpha}_n-\alpha_n\}$, we have

$$0=f'(\hat{\alpha}_n)\doteq f'(\alpha_n)+f''(\alpha_n)(\hat{\alpha}_n-\alpha_n) \tag{118}$$

Following the conclusion in paper [47, Appendix B], we can obtain

$$\begin{aligned} f_i'(\hat{\alpha}_n) &= d_i^H(\hat{\alpha}_n)\hat{Q}_{n,i}\hat{Q}_{n,i}^H a_i(\hat{\alpha}_k)+a_i^H(\hat{\alpha}_n)\hat{Q}_{n,i}\hat{Q}_{n,i}^H d_i(\hat{\alpha}_n) \\ &= 2\,\mathrm{Re}\left[a_i^H(\hat{\alpha}_n)\hat{Q}_{n,i}\hat{Q}_{n,i}^H d_i(\hat{\alpha}_n)\right] \\ &\doteq 2\,\mathrm{Re}\left[a_i^H(\hat{\alpha}_n)\Delta Q_{n,i}Q_{n,i}^H d_i(\hat{\alpha}_n)\right] \end{aligned} \tag{119}$$

$$\begin{aligned} f_i''(\alpha_k) &= 2\,\mathrm{Re}\left[d_i^H(\alpha_n)\hat{Q}_n\hat{Q}_n^H d_i(\alpha_n)+a_i^H(\alpha_n)\hat{Q}_n\hat{Q}_n^H d_i'(\alpha_n)\right] \\ &\doteq 2\left[d_i^H(\alpha_n)Q_nQ_n^H d_i(\alpha_n)\right] \end{aligned} \tag{120}$$

Substituting (20) into (26) gives

$$f_i'(\hat{\alpha}_n)\doteq -2\,\mathrm{Re}\left[s_n^{-1}e_n^T A_i^{\dagger}\Delta R_i Q_{n,i}Q_{n,i}^H d_i(\alpha_n)\right] \tag{121}$$

Therefore, the estimation errors are

$$\begin{aligned}\left(\hat{\alpha}_n-\alpha_n\right) &\doteq -\frac{f'\left(\alpha_n\right)}{f''\left(\alpha_n\right)} \\ &\doteq \frac{\sum_{i=1}^{I} 2\,\mathrm{Re}\left[s_n^{-1} e_n^T A_i^{\dagger}\Delta R_i Q_{n,i} Q_{n,i}^H d_i\left(\alpha_n\right)\right]}{\sum_{i=1}^{I} 2\left[d_i^H\left(\alpha_n\right) Q_{n,i} Q_{n,i}^H d_i\left(\alpha_n\right)\right]}\end{aligned} \tag{122}$$

Use notations in (14) and $vec\left(AXB\right)=\left(B^T\otimes A\right)vec\left(X\right)$, we have

$$\left(\hat{\alpha}_n-\alpha_n\right) \doteq -\left(s_n\rho_n\right)^{-1}\sum_{i=1}^{I}\mathrm{Re}\left(\xi_{i,n}^T\Delta r_i\right) \tag{123}$$

where $\Delta r_i = vec\left(\Delta R_i\right)$, and it completes the proof.

APPENDIX B

THE AMSE OF ITERATIVE-MUSIC

We will derive the asymptotic MSE of iterative-MUSIC without sensor location errors, sensor gain, and phase errors, which follows from (30) that

$$\begin{aligned} & E\left[\left(\hat{\alpha}_{n1}-\alpha_{n1}\right)\left(\hat{\alpha}_{n2}-\alpha_{n2}\right)\right] \\ &= \left(s_{n1}\rho_{n1}\right)^{-1}\left(s_{n2}\rho_{n2}\right)^{-1} E\left[\sum_{i=1}^{I}\mathrm{Re}\left(\xi_{i,n1}^{T}\Delta r_i\right)\sum_{j=1}^{I}\mathrm{Re}\left(\xi_{j,n2}^{T}\Delta r_j\right)^{T}\right] \\ &= \left(s_{n1}\rho_{n1}\right)^{-1}\left(s_{n2}\rho_{n2}\right)^{-1}\sum_{i=1}^{I}\sum_{j=1}^{I}E\left[\mathrm{Re}\left(\xi_{i,n1}^{T}\Delta r_i\right)\mathrm{Re}\left(\xi_{j,n2}^{T}\Delta r_j\right)^{T}\right] \\ &= \left(s_{n1}\rho_{n1}\right)^{-1}\left(s_{n2}\rho_{n2}\right)^{-1}\sum_{i=1}^{I}E\left[\mathrm{Re}\left(\xi_{i,n1}^{T}\Delta r_i\right)\mathrm{Re}\left(\xi_{i,n2}^{T}\Delta r_i\right)^{T}\right] \end{aligned} \tag{124}$$

The last term in (31) is derived because $E\left[\mathrm{Re}\left(\xi_{i,n1}^{T}\Delta r_i\right)\mathrm{Re}\left(\xi_{j,n2}^{T}\Delta r_j\right)^{T}\right]=0$ if $i\neq j$ [50]. Then, based the conclusion in [50, Appendix C], we have

$$E\left[\mathrm{Re}\left(\xi_{i,n1}^{T}\Delta r_i\right)\mathrm{Re}\left(\xi_{i,n2}^{T}\Delta r_i\right)^{T}\right]=\frac{1}{K_i}\mathrm{Re}\left(\xi_{i,n1}^{H}\left(R_i\otimes R_i^{T}\right)\xi_{i,n2}\right) \tag{125}$$

Therefore, substituting (32) into (31) we can obtain

$$E\left[\left(\hat{\alpha}_{n1}-\alpha_{n1}\right)\left(\hat{\alpha}_{n2}-\alpha_{n2}\right)\right]=\left(s_{n1}\rho_{n1}\right)^{-1}\left(s_{n2}\rho_{n2}\right)^{-1}\sum_{i=1}^{I}\frac{1}{K_i}\mathrm{Re}\left(\xi_{i,n1}^{H}\left(R_i\otimes R_i^{T}\right)\xi_{i,n2}\right) \tag{126}$$

which completes the proof.

APPENDIX C

THE CRB FOR TIME-VARYING ARRAY WRT 2D DOAS

Referred to [34], the stochastic FIM's F_θ with respect to 1D incident angle θ of static array is available:

$$F_\theta = CRB^{-1} = \frac{2K}{\sigma^2}\left\{\mathrm{Re}\left[H \odot U\right]\right\} \tag{127}$$

Where $H = D^H\left[I_0 - A\left(A^H A\right)^{-1} A^H\right]D$, $D = \left[d_1, d_2, \cdots d_N\right]$, $d_n = \frac{da(\theta)}{d\theta}|_{\theta=\theta_n}$, and $U = PA^H R^{-1} AP$.

For each iteration, the FIM's for the presented problem in this paper is given by

$$F_{i,\theta} = CRB_{i,\theta}{}^{-1} = \frac{2K}{\sigma^2}\left\{\mathrm{Re}\left[H_i \odot U_i\right]\right\} \tag{128}$$

where $H_i = D_i^H\left[I_0 - A_i\left(A_i^H A_i\right)^{-1} A_i^H\right]D_i$, $D_i = \left[d_{i,1}, d_{i,2}, \cdots d_{i,N}\right]$, $d_{i,n} = \frac{da_i(\theta)}{d\theta}|_{\theta=\theta_n}$, and $U_i = P_i A_i^H R_i^{-1} A_i P_i$.

As already stated,

$$F_\theta = \sum_{i=1}^{I} F_{i,\theta} \tag{129}$$

Omitting to the parameters $\mathrm{Re}\left(P_{mn}\right)$, $\mathrm{Im}\left(P_{mn}\right)$, σ^2, gain and phase of the signals, only consider the estimation of the elevation and azimuth angles (θ_n, ϕ_n)hereby is given by

$$\alpha = \left[\theta^T,\ \phi^T\right]^T \tag{130}$$

$$\theta=\left[\theta_1,\theta_2,\cdots\theta_N\right]^T;\ \phi=\left[\phi_1,\phi_2,\cdots\phi_N\right]^T \tag{131}$$

Thus, the submatrix of FIM associated with 2D DOA is

$$F_{i,s,2}=\begin{bmatrix}F_{i,\theta\theta}F_{i,\theta\phi}\\F_{i,\phi\theta}F_{i,\phi\phi}\end{bmatrix}=\frac{2K}{\sigma^2}\left\{\mathrm{Re}\left[D_i^H A_i^{\perp}D_i\odot 1_2 1_2^T\otimes U_i\right]\right\} \tag{132}$$

where "*i, s, 2*" denotes the 2D stochastic bound for the *i*th iteration, 1_2 represents 2x1 vectors of ones and

$$F_{i,\theta\theta}=\frac{2K}{\sigma^2}\left\{\mathrm{Re}\left[D_i^H(\theta)A_i^{\perp}D_i(\theta)\odot U_i\right]\right\} \tag{133}$$

$$F_{i,\theta\phi}=\frac{2K}{\sigma^2}\left\{\mathrm{Re}\left[D_i^H(\theta)A_i^{\perp}D_i(\phi)\odot U_i\right]\right\} \tag{134}$$

$$F_{i,\phi\theta}=\frac{2K}{\sigma^2}\left\{\mathrm{Re}\left[D_i^H(\phi)A_i^{\perp}D_i(\theta)\odot U_i\right]\right\} \tag{135}$$

$$F_{i,\phi\phi}=\frac{2K}{\sigma^2}\left\{\mathrm{Re}\left[D_i^H(\phi)A_i^{\perp}D_i(\phi)\odot U_i\right]\right\} \tag{136}$$

where $A_i(\theta,\phi)=\left[a_i(\theta_1,\phi_1),a_i(\theta_2,\phi_2),\cdots,a_i(\theta_N,\phi_N)\right]$. Thus, the system stochastic FIM is given by

$$F_{s,2}=\sum_{i=1}^{I}F_{i,s,2}=\begin{bmatrix}F_{\theta\theta}&F_{\theta\phi}\\F_{\phi\theta}&F_{\phi\phi}\end{bmatrix} \tag{137}$$

where $F_{\theta\theta}=\sum_{i=1}^{I}F_{i,\theta\theta}$, $F_{\theta\phi}=\sum_{i=1}^{I}F_{i,\theta\phi}$, $F_{\phi\theta}=\sum_{i=1}^{I}F_{i,\phi\theta}$, $F_{\phi\phi}=\sum_{i=1}^{I}F_{i,\phi\phi}$.

APPENDIX D

THE CRB OF 3D RANDOM ARRAY WRT JOINT SENSOR GAIN, PHASES, AND DOAS

Referred to [35], the likelihood function of the data is given by

$$L\left[x(1),\cdots,x(K)\right] = \frac{1}{(2\pi)^{mK}(\sigma/2)^{mK}}\exp\left\{-\frac{1}{\sigma}\sum_{k=1}^{K}\left[x(k)-As(k)\right]^{H}\cdot\left[x(k)-As(k)\right]\right\} \tag{138}$$

where σ is the variance of noise. Thus, the log-likelihood function is

$$\ln L = const - mK\ln\sigma - \frac{1}{\sigma}\sum_{k=1}^{K}\left[x^{H}(k)-s^{H}(k)A^{H}\right]\cdot\left[x(k)-As(k)\right] \tag{139}$$

First, we calculate the derivatives of (135) with respect to σ, $\left\{\overline{x}(k)\right\} \triangleq \mathrm{Re}\,x(k)$, $\left\{\tilde{x}(k)\right\} \triangleq \mathrm{Im}\,x(k)$, g, ψ, θ and ϕ. We have

$$\frac{\partial \ln L}{\partial \sigma} = \frac{mK}{\sigma} + \frac{1}{\sigma^{2}}\sum_{k=1}^{K} w^{H}(k)w(k) \tag{140}$$

$$\frac{\partial \ln L}{\partial \overline{x}(t)} = \frac{1}{\sigma}\left[A^{H}w(k) + A^{T}w^{+}(k)\right] = \frac{2}{\sigma}\mathrm{Re}\left[A^{H}w(k)\right] \tag{141}$$

$$\frac{\partial \ln L}{\partial \tilde{x}(t)} = \frac{1}{\sigma}\left[-iA^{H}w(k) + iA^{T}w^{+}(k)\right] = \frac{2}{\sigma}\mathrm{Im}\left[A^{H}w(k)\right] \tag{142}$$

$$\frac{\partial \ln L}{\partial g} = \frac{2}{\sigma}\sum_{k=1}^{K}\mathrm{Re}\left[s^{H}(k)\frac{dA^{H}}{dg}w(k)\right] = \frac{2}{\sigma}\sum_{k=1}^{K}\mathrm{Re}\left[s_{i}^{H}(k)d^{H}(g_{i})w(k)\right] \tag{143}$$

which can be written more compactly as

$$\frac{\partial \ln L}{\partial g} = \frac{2}{\sigma}\sum_{k=1}^{K} \mathrm{Re}\left[s^H(k) D_g^H w(k) \right] \tag{144}$$

Since $A = G\Psi\tilde{A}$, thus,

$$\frac{\partial \ln L}{\partial \psi} = \frac{2}{\sigma}\sum_{k=1}^{K} \mathrm{Re}\left[s^H(k) D_\psi^H w(k) \right] \tag{145}$$

$$\frac{\partial \ln L}{\partial \theta} = \frac{2}{\sigma}\sum_{k=1}^{K} \mathrm{Re}\left[s^H(k) D_\theta^H w(k) \right] \tag{146}$$

$$\frac{\partial \ln L}{\partial \phi} = \frac{2}{\sigma}\sum_{k=1}^{K} \mathrm{Re}\left[s^H(k) D_\phi^H w(k) \right] \tag{147}$$

To proceed, we need the following four results.

$$R1: Ew^H(k) w(k) w^H(t) w(t) = \begin{cases} m^2\sigma^2 & for\, k \neq t \\ m(m+1)\sigma^2 & for\, k = t \end{cases} \tag{148}$$

$$R2: Ew^H(k) w(k) w^T(t) = 0 \text{ for all } k \text{ and } t \tag{149}$$

$$\begin{aligned} R3: \mathrm{Re}(x)\mathrm{Re}(y^T) &= \frac{1}{2}\left[\mathrm{Re}(xy^T) + \mathrm{Re}(xy^H) \right] \\ \mathrm{Im}(x)\mathrm{Im}(y^T) &= -\frac{1}{2}\left[\mathrm{Re}(xy^T) - \mathrm{Re}(xy^H) \right] \\ \mathrm{Re}(x)\mathrm{Im}(y^T) &= \frac{1}{2}\left[\mathrm{Im}(xy^T) - \mathrm{Im}(xy^H) \right] \end{aligned} \tag{150}$$

R4: Let H be a nonsingular complex matrix and denote its inverse by $B = H^{-1}$. Then

$$\begin{bmatrix} \bar{H} & -\tilde{H} \\ \tilde{H} & \bar{H} \end{bmatrix}^{-1} = \begin{bmatrix} \bar{B} & -\tilde{B} \\ \tilde{B} & \bar{B} \end{bmatrix} \tag{151}$$

Those four rules are proved in [37, Appendix E]

Turn now to the evaluation of the CRB covariance matrix, which is given by

$$\Omega = \left(E\varphi\varphi^T \right)^{-1} \tag{152}$$

where

$$\varphi^T = \partial \ln L \Big/ \partial \left[\sigma \overline{s}^T(1) \overline{s}^T(1) \cdots \tilde{s}^T(K) \tilde{s}^T(K) g^T \cdot \psi^T \theta^T \phi^T \right] \tag{153}$$

Using R1, we obtain

$$\begin{aligned} & E\left[\frac{\partial \ln L}{\partial \sigma} \right]^2 \\ & = \frac{m^2 K^2}{\sigma^2} - 2\frac{mK}{\sigma^3} \sum_{k=1}^{K} E w^H(k) w(k) + \frac{1}{\sigma^4} \sum_{k=1}^{K} \sum_{t=1}^{K} E w^H(k) w(k) w^H(t) w(t) \\ & = \frac{m^2 K^2}{\sigma^2} - 2\frac{m^2 K^2}{\sigma^2} + \frac{Km}{\sigma^2} \left[(K-1)m + (m+1) \right] = \frac{mK}{\sigma^2} \end{aligned} \tag{154}$$

Using R2, we note that $\partial \ln L / \partial \sigma$ is not correlated with any of the other derivatives.

Next, we use R3 and the fact that $E w(k) w^T(t) = 0$ for all *k* and *t* to obtain

$$E\left[\frac{\partial \ln L}{\partial \overline{s}(p)} \right] \left[\frac{\partial \ln L}{\partial \overline{s}(t)} \right]^T = \frac{4}{\sigma^2} \frac{1}{2} \mathrm{Re}\left[E A^H w(p) w^H(t) A \right] = \frac{2}{\sigma} \mathrm{Re}\left[A^H A \right] \delta_{p,t} \tag{155}$$

$$E\left[\frac{\partial \ln L}{\partial \overline{s}(p)} \right] \left[\frac{\partial \ln L}{\partial \tilde{s}(t)} \right]^T = -\frac{4}{\sigma^2} \frac{1}{2} \mathrm{Im}\left[E A^H w(p) w^H(t) A \right] = -\frac{2}{\sigma} \mathrm{Im}\left[A^H A \right] \delta_{p,t} \tag{156}$$

$$E\left[\frac{\partial \ln L}{\partial \overline{s}(t)} \right] \left[\frac{\partial \ln L}{\partial g} \right]^T = \frac{4}{\sigma^2} \sum_{k=1}^{K} \frac{1}{2} \mathrm{Re}\left[E A^H w(t) w^H(k) D_g s(k) \right] = \frac{2}{\sigma} \mathrm{Re}\left[D_g s(t) \right] \tag{157}$$

$$E\left[\frac{\partial \ln L}{\partial \overline{s}(t)} \right] \left[\frac{\partial \ln L}{\partial \psi} \right]^T = \frac{4}{\sigma^2} \sum_{k=1}^{K} \frac{1}{2} \mathrm{Re}\left[E A^H w(t) w^H(k) D_\psi S(k) \right] = \frac{2}{\sigma} \mathrm{Re}\left[A^H D_\psi S(t) \right] \tag{158}$$

$$E\left[\frac{\partial \ln L}{\partial \overline{s}(t)} \right] \left[\frac{\partial \ln L}{\partial \theta} \right]^T = \frac{4}{\sigma^2} \sum_{k=1}^{K} \frac{1}{2} \mathrm{Re}\left[E A^H w(t) w^H(k) D_\theta S(k) \right] = \frac{2}{\sigma} \mathrm{Re}\left[A^H D_\theta S(t) \right] \tag{159}$$

$$E\left[\frac{\partial \ln L}{\partial \tilde{s}(p)}\right]\left[\frac{\partial \ln L}{\partial \tilde{s}(t)}\right]^T = \frac{4}{\sigma^2}\frac{1}{2}\mathrm{Re}\left[EA^H w(p) w^H(t) A\right] = \frac{2}{\sigma}\mathrm{Re}\left[A^H A\right]\delta_{p,t} \tag{160}$$

$$\begin{aligned} E\left[\frac{\partial \ln L}{\partial \tilde{s}(p)}\right]\left[\frac{\partial \ln L}{\partial g}\right]^T &= \frac{4}{\sigma^2}\sum_{k=1}^{K}\left(-\frac{1}{2}\right)\mathrm{Im}\left[ES^H(k) D_g^H A^H w(k) w^H(p) A\right]^T \\ &= -\frac{2}{\sigma}\mathrm{Im}\left[S^H(p) D_g^H A\right]^T = \frac{2}{\sigma}\mathrm{Im}\left[A^H D_g S(p)\right] \end{aligned} \tag{161}$$

$$E\left[\frac{\partial \ln L}{\partial \tilde{s}(p)}\right]\left[\frac{\partial \ln L}{\partial \psi}\right]^T = \frac{2}{\sigma}\mathrm{Im}\left[A^H D_\psi S(p)\right] \tag{162}$$

$$E\left[\frac{\partial \ln L}{\partial \tilde{s}(p)}\right]\left[\frac{\partial \ln L}{\partial \theta}\right]^T = \frac{2}{\sigma}\mathrm{Im}\left[A^H D_\theta S(p)\right] \tag{163}$$

$$\begin{aligned} E\left[\frac{\partial \ln L}{\partial g}\right]\left[\frac{\partial \ln L}{\partial g}\right]^T &= \frac{4}{\sigma^2}\frac{1}{2}\sum_{k=1}^{K}\sum_{p=1}^{K}\mathrm{Re}\left[ES^H(k) D_g^H \cdot w(k) w^H(p) D S(p)\right] \\ &= \frac{2}{\sigma}\sum_{k=1}^{K}\mathrm{Re}\left[S^H(k) D_g^H D_g S(k)\right] = F_{gg} \end{aligned} \tag{164}$$

$$E\left[\frac{\partial \ln L}{\partial g}\right]\left[\frac{\partial \ln L}{\partial \psi}\right]^T = \frac{2}{\sigma}\sum_{k=1}^{K}\mathrm{Re}\left[S^H(k) D_g^H D_\psi S(k)\right] = F_{g\psi} \tag{165}$$

$$E\left[\frac{\partial \ln L}{\partial g}\right]\left[\frac{\partial \ln L}{\partial \theta}\right]^T = \frac{2}{\sigma}\sum_{k=1}^{K}\mathrm{Re}\left[S^H(k) D_g^H D_\theta S(k)\right] = F_{g\theta} \tag{166}$$

$$E\left[\frac{\partial \ln L}{\partial \psi}\right]\left[\frac{\partial \ln L}{\partial \psi}\right]^T = \frac{2}{\sigma}\sum_{k=1}^{K}\mathrm{Re}\left[S^H(k) D_\psi^H D_\psi S(k)\right] = F_{\psi\psi} \tag{167}$$

$$E\left[\frac{\partial \ln L}{\partial \psi}\right]\left[\frac{\partial \ln L}{\partial \theta}\right]^T = \frac{2}{\sigma}\sum_{k=1}^{K}\mathrm{Re}\left[S^H(k) D_\psi^H D_\theta S(k)\right] = F_{\psi\theta} \tag{168}$$

$$E\left[\frac{\partial \ln L}{\partial \theta}\right]\left[\frac{\partial \ln L}{\partial \theta}\right]^T = \frac{2}{\sigma}\sum_{k=1}^{K}\mathrm{Re}\left[S^H(k) D_\theta^H D_\theta S(k)\right] = F_{\theta\theta} \tag{169}$$

Note the following notations: $\text{var}_{CR}(\sigma) = \sigma^2 / mK$, $H = \frac{2}{\sigma} A^H A$, $B = H^{-1}$, and

$$\Delta_{gk} = \frac{2}{\sigma} A^H D_g S(k) \qquad \Delta_{\psi k} = \frac{2}{\sigma} A^H D_\psi S(k)$$

$$\Delta_{\theta k} = \frac{2}{\sigma} A^H D_\theta S(k) \qquad \Delta_{\phi k} = \frac{2}{\sigma} A^H D_\phi S(k)$$

Observe that since the matrix H is Hermitian, its imaginary part must be skew-symmetric $\tilde{H}^T = -\tilde{H}$. Using the notation above, we get

$$\Omega = \begin{bmatrix} \text{var}_{CR}^{-1}(\sigma) & 0 & 0 & 0 & 0 & 0 & 0 & 0 \\ 0 & \begin{matrix} \bar{H} & -\tilde{H} \\ \tilde{H} & \bar{H} \end{matrix} & 0 & 0 & \begin{matrix} \bar{\Delta}_{g1} \\ \bar{\Delta}_{g1} \end{matrix} & \begin{matrix} \bar{\Delta}_{\psi 1} \\ \bar{\Delta}_{\psi 1} \end{matrix} & \begin{matrix} \bar{\Delta}_{\theta 1} \\ \bar{\Delta}_{\theta 1} \end{matrix} & \begin{matrix} \bar{\Delta}_{\phi 1} \\ \bar{\Delta}_{\phi 1} \end{matrix} \\ 0 & 0 & \ddots & 0 & \vdots & \vdots & \vdots & \vdots \\ 0 & 0 & 0 & \begin{matrix} \bar{H} & -\tilde{H} \\ \tilde{H} & \bar{H} \end{matrix} & \begin{matrix} \bar{\Delta}_{gK} \\ \bar{\Delta}_{gK} \end{matrix} & \begin{matrix} \bar{\Delta}_{\psi K} \\ \bar{\Delta}_{\psi K} \end{matrix} & \begin{matrix} \bar{\Delta}_{\theta K} \\ \bar{\Delta}_{\theta K} \end{matrix} & \begin{matrix} \bar{\Delta}_{\phi K} \\ \bar{\Delta}_{\phi K} \end{matrix} \\ 0 & \bar{\Delta}_{g1}^T & \tilde{\Delta}_{g1}^T & \cdots & \bar{\Delta}_{gK}^T & \tilde{\Delta}_{gK}^T & F_{gg} & F_{g\psi} & F_{g\theta} & F_{g\phi} \\ 0 & \bar{\Delta}_{\psi 1}^T & \tilde{\Delta}_{\psi 1}^T & \cdots & \bar{\Delta}_{\psi K}^T & \tilde{\Delta}_{\psi K}^T & F_{\psi g} & F_{\psi\psi} & F_{\psi\theta} & F_{\psi\phi} \\ 0 & \bar{\Delta}_{\theta 1}^T & \tilde{\Delta}_{\theta 1}^T & \cdots & \bar{\Delta}_{\theta K}^T & \tilde{\Delta}_{\theta K}^T & F_{\theta g} & F_{\theta\psi} & F_{\theta\theta} & F_{\theta\phi} \\ 0 & \bar{\Delta}_{\phi 1}^T & \tilde{\Delta}_{\phi 1}^T & \cdots & \bar{\Delta}_{\phi K}^T & \tilde{\Delta}_{\phi K}^T & F_{\phi g} & F_{\theta\phi} & F_{\phi\theta} & F_{\phi\phi} \end{bmatrix}^{-1} \tag{170}$$

The expression for $\text{var}_{CR}^{-1}(\sigma)$ is proven. Then we use the standard result on the inverse of a partitioned matrix, and R4 to obtain the CRB.

$$CRB^{-1}\left(g,\psi,\theta,\phi\right)=\begin{bmatrix} F_{gg} & F_{g\psi} & F_{g\theta} & F_{g\phi} \\ F_{\psi g} & F_{\psi\psi} & F_{\psi\theta} & F_{\psi\phi} \\ F_{\theta\psi} & F_{\theta\psi} & F_{\theta\theta} & F_{\theta\phi} \\ F_{\phi g} & F_{\theta\phi} & F_{\phi\theta} & F_{\phi\phi} \end{bmatrix}-\begin{bmatrix} \overline{\Delta}_{g1}^{T} & \tilde{\Delta}_{g1}^{T} & \cdots & \overline{\Delta}_{gK}^{T} & \tilde{\Delta}_{gK}^{T} \\ \overline{\Delta}_{\psi 1}^{T} & \tilde{\Delta}_{\psi 1}^{T} & \cdots & \overline{\Delta}_{\psi K}^{T} & \tilde{\Delta}_{\psi K}^{T} \\ \overline{\Delta}_{\theta 1}^{T} & \tilde{\Delta}_{\theta 1}^{T} & \cdots & \overline{\Delta}_{\theta K}^{T} & \tilde{\Delta}_{\theta K}^{T} \\ \overline{\Delta}_{\phi 1}^{T} & \tilde{\Delta}_{\phi 1}^{T} & \cdots & \overline{\Delta}_{\phi K}^{T} & \tilde{\Delta}_{\phi K}^{T} \end{bmatrix}$$
$$\cdot\begin{bmatrix} \overline{B} & -\tilde{B} & & 0 & \\ \tilde{B} & \overline{B} & & & 0 \\ & 0 & \ddots & & \\ & & & \overline{B} & -\tilde{B} \\ & 0 & & \tilde{B} & \overline{B} \end{bmatrix}\begin{bmatrix} \overline{\Delta}_{g1} & \overline{\Delta}_{\psi 1} & \overline{\Delta}_{\theta 1} & \overline{\Delta}_{\phi 1} \\ \tilde{\Delta}_{g1} & \tilde{\Delta}_{\psi 1} & \tilde{\Delta}_{\theta 1} & \tilde{\Delta}_{\phi 1} \\ \vdots & \vdots & \vdots & \vdots \\ \overline{\Delta}_{gK} & \overline{\Delta}_{\psi K} & \overline{\Delta}_{\theta K} & \overline{\Delta}_{\phi K} \\ \tilde{\Delta}_{gK} & \tilde{\Delta}_{\psi K} & \tilde{\Delta}_{\theta K} & \tilde{\Delta}_{\phi K} \end{bmatrix} \tag{171}$$

Next, observe that

$$\begin{bmatrix} \overline{B} & -\tilde{B} \\ \tilde{B} & \overline{B} \end{bmatrix}\begin{bmatrix} \overline{\Delta}_{g} & \overline{\Delta}_{\psi} & \overline{\Delta}_{\theta} & \overline{\Delta}_{\phi} \\ \tilde{\Delta}_{g} & \tilde{\Delta}_{\psi} & \tilde{\Delta}_{\theta} & \tilde{\Delta}_{\phi} \end{bmatrix}$$
$$=\begin{bmatrix} \overline{B}\overline{\Delta}_{g}-\tilde{B}\tilde{\Delta}_{g} & \overline{B}\overline{\Delta}_{g}-\tilde{B}\tilde{\Delta}_{g} & \overline{B}\overline{\Delta}_{g}-\tilde{B}\tilde{\Delta}_{g} & \overline{B}\overline{\Delta}_{g}-\tilde{B}\tilde{\Delta}_{g} \\ \tilde{B}\overline{\Delta}_{g}+\overline{B}\tilde{\Delta}_{g} & \tilde{B}\overline{\Delta}_{g}+\overline{B}\tilde{\Delta}_{g} & \tilde{B}\overline{\Delta}_{g}+\overline{B}\tilde{\Delta}_{g} & \tilde{G}\overline{\Delta}_{g}+\overline{B}\tilde{\Delta}_{g} \end{bmatrix} \tag{172}$$
$$=\begin{bmatrix} \overline{B\Delta_{g}} & \overline{B\Delta_{\psi}} & \overline{B\Delta_{\theta}} & \overline{B\Delta_{\phi}} \\ \widetilde{B\Delta_{g}} & \widetilde{B\Delta_{\psi}} & \widetilde{B\Delta_{\theta}} & \widetilde{B\Delta_{\phi}} \end{bmatrix}$$

and that

$$\begin{aligned}
&\begin{bmatrix} \overline{\Delta}_g^T & \tilde{\Delta}_g^T \\ \overline{\Delta}_\psi^T & \tilde{\Delta}_\psi^T \\ \overline{\Delta}_\theta^T & \tilde{\Delta}_\theta^T \\ \overline{\Delta}_\phi^T & \tilde{\Delta}_\phi^T \end{bmatrix} \begin{bmatrix} \overline{B\Delta_g} & \overline{B\Delta_\psi} & \overline{B\Delta_\theta} & \overline{B\Delta_\phi} \\ \widetilde{B\Delta_g} & \widetilde{B\Delta_\psi} & \widetilde{B\Delta_\theta} & \widetilde{B\Delta_\phi} \end{bmatrix} \\
&= \mathrm{Re}\begin{bmatrix} \Delta_g^H B\Delta_g & \Delta_g^H B\Delta_\psi & \Delta_g^H B\Delta_\theta & \Delta_g^H B\Delta_\phi \\ \Delta_\psi^H B\Delta_g & \Delta_\psi^H B\Delta_\psi & \Delta_\psi^H B\Delta_\theta & \Delta_\psi^H B\Delta_\phi \\ \Delta_\theta^H B\Delta_g & \Delta_\theta^H B\Delta_\psi & \Delta_\theta^H B\Delta_\theta & \Delta_\theta^H B\Delta_\phi \\ \Delta_\phi^H B\Delta_g & \Delta_\phi^H B\Delta_\psi & \Delta_\theta^H B\Delta_\theta & \Delta_\phi^H B\Delta_\phi \end{bmatrix}
\end{aligned} \tag{173}$$

Therefore,

$$\begin{aligned}
CRB^{-1}(g,\psi,\theta,\phi) &= \begin{bmatrix} F_{gg} & F_{g\psi} & F_{g\theta} & F_{g\phi} \\ F_{\psi g} & F_{\psi\psi} & F_{\psi\theta} & F_{\psi\phi} \\ F_{\theta\psi} & F_{\theta\psi} & F_{\theta\theta} & F_{\theta\phi} \\ F_{\phi g} & F_{\theta\phi} & F_{\phi\theta} & F_{\phi\phi} \end{bmatrix} \\
&\quad - \sum_{k=1}^{K} \mathrm{Re}\begin{bmatrix} \Delta_{gk}^H B\Delta_{gk} & \Delta_{gk}^H B\Delta_{\psi k} & \Delta_{gk}^H B\Delta_{\theta k} & \Delta_{gk}^H B\Delta_{\phi k} \\ \Delta_{\psi k}^H B\Delta_{gk} & \Delta_{\psi k}^H B\Delta_{\psi k} & \Delta_{\psi k}^H B\Delta_{\theta k} & \Delta_{\psi k}^H B\Delta_{\phi k} \\ \Delta_{\theta k}^H B\Delta_{gk} & \Delta_{\theta k}^H B\Delta_{\psi k} & \Delta_{\theta k}^H B\Delta_{\theta k} & \Delta_{\theta k}^H B\Delta_{\phi k} \\ \Delta_{\phi k}^H B\Delta_{gk} & \Delta_{\phi k}^H B\Delta_{\psi k} & \Delta_{\theta k}^H B\Delta_{\theta k} & \Delta_{\phi k}^H B\Delta_{\phi k} \end{bmatrix} \\
&= \begin{bmatrix} Y_{gg} & Y_{g\psi} & Y_{g\theta} & Y_{g\phi} \\ Y_{\psi g} & Y_{\psi\psi} & Y_{\psi\theta} & Y_{\psi\phi} \\ Y_{\theta\psi} & Y_{\theta\psi} & Y_{\theta\theta} & Y_{\theta\phi} \\ Y_{\phi g} & Y_{\theta\phi} & Y_{\phi\theta} & Y_{\phi\phi} \end{bmatrix}
\end{aligned} \tag{174}$$

where

$$\begin{aligned}
Y_{gg} &= \frac{2}{\sigma}\sum_{k=1}^{K} \mathrm{Re}\left[S^H(k) D_g^H D_g S(k) - S^H(k) D_g^H A\left(A^H A\right)^{-1} A^H D S(k) \right] \\
&= \frac{2}{\sigma}\sum_{k=1}^{K} \mathrm{Re}\left\{ S^H(k) D_g^H A^{\perp} D_g S(k) \right\}
\end{aligned} \tag{175}$$

$$A^{\perp} = \left[I - A\left(A^{H} A \right)^{-1} A^{H} \right] \tag{176}$$

$$Y_{g\psi} = \frac{2}{\sigma} \sum_{k=1}^{K} \mathrm{Re}\left\{ S^{H}(k) D_{g}^{H} A^{\perp} D_{\psi} S(k) \right\} \tag{177}$$

$$Y_{g\theta} = \frac{2}{\sigma} \sum_{k=1}^{K} \mathrm{Re}\left\{ S^{H}(k) D_{g}^{H} A^{\perp} D_{\theta} S(k) \right\} \tag{178}$$

$$Y_{g\phi} = \frac{2}{\sigma} \sum_{k=1}^{K} \mathrm{Re}\left\{ S^{H}(k) D_{g}^{H} A^{\perp} D_{\phi} S(k) \right\} \tag{179}$$

$$Y_{\psi g} = \frac{2}{\sigma} \sum_{k=1}^{K} \mathrm{Re}\left\{ S^{H}(k) D_{\psi}^{H} A^{\perp} D_{g} S(k) \right\} \tag{180}$$

$$Y_{\psi\psi} = \frac{2}{\sigma} \sum_{k=1}^{K} \mathrm{Re}\left\{ S^{H}(k) D_{\psi}^{H} A^{\perp} D_{\psi} S(k) \right\} \tag{181}$$

$$Y_{\psi\theta} = \frac{2}{\sigma} \sum_{k=1}^{K} \mathrm{Re}\left\{ S^{H}(k) D_{\psi}^{H} A^{\perp} D_{\theta} S(k) \right\} \tag{182}$$

$$Y_{\psi\phi} = \frac{2}{\sigma} \sum_{k=1}^{K} \mathrm{Re}\left\{ S^{H}(k) D_{\psi}^{H} A^{\perp} D_{\phi} S(k) \right\} \tag{183}$$

$$Y_{\theta g} = \frac{2}{\sigma} \sum_{k=1}^{K} \mathrm{Re}\left\{ S^{H}(k) D_{\theta}^{H} A^{\perp} D_{g} S(k) \right\} \tag{184}$$

$$Y_{\theta\psi} = \frac{2}{\sigma} \sum_{k=1}^{K} \mathrm{Re}\left\{ S^{H}(k) D_{\theta}^{H} A^{\perp} D_{\psi} S(k) \right\} \tag{185}$$

$$Y_{\theta\theta} = \frac{2}{\sigma} \sum_{k=1}^{K} \mathrm{Re}\left\{ S^{H}(k) D_{\theta}^{H} A^{\perp} D_{\theta} S(k) \right\} \tag{186}$$

$$Y_{\theta\phi} = \frac{2}{\sigma} \sum_{k=1}^{K} \mathrm{Re}\left\{ S^{H}(k) D_{\theta}^{H} A^{\perp} D_{\phi} S(k) \right\} \tag{187}$$

$$Y_{\phi g} = \frac{2}{\sigma} \sum_{k=1}^{K} \mathrm{Re}\left\{ S^{H}(k) D_{\phi}^{H} A^{\perp} D_{g} S(k) \right\} \tag{188}$$

$$Y_{\phi\psi} = \frac{2}{\sigma}\sum_{k=1}^{K}\mathrm{Re}\left\{S^{H}\left(k\right)D_{\phi}^{H}A^{\perp}D_{\psi}S\left(k\right)\right\} \tag{189}$$

$$Y_{\phi\theta} = \frac{2}{\sigma}\sum_{k=1}^{K}\mathrm{Re}\left\{S^{H}\left(k\right)D_{\phi}^{H}A^{\perp}D_{\theta}S\left(k\right)\right\} \tag{190}$$

$$Y_{\phi\phi} = \frac{2}{\sigma}\sum_{k=1}^{K}\mathrm{Re}\left\{S^{H}\left(k\right)D_{\phi}^{H}A^{\perp}D_{\phi}S\left(k\right)\right\} \tag{191}$$

APPENDIX E

DERIVATION OF THE FIM WITH SENSOR GAIN, PHASE AND POSITION ERRORS

We derived the FIM with respect to DOAs in Appendix A of our previously published paper [55]. Omitting to the parameters $\mathrm{Re}(P_{mn})$, $\mathrm{Im}(P_{mn})$ and σ^2, we only consider incident signal angles θ, ϕ, sensor gain g, sensor phase ψ and sensor location errors u, v, w along x-axis, y-axis and z-axis. The collection of unknown parameters we consider is given by

$$\eta = \left[g^T, \psi^T, \theta^T, \phi^T, u^T, v^T, w^T \right]^T \tag{192}$$

Since the array structure varies as the UAVs morph, we use iterative-MUSIC algorithm to estimate the incident angles.

The system stochastic FIM associated with 2-D DOAs is given in Appendix C,

$$F_{s,2} = \sum_{i=1}^{I} F_{i,s,2} = \begin{bmatrix} F_{\theta\theta} & F_{\theta\phi} \\ F_{\phi\theta} & F_{\phi\phi} \end{bmatrix} \tag{193}$$

$$F_{i,s,2} = \begin{bmatrix} F_{i,\theta\theta} F_{i,\theta\phi} \\ F_{i,\phi\theta} F_{i,\phi\phi} \end{bmatrix} = \frac{2K}{\sigma^2} \left\{ \mathrm{Re}\left[D_i^H A_i^{\perp} D_i \odot \mathbf{1}_2 \mathbf{1}_2^T \otimes U_i \right] \right\} \tag{194}$$

Therefore, the FIM associated with sensor gain, phase, position errors, and DOAs can be obtained as

$$
\begin{aligned}
&F_{i,s,7}\left(g,\psi,\theta,\phi,u,v,w\right)\\
&=\begin{bmatrix}
F_{i,gg} & F_{i,g\psi} & F_{i,g\theta} & F_{i,g\phi} & F_{i,gu} & F_{i,gv} & F_{i,gw}\\
F_{i,\psi g} & F_{i,\psi\psi} & F_{i,\psi\theta} & F_{i,\psi\phi} & F_{i,\psi u} & F_{i,\psi v} & F_{i,\psi w}\\
F_{i,\theta g} & F_{i,\theta\psi} & F_{i,\theta\theta} & F_{i,\theta\phi} & F_{i,\theta u} & F_{i,\theta v} & F_{i,\theta w}\\
F_{i,\phi g} & F_{i,\phi\psi} & F_{i,\phi\theta} & F_{i,\phi\phi} & F_{i,\phi u} & F_{i,\phi v} & F_{i,\phi w}\\
F_{i,ug} & F_{i,u\psi} & F_{i,u\theta} & F_{i,u\phi} & F_{i,uu} & F_{i,uv} & F_{i,uw}\\
F_{i,vg} & F_{i,v\psi} & F_{i,v\theta} & F_{i,v\phi} & F_{i,vu} & F_{i,vv} & F_{i,vw}\\
F_{i,wg} & F_{i,w\psi} & F_{i,w\theta} & F_{i,w\phi} & F_{i,wu} & F_{i,wv} & F_{i,ww}
\end{bmatrix}\\
&=\frac{2K}{\sigma^2}\left\{\mathrm{Re}\left[\tilde{D}_i^H\tilde{A}_i^{\perp}\tilde{D}_i\odot 1_7 1_7^T\otimes\tilde{U}_i\right]\right\}
\end{aligned}
\tag{195}
$$

$$
F_{s,7}=\sum_{i=1}^{I}F_{i,s,7} \tag{196}
$$

herein

$$
\tilde{D}_i=\begin{bmatrix}\tilde{d}_{i,g} & \tilde{d}_{i,\psi} & \tilde{d}_{i,\theta} & \tilde{d}_{i,\phi} & \tilde{d}_{i,u} & \tilde{d}_{i,v} & \tilde{d}_{i,w}\end{bmatrix} \tag{197}
$$

$$
\tilde{A}_i^{\perp}=I_0-\tilde{A}_i\left(\tilde{A}_i^H\tilde{A}_i\right)^{-1}\tilde{A}_i^H \tag{198}
$$

$$
\tilde{U}_i=P\tilde{A}_i^H\tilde{R}_i^{-1}\tilde{A}_iP \tag{199}
$$

where

$$
\tilde{d}_{i,g}=\frac{d}{dg}\tilde{a}_i\left(\alpha,\beta,\delta\right)=\tilde{a}_i\left(\alpha,\beta,\delta\right)/g_i \tag{200}
$$

$$
\tilde{d}_{i,\psi}=\frac{d}{d\psi}\tilde{a}_i\left(\alpha,\beta,\delta\right)=j\tilde{a}_i\left(\alpha,\beta,\delta\right) \tag{201}
$$

$$
\tilde{d}_{i,u}=\frac{d}{du}\tilde{a}_i\left(\alpha,\beta,\delta\right)=j\frac{2\pi}{\lambda}\tilde{a}_i\left(\alpha,\beta,\delta\right)\sin\theta\cos\phi \tag{202}
$$

$$
\tilde{d}_{i,v}=\frac{d}{dv}\tilde{a}_i\left(\alpha,\beta,\delta\right)=j\frac{2\pi}{\lambda}\tilde{a}_i\left(\alpha,\beta,\delta\right)\sin\theta\sin\phi \tag{203}
$$

$$\tilde{d}_{i,w} = \frac{d}{dw}\tilde{a}_i\left(\alpha,\beta,\delta\right) = j\frac{2\pi}{\lambda}\tilde{a}_i\left(\alpha,\beta,\delta\right)\cos\theta \tag{204}$$

$$\tilde{d}_{i,\theta} = \frac{d}{d\theta}\tilde{a}_i\left(\alpha,\beta,\delta\right) = j\frac{2\pi}{\lambda}\tilde{b}_i\tilde{a}_i\left(\alpha,\beta,\delta\right) \tag{205}$$

$$\tilde{d}_{i,\phi} = \frac{d}{d\phi}\tilde{a}_i\left(\alpha,\beta,\delta\right) = j\frac{2\pi}{\lambda}\tilde{q}_i\tilde{a}_i\left(\alpha,\beta,\delta\right) \tag{206}$$

where

$$\tilde{b}_i = \tilde{x}_i\cos\theta\cos\phi + \tilde{y}_i\cos\theta\sin\phi - \tilde{z}_i\sin\theta \tag{207}$$

$$\tilde{q}_i = -\tilde{x}_i\sin\theta\sin\phi + \tilde{y}_i\sin\theta\cos\phi \tag{208}$$

Finally, we obtain

$$CRB = F_{s,7}^{-1} \tag{209}$$